MINNESOTA GEOLOGICAL SURVEY
D.L. Southwick, *Director*

GEOLOGIC SETTING AND DESCRIPTIVE GEOCHEMISTRY OF ARCHEAN SUPRACRUSTAL AND HYPABYSSAL ROCKS, SOUDAN-BIGFORK AREA, NORTHERN MINNESOTA: IMPLICATIONS FOR METALLIC MINERAL EXPLORATION

D.L. Southwick, T.J. Boerboom and M.A. Jirsa

Report of Investigations 51
ISSN 0076-9177

UNIVERSITY OF MINNESOTA
Saint Paul — 1998

GEOLOGIC SETTING AND DESCRIPTIVE GEOCHEMISTRY OF ARCHEAN SUPRACRUSTAL AND HYPABYSSAL ROCKS, SOUDAN-BIGFORK AREA, NORTHERN MINNESOTA: IMPLICATIONS FOR METALLIC MINERAL EXPLORATION

Minnesota Geological Survey
2642 University Avenue West
Saint Paul, Minnesota 55114-1057

Telephone: 612-627-4780
Fax: 612-627-4778
E-mail address: mgs@gold.tc.umn.edu
Web site: http://geolab.geo.umn.edu/mgs

ISSN 0076-9177

CONTENTS

Page

FIGURES

FIGURES continued.

Page

TABLES

Page

APPENDIX TABLES

GEOLOGIC SETTING AND DESCRIPTIVE GEOCHEMISTRY OF ARCHEAN SUPRACRUSTAL AND HYPABYSSAL ROCKS, SOUDAN-BIGFORK AREA, NORTHERN MINNESOTA: IMPLICATIONS FOR METALLIC MINERAL EXPLORATION

D.L. Southwick, T.J. Boerboom and M.A. Jirsa

ABSTRACT

Geochemical data are presented for a suite of samples chosen to represent as nearly as possible the compositions of unaltered rocks within the Archean greenstone belt of the Soudan-Bigfork area in northern Minnesota. These data are interpreted within the stratigraphic and structural framework provided by geologic mapping, and are used to deduce probable depositional and tectonic environments for the volcanic and sedimentary sequences described. In addition, the data indicate regional differences in intrinsic mineral potential, as judged from the presence or absence of geochemically favorable rock types associated with economic deposits of metallic minerals elsewhere in the Superior Province.

The greenstone belt as a whole has attributes consistent with development in an oceanic volcanic-arc setting that is broadly analogous to modern arcs of the western Pacific basin. Supracrustal rocks in the Soudan belt (southern portion of the Soudan-Bigfork area) include a lower volcanic cycle that consists of the upper parts of a calc-alkaline volcanic edifice which evolved with time from a submarine basaltic pile into an emergent or nearly emergent dacitic eruptive center, and an upper cycle that represents submarine fan deposits mingled in time and space with tholeiitic basalt of possible back-arc origin. The Newton belt (northern portion of the Soudan-Bigfork area) consists of several fault slices made up chiefly of tholeiitic basalt and pyroclastic and epiclastic dacitic rocks. Because of structural shuffling and imbrication, the rock sequences within the Newton belt cannot be reliably correlated from slice to slice, which handicaps paleotectonic interpretation. Geochemically they are consistent with a back-arc origin.

Basaltic sequences in the Soudan belt are evolved to iron-enriched compositions and exhibit very low background values for gold. Basaltic sequences in the Newton belt are moderately more magnesian and auriferous, and therefore may be somewhat better candidates for harboring economic gold deposits. The dacitic rocks of the Soudan belt fall into the least favorable geochemical category for hosting massive-sulfide deposits, based on empirical associations throughout the Superior Province, whereas the geochemical attributes of dacitic rocks in the Newton belt remain inadequately characterized in this respect. Differentiated gabbro-pyroxenite-peridotite sills are absent from the Soudan belt but are characteristic of the Newton belt. Peridotite sills within the Deer Lake Complex contain subeconomic amounts of magmatic Cu-Ni sulfide minerals and are petrologically reasonable, but untested, candidates for hosting platinum-group minerals. On the basis of these broad lithogeochemical criteria, the mineral potential of the Newton belt would appear to warrant serious further investigation.

INTRODUCTION

Exploration geologists generally agree that good geologic maps are the first and most basic requirements for systematic mineral exploration in Archean greenstone belts. Most would also agree that for modern exploration practice it is almost as important to know the detailed geochemical characteristics of the rock types in a regional target area as it is to know the distribution of rock units in space and time. It is increasingly clear that the types of

metallic mineral deposits expected within an orogenic belt of any age are related to the specific tectonic environments where the host rocks were formed (Mitchell and Garson, 1981; Sawkins, 1990; Barley and Groves, 1992). Consequently, the early stages of systematic mineral exploration in a structurally complex, heterolithic, convergent-margin orogen, such as an Archean greenstone belt, tend to center around deduction of the petrotectonic origins of the lithostratigraphic terranes of which the orogen is composed. This process requires the integration and interpretation of information on the stratigraphy, physical attributes, structural position, and chemical composition of the rock sequences that make up each terrane. The results will shape the broader aspects of an exploration strategy by guiding the selection of specific geological targets within a terrane that hold the greatest potential for eventual mineral discovery.

The linkage between deposit type and tectonic environment within convergent-margin regimes rests chiefly on observations and inferences from Phanerozoic orogens,

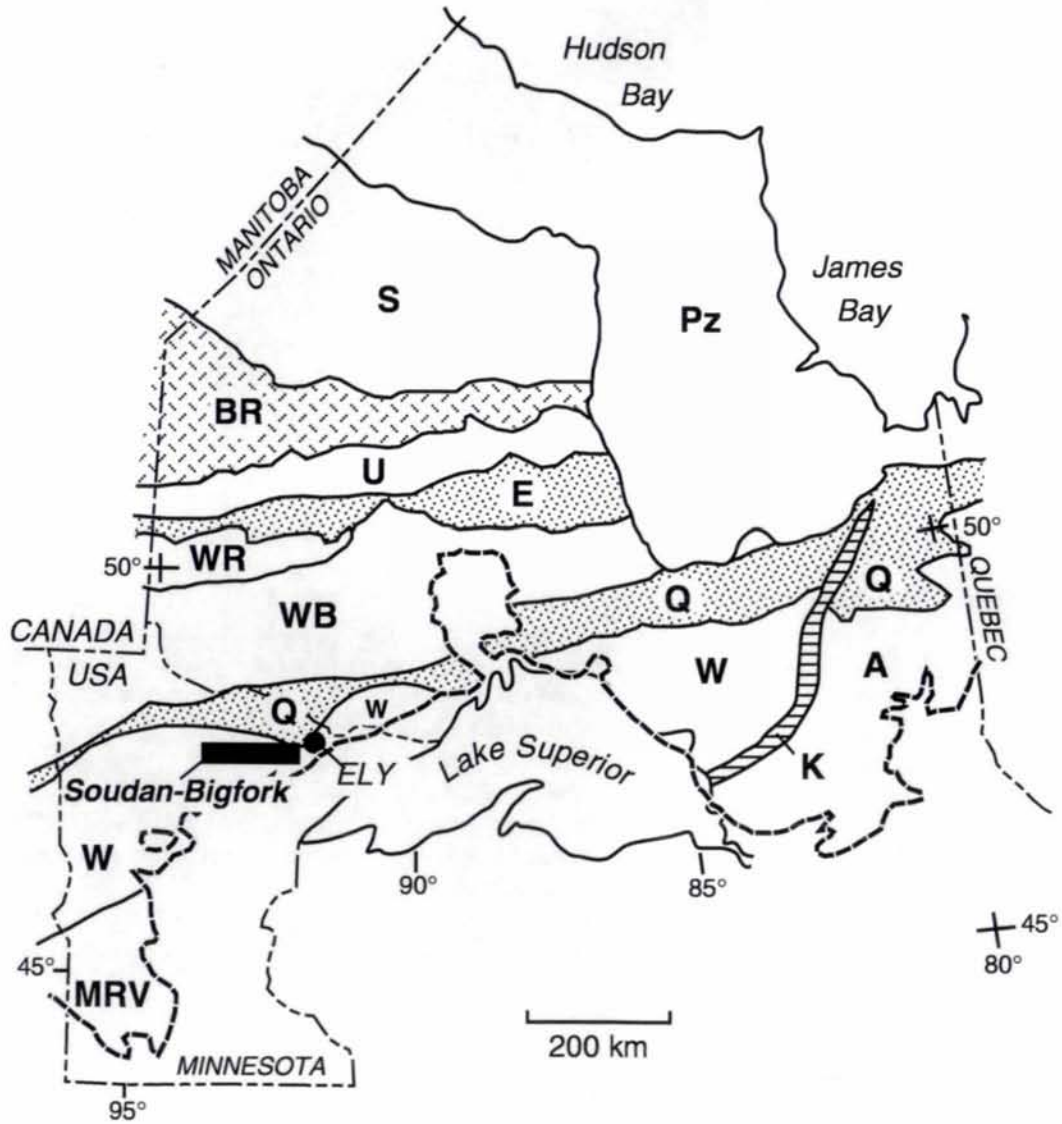

Figure 1. Approximate location of the Soudan-Bigfork area (area A of Fig. 2) of the Vermilion district in the Wawa subprovince, with respect to other subprovinces of the Superior Province of the Canadian Shield. Subprovince names: S, Sachigo; BR, Berens River; U, Uchi; E, English River; WR, Winnipeg River; WB, Wabigoon; Q, Quetico; W, Wawa; A, Abitibi; MRV, Minnesota River Valley; K, Kapuskasing structural zone. Pz = Paleozoic rocks in Hudson lowland. Dashed line marks edge of post-Archean rocks to the south. Map modified from Ontario Geological Survey (1992) and various Minnesota sources.

mostly of Cenozoic age and on the Pacific Rim. The rationale pertains by analogy to the Archean greenstone belts, despite the inherently greater difficulty in establishing the details of their tectonic evolution (Thurston and Chivers, 1990; La Fleche and others, 1992; Taira and others, 1992; Kerrich and Wyman, 1996). High-quality geochemical data are of preeminent value in this task. The interpretive keys lie mainly in the original, igneous geochemistry of the volcanic sequences and subvolcanic intrusions that are now dismembered, tectonically reassembled and variably metamorphosed. Because information on original rock compositions is critical, analyses of unaltered, unmineralized, more or less pristine rocks are of greatest value. Indeed, a lack of chemical data from suitably fresh rock samples may seriously handicap the regional evaluation of a greenstone belt that otherwise is well mapped. Many chemical analyses obtained by earlier generations of exploration geologists are not well suited for tectonic interpretation because the samples were not selected to represent as closely as possible the original, unmodified rock compositions. Until recently this has been the case in Minnesota.

Chemical data from unaltered rock types are also applicable to the development of more specific exploration strategies for lode gold, volcanic-hosted base-metal sulfide deposits, or other deposit types common to convergent-margin settings, including the Archean greenstone belts (Lesher and others, 1986; Swinden and others, 1989; Barnes and others, 1995; Stolz, 1995; Galley, 1996). Therefore, the basic geochemical data assembled for the purpose of determining tectonic environments also contribute to a preliminary assessment of the probability of mineral discovery, insofar as probability can be judged from the presence or absence of geochemical favorability criteria in the potential host rocks. Geochemical favorability criteria are highly developed for the volcanic sequences associated with base-metal massive-sulfide deposits (Galley, 1996, and references therein) and for the volcanic sequences associated with the so-called komatiitic class of Cu-Ni-PGE deposits (Barnes and others, 1995; Lesher and Stone, 1996). General geochemical criteria are also applied to exploration for various lode-gold deposit types (Poulsen, 1996), although their efficacy in delineating favorable gold targets is open to debate (Card and others, 1989; Robert, 1996).

CONTEXT AND PURPOSE OF THIS STUDY

The primary objective here is to present an improved geochemical database for the supracrustal and subvolcanic rocks in the Soudan-Bigfork area of the western Vermilion district in northeastern Minnesota. We interpret the data in the context of stratigraphic, structural, and lithologic factors determined over several decades of geologic mapping.

The Vermilion district (Clements, 1903; Sims, 1972a) is a strike-parallel segment of a greenstone belt within the Wawa subprovince of the Superior Province of the Canadian Shield (Fig. 1). As presently used, the terms "Vermilion district" or "Vermilion district greenstone belt" refer to a belt of Archean supracrustal rocks that extends at least 300 km west to east and 50 to 70 km from north to south, as delineated by geophysical maps. Archean rocks of the Vermilion district greenstone belt are exposed intermittently to the east of longitude 93°75'W. (Fig. 2). West of there they are overlain locally by erosional remnants of flat-lying marine sedimentary rocks of Mesozoic age and a ubiquitous blanket of Quaternary glacial deposits. The Soudan-Bigfork area is a subarea of the western Vermilion district (Figs. 1 and 2), and consists of 26 quadrangles where detailed geologic mapping has recently been completed by Minnesota Geological Survey staff. Although the Vermilion district was a significant source of iron ore prior to the cessation of mining in 1962, repeated episodes of exploration for nonferrous metals over the past 130 years have generally been disappointing.

Worldwide, there is a vast published literature concerned with the regional geochemistry of Archean supracrustal rocks, numbering many hundreds of separate studies and thousands of rock analyses (e.g. Ho and others, 1990; La Fleche and others, 1992; Grunsky and others, 1992). The geochemistry of Minnesota's Archean greenstone belts is not well characterized in comparison to areas of similar size and equivalent mineral potential in Canada or Australia. Prior to 1990, the only widely available geochemical data were in papers by Green (1970), Jahn and others (1974), Arth and Hanson (1975), and Schulz (1980, 1982). Most of this published work pertained to the eastern, best-exposed part of the Vermilion district near Ely, Minnesota (some 20 km east of area A on Fig. 2; see also Fig. 1) and therefore characterizes only a restricted stratigraphic section in a small segment of a single greenstone belt.

In 1989, the Natural Resources Research Institute (NRRI) and the Minnesota Geological Survey (MGS) began a cooperative effort to codify the geochemical database for Archean supracrustal rocks in northern Minnesota. The results were provided in print and electronic formats as a massive open-file report by Englebert and Hauck (1991). The compilation process involved (1) screening, organizing, and tabulating geochemical data that exploration companies had acquired and released to the public; (2) assembling all unpublished, well-documented geochemical data from government files; and (3) tabulating new analytical data from sample suites collected during geologic mapping in the Vermilion district and its

westward extensions (Jirsa and others, 1991; Southwick, 1993), as well as that in the greenstone-belt rocks of the Virginia horn in the footwall of the Mesabi Iron Range (Welsh and others, 1991; see Fig. 2).

This report covers a selected subset of the data compiled by Englebert and Hauck (1991), together with analyses that have been newly acquired or exhumed from archives since that compilation was made. Only analyses of unsheared, unaltered rocks are considered. The geochemical data are discussed and interpreted within the framework of structural subdivisions and stratigraphic units recognized through geologic mapping in the Soudan-Bigfork area (Southwick, 1993; area A of Fig. 2). This approach leads naturally to considerations of the original tectonic settings in which the supracrustal rocks of the western Vermilion district were deposited, and various implications for metallic mineral exploration. The geochemistry of rocks in the Virginia horn is not considered in this study. That will be the subject of a separate report that will augment recently completed geologic mapping (Jirsa and others, 1998; Jirsa, 1998).

GEOLOGY OF THE SOUDAN-BIGFORK AREA

Regional Geologic Relations

In the historically defined (Clements, 1903) Vermilion district, i.e. the greenstone belt rocks that extend eastward from longitude 92°50'W., supracrustal rock sequences are confined to a narrow zone between the Vermilion Granitic Complex on the north (within the Quetico subprovince) and the Giants Range batholith on the south (within the Wawa subprovince). The area underlain by Archean supracrustal rocks widens abruptly to the west (Jirsa and Boerboom, 1990; Jirsa, 1990; Jirsa and others, 1991, 1992), and is divisible into two distinct panels that differ markedly in large-scale structural style (Fig. 3). The southern panel (the Soudan belt) is characterized by prominent arcuate folds and curvilinear structural trends. The northern panel (the Newton belt) lacks large fold structures and is interpreted to consist of a deck of fault-bounded, homoclinal, dominantly north-facing stratigraphic packets. The boundary between these contrasting structural panels can be traced geophysically across the width of Minnesota, and has been informally designated the Leech Lake structural disconformity (Jirsa and others, 1992). This designation, though cumbersome, emphasizes that the boundary appears to have both structural and stratigraphic aspects. It is rather clearly a zone of faulting in some places and an unconformity in others. Where the boundary has been disrupted by complex displacements on younger strike-slip faults, as, for example, in the western part of the Soudan-Bigfork area (Fig. 3), its original attributes and even its trace become somewhat obscure. Nevertheless, the disconformity is readily delineated on regional-scale geophysical maps, and the feature, whatever its origin, appears to be a boundary between tectonic domains of fundamentally different structural architecture.

In the central and eastern parts of the Vermilion district, the Leech Lake structural disconformity is interpreted to coincide with the Mud Creek shear zone (Hudleston and others, 1988) and segments of the traces of the Vermilion and Wolf Lake faults (Sims and Southwick, 1985). It continues westward across the Soudan-Bigfork area, essentially as the inferred trace of the Mud Creek shear zone (Fig. 3), and is displaced southward by sinistral offset on the Bear River fault. The structural panel south of the disconformity, characterized by regional-scale folds, is informally termed the Soudan belt (Jirsa and others, 1992). The panel north of the disconformity, characterized by homoclinal fault slices, is informally termed the Newton belt.

Structure and Stratigraphy of the Soudan Belt

The best defined large fold in the Soudan belt is the Tower-Soudan anticline (Sims and Southwick, 1985; Southwick, 1993) which plunges steeply toward the west or northwest and is overturned toward the southwest (Fig. 3). It is very nearly a vertical fold (Ramsay and Huber, 1987), inasmuch as its hinge locally approaches a vertical orientation. A second fold comparable to this is the Sherry Lake anticline, located near the west end of the Soudan-Bigfork area (Fig. 3). It plunges steeply to the north or northeast and appears to have been significantly reoriented during late folding (F_3) and the rise of granitoid plutons (Jirsa and others, 1992).

The stratigraphic sequence delineating both of these major anticlines consists of lower and upper units of mafic volcanic rocks that are separated from each other by a unit composed of mafic to felsic fragmental rocks and iron-formation (Table 1). The lower volcanic unit (BLLE on Fig. 3) contains pillowed and massive flows of tholeiitic to calc-alkalic composition, many diabase sills of similar composition, and local fragmental units that probably were pillow-breccia and reworked flow-top rubble (Schulz, 1980). Pillows typically form irregular shapes and are vesiculated. This unit is overlain gradationally by a sequence that consists of thin basalt flows, detrital rocks of basaltic to dacitic composition that range from thin-bedded and fine-grained to thick-bedded and rubbly, and by laminated magnetite-chert iron-formation of the iron-formation unit. The upper volcanic unit (SLUE on Fig. 3) is in sharp stratigraphic contact with the underlying iron-formation unit in most places; locally

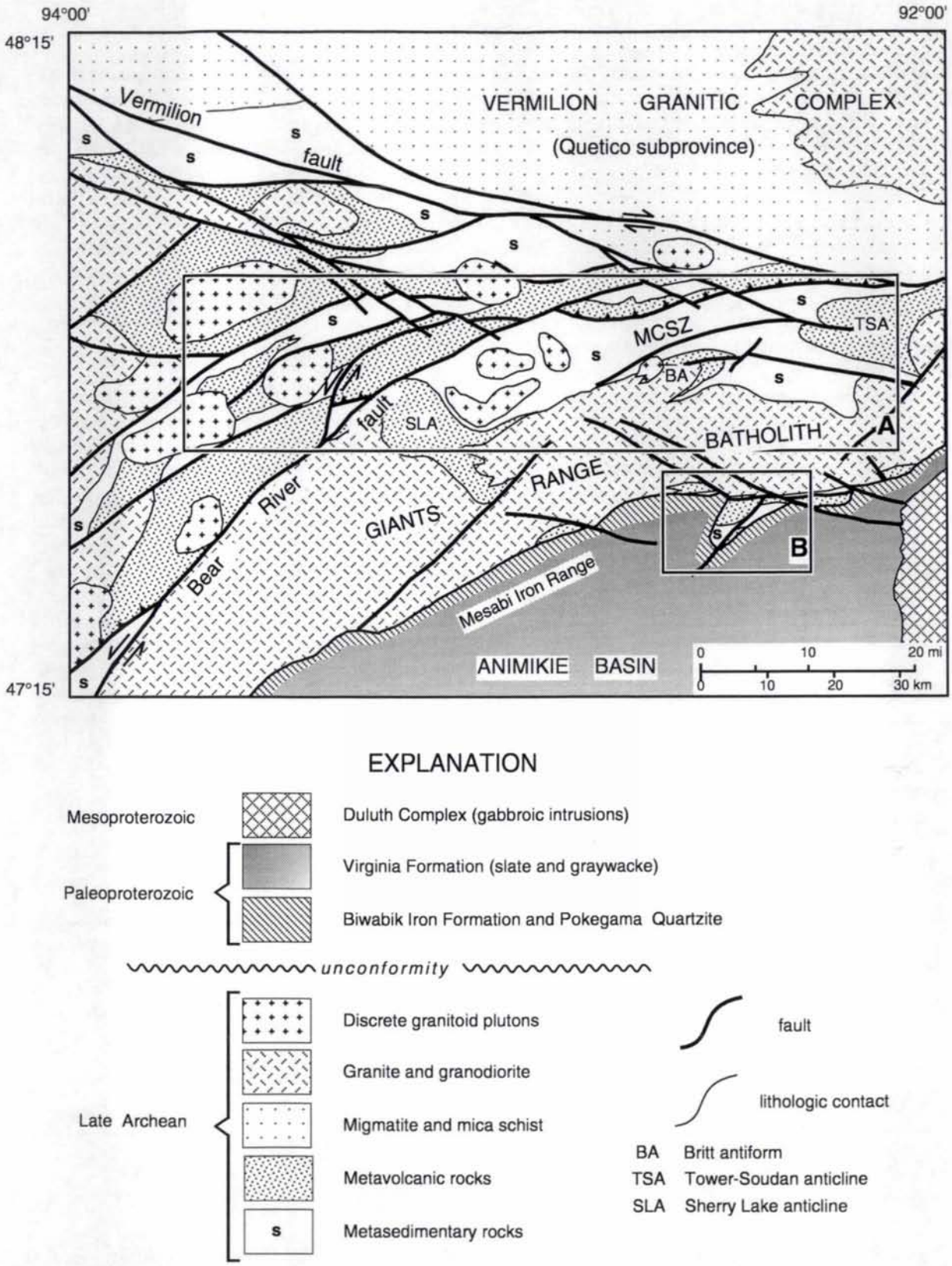

Figure 2. Bedrock geology of part of the western Vermilion district of northern Minnesota showing the Soudan-Bigfork area (A) and the Virginia horn (B). Geology modified from Morey (1996). The Soudan belt is bounded by the Mud Creek shear zone (MCSZ), the Bear River fault, and the Giants Range batholith. The Newton belt lies between the Vermilion fault on the north and the combined traces of the Mud Creek shear zone and the Bear River fault on the south. Displacement sense of major faults shown by standard ornamentation.

there is evidence for stratigraphic unconformity between the two. The upper volcanic unit is for the most part a monotonously uniform sequence of tholeiitic pillow basalts. The pillows are typically ovoid, smooth, thin rinded, and without vesicles, all of which suggest extrusion under deep water (Schulz, 1980). The stratigraphic order of rock units is well established from the consistent orientation and wide distribution of evidence for younging within the pillowed sequences of basaltic rocks in both major anticlines.

In the Tower-Soudan area, the lower volcanic unit, the iron-formation unit, and the upper volcanic unit constitute the informally named Lower member, the formally named Soudan Iron-formation Member, and the informally-named Upper member, respectively, of the Ely Greenstone (Morey and others, 1970; Schulz, 1980). A similar lithologic sequence is documented from the Sherry Lake anticline (Fig. 3), where the lower volcanic unit is termed the Bear Lake sequence, the iron-formation unit is unnamed, and the upper volcanic unit is termed the Sherry Lake sequence. Lithologic units within the Sherry Lake anticline have not been formally correlated with the Ely Greenstone, despite their similarities (Jirsa, 1988, and Table 1).

A thick sedimentary unit composed of dacitic volcaniclastic rocks and turbiditic graywacke and shale derived from dacitic sources stratigraphically overlies rocks of the iron-formation unit, or the lower volcanic unit where iron-formation is missing. These dacitic volcaniclastic rocks constitute the Lake Vermilion Formation, which is laterally equivalent to some rocks in the upper volcanic unit (Morey and others, 1970). Rocks of the Lake Vermilion Formation range from essentially unsorted and unstratified dacite rubble at one extreme to finely laminated and graded, reworked ash and fine-grained epiclastic detritus at the other, with the greater part of the unit consisting of lithic graywacke and associated shale (Ojakangas, 1972a, 1972b). As a whole, the Lake Vermilion Formation has the sedimentological attributes of a turbiditic slope-and-fan assemblage deposited around and among volcanic islands that had evolved to the stage of producing dacite as their primary output (Ojakangas, 1985).

Where the Upper member of the Ely Greenstone is missing in the Tower-Soudan area, the contact between the Soudan Iron-formation Member of the Ely Greenstone and the overlying Lake Vermilion Formation is locally an unconformity (Sims and Southwick, 1980; Southwick, 1993). In the same area, mafic volcanic rocks assigned to the Upper member of the Ely Greenstone are interstratified with sedimentary rocks of the Lake Vermilion Formation (Schulz, 1980). A similar relationship exists in equivalent rock types around the Sherry Lake anticline. The implications are (1) that the upper volcanic unit in the Soudan-Bigfork area was deposited penecontemporaneously with the Lake Vermilion Formation, and (2) that there was a depositional hiatus between the Soudan Iron-formation Member and the Upper member of the Ely Greenstone.

Table 1. Stratigraphic terminology for the Soudan belt. Adapted from Morey and others (1970), Schulz (1980) and Jirsa (1990).

Informal unit term	Rock types	Sherry Lake anticline	Tower-Soudan anticline
sedimentary unit	Lithic wacke, dacitic wacke and related rocks	Lake Vermilion Formation	Lake Vermilion Formation
upper volcanic unit	Tholeiitic pillow basalt; nonvesiculated homogeneous flows	Sherry Lake sequence	Upper member, Ely Greenstone
~~	~~~~~~~~~~	local unconformity	~~~~~~~~~~
iron-formation unit	Cherty, laminated iron-formation commonly interbedded with basaltic, andesitic and dacitic flows, and their epiclastic equivalents	Unnamed iron-formation	Soudan Iron-formation Member, Ely Greenstone
lower volcanic unit	Tholeiitic to calc-alkalic basalt; massive to pillowed flows interbedded with andesitic, dacitic flows and epiclastic volcanic rocks towards the top of the unit	Bear Lake sequence	Lower member, Ely Greenstone

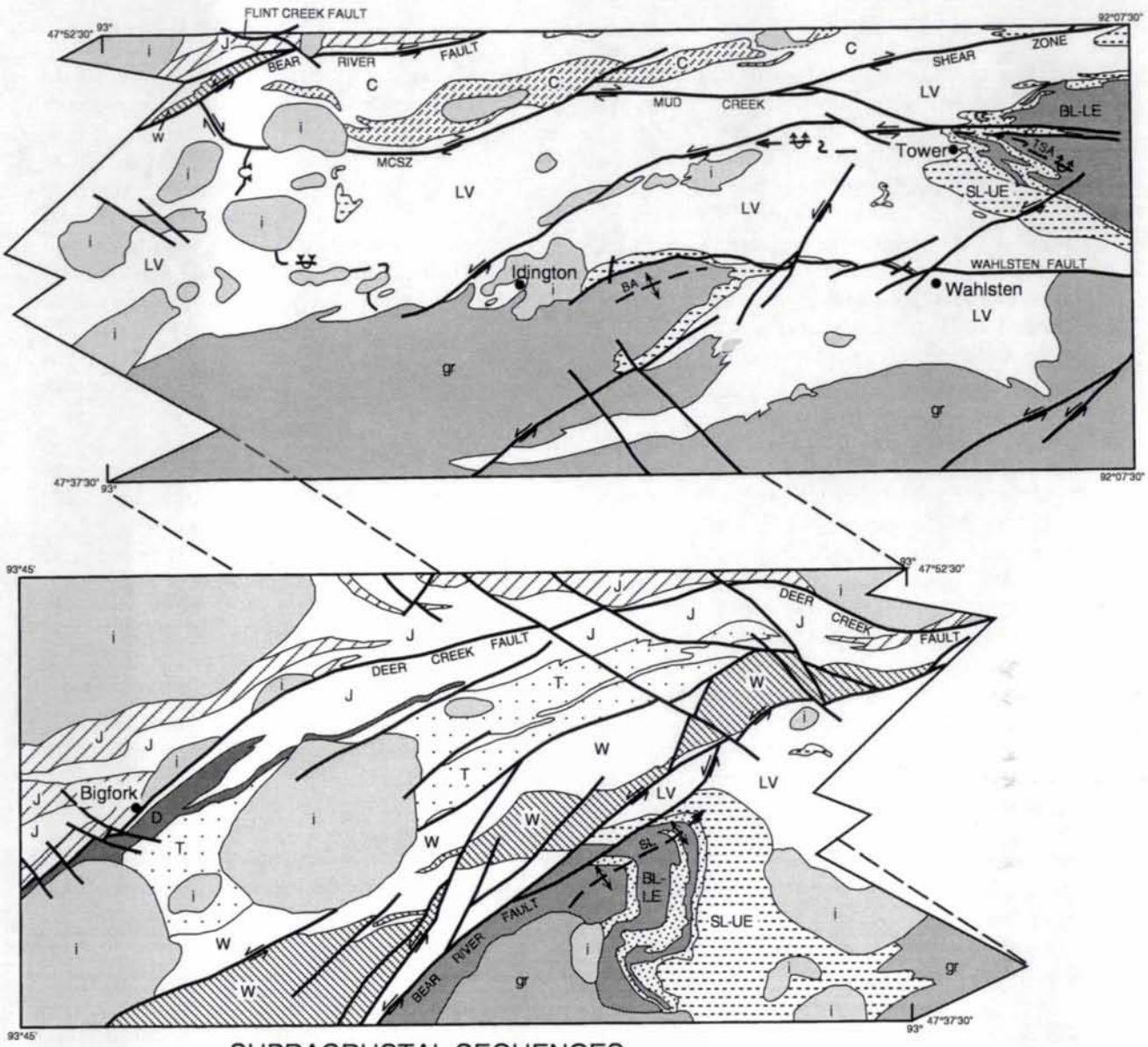

Figure 3. Simplified bedrock geology of the Soudan-Bigfork area showing major faults and the distribution of rock sequences. Unpatterned areas are predominantly sedimentary and dacitic volcanic rocks; symbol LV denotes sedimentary rocks of the Lake Vermilion Formation. See Figures 1 and 2 for location of the Soudan-Bigfork area.

The original distribution of sedimentary lithofacies within the Lake Vermilion Formation cannot be reconstructed precisely because of structural complexities. In general, coarse felsic detritus is more abundant in stratigraphically lower parts of the section, near contacts with underlying rocks of the lower volcanic unit or iron-formation unit in the cores of the large F_1 anticlines. Stratigraphically higher parts of the section exposed on the long limbs of F_1 folds are dominated by more distal, resedimented felsic tuff that is interbedded with graywacke and argillite of diverse but predominantly dacitic provenance.

Physical evidence for the depositional environment of the volcanic and sedimentary rocks indicates a geographically and temporally irregular transition from relatively shallow water volcanism, represented by the Lower member of the Ely Greenstone and parts of the Soudan Iron-formation Member and their lithologic equivalents, to deeper-water eruption of tholeiitic basalt (Upper member of the Ely Greenstone and equivalents). The transition was more or less coeval with dacitic eruptions from nearby centers (Schulz, 1980; Ojakangas, 1985). The dacitic volcanic centers stood as topographic highs and shed detritus, largely of pyroclastic origin, into the surrounding marine basins where it was reworked and redeposited as lithic graywacke and associated sedimentary rocks. The transitions from mafic to felsic volcanism and from shallow- to deep-water depositional environments were clearly episodic and complex. Local and perhaps regional unconformities, soft-sediment deformation features, and abrupt facies changes in the Lake Vermilion Formation all attest to sedimentation in a tectonically and volcanically active setting (Southwick and others, 1993). Indeed, the assemblage of depositional environments inferred for these Archean rocks, mainly from stratigraphic principles, accords remarkably well with the now-emerging picture of volcanism and sedimentation in active, rifted volcanic arcs of the western Pacific (Clift, 1995; Marsaglia and others, 1995).

The approximate contemporaneity of volcanism, sedimentation and deformation is also indicated by the characteristics of the earliest deformational events to affect the supracrustal rocks (Hudleston, 1976; Hudleston and others, 1988; Jirsa and others, 1992). Although later folding events and metamorphism (i.e. superimposed F_2 folds and associated S_2 and L_2 fabric elements) have obscured many details of the earlier folding, it is reasonably certain that F_1 folds were widely developed in the Soudan belt and that they formed under essentially nonmetamorphic conditions. Furthermore, the larger of these early folds involved thick sequences of volcanic and sedimentary strata, including the volcanic units in the core zones of the Tower-Soudan and Sherry Lake anticlines.

Recent mapping and structural studies support the following inferences about F_1 folding in the Soudan-Bigfork area:

1. The larger F_1 structures have dimensions on the scale of kilometers. This is indicated by the large areas within which easterly plunging F_2 folds face downward and westward in the S_2 cleavage (Jirsa and others, 1991, 1992), which requires that the stratigraphic sequence was inverted over large areas prior to F_2 folding. Such broad areas of inverted stratigraphy imply the existence of F_1 fold nappes and extensive preservation of their inverted lower limbs.

2. Outcrop-scale F_1 folds occur chiefly in sequences of thin-bedded sedimentary rocks (iron-formation and medial to distal turbidite sequences). Morphologically they include tight to isoclinal folds of diverse shapes and styles, including sheath folds and zones of complex fold interference, that are suggestive of soft-sediment origin. Axial-planar F_1 fabric is weak or absent. Most of the interference structures, including all those interpreted as sheath folds, are the result of soft-sediment and associated early tectonic deformation, both of which are assigned to D_1. They are not the result of superposition of F_2 folds on F_1 folds, as removal of the D_2 strain (Schultz-Ela and Hudleston, 1991) does not remove the sheath folds.

3. The Tower-Soudan and Sherry Lake anticlines are regional F_1 structures in which relatively massive metavolcanic rocks (the Ely Greenstone and equivalents) are overlain by massively to thinly bedded volcaniclastic and sedimentary strata (Lake Vermilion Formation and associated rocks). The massive rocks in the anticlinal cores accommodated F_1 folding under conditions that did not produce fabric in overlying sedimentary strata, but must instead have involved brittle slip on innumerable surfaces. This implies that many, if not most, of the contacts between the volcanic and sedimentary units in these anticlines are likely to have been decollements. Field study affirms that many of these contacts are indeed slip surfaces (Southwick, 1993), but the time when shearing occurred (i.e. D_1, D_2 or both) has not yet been resolved.

To sum up, the stratigraphic, lithologic, and D_1 structural attributes of supracrustal rocks in the Soudan belt of the Soudan-Bigfork area are all consistent with syntectonic evolution in a convergent-margin tectonic setting. The sedimentary rocks may represent an accretionary wedge assemblage that lay outboard of an evolved island-arc; it was deforming dynamically at moderate depths while sedi-

mentation and volcanism were continuing at the surface. Sedimentary materials in the deforming zone appear to have been capable of deformation by boundary-slip processes (Knipe, 1986) inasmuch as virtually no penetrative cleavage accompanied development of F_1 folds (Hudleston, 1976; Hudleston and others, 1988; Schulz-Ela and Hudleston, 1991). Thus it is reasonable to infer that the sedimentary components probably were wet and unlithified in the zone of F_1 deformation (MacKay and Moore, 1990; DiTullio and Byrne, 1990; Kimura and others, 1989).

Units of more massive and less hydrated volcanic rock that were involved in F_1 deformation would also have yielded by internal slip on pillow margins, fragment boundaries, and other primary or secondary fracture surfaces. Internal slip in both sedimentary and volcanic rocks

Table 2. Sequence terminology for the Newton belt, modified from Jirsa (1990). Internal unit labels are those on the geologic map compiled by Southwick (1993), which should be consulted for further clarification.

Sequence name	Mapped internal units		Sequence contacts
Joy Lake	jms:	metasedimentary rocks, chiefly graywacke; also felsic tuff and rare felsic flows	South: Bear River fault and lithologic contacts with other Newton belt sequences (mainly tmv, wmv).
	jmv:	metavolcanic rocks; mainly tholeiitic metabasalt	North: poorly defined; in part the faulted contact with Quetico subprovince rocks.
Deer Lake	dmv:	metavolcanic rocks; mainly Mg-tholeiite and Fe-komatiite; host to differentiated mafic sills of the Deer Lake Complex	South: lithologic contact between tmv and dmv. North: lithologic contact between dmv and jms.
Thistledew Lake	tgs:	metagraywacke, slate, dacitic tuff; minor chert, argillite	South: web of unnamed faults and lithologic contacts. North: same; much of boundary is lithologic contact between tmv and jms.
	tmv:	metavolcanic rocks; mainly tholeiitic metabasalt	
Wilson Lake	wms:	diverse metasedimentary and felsic metavolcanic rocks: mainly metagraywacke, slate, argillite, and dacitic tuff	South: Bear River fault. North: web of unnamed faults and lithologic contacts.
	wfx:	felsic and intermediate meta-volcanic rocks; includes flows, tuffs and agglomerates	
	wmv:	mafic and intermediate meta-volcanic rocks; chiefly tholeiitic metabasalt and meta-andesite	
Cook	cms:	metagraywacke and argillite	South: Mud Creek shear zone. North: Bear River fault.
	cmv:	metavolcanic rocks; mainly tholeiitic metabasalt	

may have been facilitated by synkinematic growth of secondary hydrous minerals (clay minerals, chlorite) on the slip surfaces, as well as by hydraulic effects (Platt, 1990).

Early F_1 deformation in this convergent-margin setting was followed by transpressional deformation at greater depth, under greenschist to amphibolite facies metamorphic conditions. F_2 folds and the associated regional fabrics (S_2 cleavage, L_2 lineation) were imposed on the rocks during transpressional deformation (Hudleston and others, 1988; Schultz-Ela and Hudleston, 1991; Jirsa and others, 1992). Although D_2 elements are the predominant structures observed at the outcrop scale, it appears that the major distribution of rock types at map scale was achieved during D_1.

The Britt antiform (Fig. 3) is a large F_3 fold that affects the inverted limb of a major F_1 nappe. Stratigraphic tops in the metabasalt unit that outlines the Britt fold face towards the fold core, but the rocks dip away from the core; thus the Britt fold is an antiformal syncline. F_3 folding is interpreted to be an arching or doming associated with the emplacement of batholiths.

Structure and Stratigraphy of the Newton Belt

The Newton belt lacks the large folds that are characteristic of the Soudan belt, and is instead typified by an abundance of homoclinal, north-facing fault panels (Fig. 3). As a further contrast, the Newton belt contains local sequences of relatively primitive mafic volcanic rocks, including Mg-tholeiites and komatiites (Green and Schulz, 1977; Schulz, 1980, 1982) that are not represented, or at least are not abundant, in the Soudan belt. Rocks with these more primitive compositions occur principally in the Newton Lake Formation (Morey and others, 1970; Schulz, 1982) and in the Deer Lake sequence (Jirsa, 1990; Fig. 3). The Newton Lake Formation lies outside the Soudan-Bigfork area, and is not considered further in this report.

Other supracrustal rock types within the Newton belt are: (1) monotonously uniform, pillowed tholeiite (comparable lithologically to the Upper member of the Ely Greenstone); (2) graywacke, shale, breccia, and tuff-breccia of principally dacitic provenance (comparable lithologically to the Lake Vermilion Formation); (3) mixed sequences of interbedded mafic and felsic volcaniclastic rocks that commonly contain thin units of laminated iron-formation (comparable lithologically to the Soudan Iron-formation Member of the Ely Greenstone); and (4) vesicular, irregularly pillowed basalt with "shallow water" attributes (comparable lithologically to the Lower member of the Ely Greenstone). Recent mappers in this heavily faulted and rather poorly exposed terrane have not correlated the rock units of the Newton belt with named stratigraphic units in the Soudan belt because neither age equivalence nor lateral continuity can be proved (Jirsa and Boerboom, 1990; Jirsa, 1990). Instead, an informal system of sequence names has been applied to the Newton-belt units (Table 2) that is intended for strictly local usage.

The structural contrasts between the Soudan and Newton belts are most easily explained if their differing structural styles were established early, prior to D_2. The rock units in the Newton belt may have responded to D_1 accretionary compression by forming stacks of thrust-nappes rather than fold nappes. This response may have been favored by a stratigraphic sequence that was composed chiefly of mechanically strong, thick volcanic units interleaved with thin units of relatively incompetent sedimentary rock. The Soudan belt may have been a favored locus for fold-nappe development for just the opposite reason; the stratigraphic succession there was dominated by thick units of incompetent sedimentary rock (Lake Vermilion Formation) and contained only thin units of competent and massive volcanic rock.

Once thickened by D_1 imbricate thrusting, the rocks destined to become the Newton belt were even more resistant to buckling, and tended to subdivide on strike-slip fault systems that were oriented in the regional plane of maximum shear during D_2 transpression. The response in D_2 was dominated by layer-parallel flattening and shear rather than folding. Whatever the true structural dynamics may have been within the Newton belt, the net result of (1) D_1 thrust imbrication (speculative at this point), (2) D_2 strike-slip and dip-slip faulting, and (3) further faulting that outlasted D_2 was a complex web of subvertical fault slices. The original stratigraphic sequence has been severely dismembered by this repeated faulting.

Sedimentary Environments in the Abitibi Subprovince: Possible Minnesota Analogs

Ojakangas (1985) has pointed out that the Vermilion district greenstone belt contains a greater proportion of sedimentary rock than most other greenstone belts in the Superior Province. However, many individual supracrustal belts within the Abitibi subprovince in Canada also contain large amounts of sedimentary rock. This raises the question as to whether the Soudan and Newton belts of Minnesota and the greenstone belts of the Abitibi subprovince have more in common than a broadly similar position near the south margin of the Superior Province.

Four sedimentary cycles, designated 1-4 from oldest to youngest, are now recognized within sedimentary and volcanic rocks of the Abitibi subprovince in Quebec (Mueller and Donaldson, 1992; Mueller and others, 1996). Two of these (cycles 1 and 3) are dominantly accumulations of deep-water turbiditic wackes and two (cycles 2

and 4) are molasse-like accumulations of shallow-marine and fluvial facies. For the most part, the turbiditic sedimentary rocks of cycle 1 (2720-2730 Ma) occur in linear basins in the monocyclic volcanic segment of the northern volcanic zone of the Abitibi (Chown and others, 1992). They are located on the northern margins of submarine, mafic to felsic volcanic piles that are interpreted to have been individual volcanic centers or a distributed island arc. Thin, laterally continuous units of laminated iron-formation are commonly interbedded with the turbiditic rocks in these basins; the iron-formation appears to take the place of benthic mudstone in some graded couplets, suggesting that (1) sedimentation took place in deep water and (2) chemical precipitation of iron-rich minerals was a background depositional process. Turbiditic rocks of sedimentary cycle 3 (2700-2687 Ma) occur intermittently in collisional flysch-type basins along the fault-delineated tectonic boundary between the northern and southern volcanic zones of the Abitibi subprovince (Mueller and others, 1996). The fill in the cycle 3 basins is similar to that in cycle 1 basins in terms of lithology and facies architecture (Mueller and Donaldson, 1992), except that less iron-formation is interstratified with the volcaniclastic rocks of cycle 3.

There are intriguing compositional, sedimentological, and tectonic similarities between the felsic metasedimentary sequences of the Soudan-Bigfork area of Minnesota and the turbiditic rocks of cycles 1 and 3 of the western Abitibi subprovince (Mueller and Donaldson, 1992). Among the parallels between the Lake Vermilion Formation and the rocks of Abitibi cycle 1 are (1) the similarity of the geochemically inferred heterolithic source terranes (La Fleche and Camire, 1996), and (2) the position of the sedimentary accumulations on the flanks of submarine volcanic piles. On the other hand, the great thickness of the Lake Vermilion Formation (at least 1 km; Ojakangas, 1985) and its spatial association with major faults (most notably the Mud Creek shear zone) suggest a possible parallel with Abitibi cycle 3 sedimentary rocks.

Further efforts to document the details of this regional analog, particularly the acquisition of radiometric dates and the development of a timescale for deposition and deformation in the Soudan-Bigfork area, could yield information of considerable economic significance. For example, it would be useful to establish the temporal and spatial relationships between sedimentary rocks of the Lake Vermilion Formation and movement on the Mud Creek shear zone (Hudleston and others, 1988). It would then be useful to compare these data and interpretations with those for cycle-3 sedimentation and the movement history on the heavily mineralized Destor-Porcupine-Manneville fault zone in the western Abitibi subprovince. If the analogy should hold, it should spur interest in exploring for epithermal vein systems associated with fault disruption of thick volcaniclastic prisms close to the Mud Creek shear zone and farther west along the Leech Lake structural disconformity in north-central Minnesota.

Intrusive Rocks Within the Supracrustal Successions

The Soudan and Newton belts contain four broadly distinctive types of interior intrusions: (1) hypabyssal, subvolcanic sills and dikes of diabase and gabbro; (2) hypabyssal, subvolcanic sills and dikes of quartz-plagioclase porphyry; (3) a suite of lamprophyre sills and dikes emplaced over a span of time that brackets D_2 deformation; and (4) minor- to meso-scale plugs and stocks of granitic rock that also bracket D_2 and are divisible into quartz-bearing (granite-granodiorite) and quartz-poor (pyroxenite-syenite-diorite) suites (Jirsa and others, 1991; Southwick, 1993). The subvolcanic intrusions of groups (1) and (2) are more or less coeval with enclosing or superjacent volcanic and fragmental rocks of equivalent composition.

Larger granitic masses of various types intrude the Soudan and Newton belts near or at their margins; these granitic rocks are related to the flanking Giants Range batholith and Vermilion Granitic Complex and thus are mainly external to the greenstone belt proper. Neither the flanking granitic rocks nor the internal granitic plugs and stocks [group (4) above] are considered further here.

Hypabyssal, Subvolcanic Intrusions: Diabase and Gabbro

Sills of relatively massive and weakly deformed metadiabase occur in small quantity throughout the mafic volcanic sequences of both the Soudan and Newton belts. For the most part these are not modally layered or otherwise differentiated. Where metamorphosed under conditions of the mid- to upper-greenschist facies, they consist dominantly of medium-grained plagioclase and actinolitic green amphibole that pseudomorphs originally ophitic clinopyroxene. The metadiabase also includes smaller amounts of epidote, clinozoisite, chlorite, and leucoxene. Although sills of this type are widely distributed, they appear to be somewhat more abundant in the Lower member of the Ely Greenstone of the Soudan belt than elsewhere.

Complexes of strongly differentiated mafic sills that contain a significant proportion of pyroxenitic and peridotitic rocks in their basal portions are seemingly confined to the Newton belt. The Deer Lake Complex of the Deer Lake sequence (Fig. 3) is an example; it was first mapped and described by Berkley (1972) and Berkley and Himmelberg (1978), and later remapped in greater detail by Jirsa (1990). The presence of magmatic sulfides in the basal ultramafic zones of sills in the Deer Lake Complex (Ripley, 1978) has prompted several episodes of ex-

ploration drilling, as yet without economic results. Comparable differentiated sills occur within the Newton Lake Formation near Ely (Schulz, 1980), some distance east of the present study area.

Hypabyssal, Subvolcanic Intrusions:
Quartz-plagioclase Porphyry

Quartz-plagioclase porphyry most commonly forms quasi-conformable sheet-like bodies that range in thickness from 1 to 100 meters and from a few tens of meters to several kilometers in strike length. Although most large porphyry intrusions are effectively parallel to the plane of primary layering in the enclosing supracrustal rocks, their contacts are locally discordant to the primary layering. A few porphyry bodies are plug-like in shape. In the Soudan belt, the porphyry intrusions are most abundant in the uppermost parts of the lower volcanic unit, throughout the iron-formation unit, and in the lower parts of the Lake Vermilion Formation and laterally correlative units. Porphyry is especially abundant in the vicinity of Stuntz Bay, Armstong Bay, and Ely Island in the east end of Lake Vermilion, and eastward from there along the Armstrong River [Fig. 3; see Sims and Southwick (1980, 1985) and Southwick (1993) for detailed locations]. In this area porphyry is closely associated with (1) massively bedded dacite tuff and tuff-breccia; (2) virtually monomict dacite conglomerate (agglomerate of Sims, 1972b); and (3) thick-bedded to rhythmically medium-bedded dacitic wacke, all assigned to the Lake Vermilion Formation. This rock association strongly suggests deposition and subvolcanic intrusion in proximity to a dacitic volcanic center, possibly on the flank of an emergent volcanic island (Ojakangas, 1985; Southwick and others, 1993).

Petrographically, the porphyry is quartz- and plagioclase-phyric. The quartz phenocrysts are monocrystalline, variably resorbed, and weakly undulatory; they range in diameter from 2 to 12 mm and typically compose about 2 to 10 percent of the phenocryst population. The plagioclase phenocrysts are smaller and more abundant than the quartz phenocrysts. They range from 1 to 5 mm in length, are variably sericitized, and are unzoned except for a small fraction of anomalously large individuals that may be xenocrysts. Small mafic phenocrysts constitute 1 or 2 percent of the phenocryst population; most were hornblende that is now pseudomorphed by secondary chlorite, epidote, carbonate, and opaques, and fewer were biotite, now pseudomorphed by chlorite and sericite. The groundmass of the porphyry is a recrystallized aggregate of quartz and plagioclase together with lesser amounts of secondary sericite, clinozoisite, carbonate, chlorite, and leucoxene. The groundmass typically carries a variably developed S_2 fabric.

Porphyry in which quartz makes up about 5-10 percent of the total phenocrysts is seemingly distinct from porphyry in which quartz makes up less than 2 percent of the total phenocrysts. Although this distinction was not applied in the field, it serves as the basis for dividing the porphyries into quartz-prominent and plagioclase-prominent subtypes for the purpose of geochemical interpretation.

Lamprophyre Dikes and Sills

Hornblende- and pyroxene-rich mafic rocks classed as lamprophyres are present throughout the Soudan-Bigfork area. Included among them are (1) dike-like to podiform masses that carry moderately to strongly developed tectonic fabric ascribable to D_2; (2) less pervasively deformed dikes and irregular plug-like masses spatially associated with granitoid intrusions of the pyroxenite-syenite-diorite suite; and (3) narrow dikes that generally lack deformational fabrics and therefore are interpreted as post-D_2 intrusions. The dikes of type (3) tend to be porphyritic, with phenocrysts of hornblende and pyroxene in varying proportions. Many of the irregular or plug-like bodies of type (2) contain abundant aegerine or related Na-pyroxene, either as the sole mafic phase or together with an amphibole. Strongly deformed rocks of groups (1) and (2) tend to be of uniform grain size and dominated modally by hornblende. Small, polymineralic felsic clots or segregations ("ocelli") occur locally in lamprophyres of all three categories; panidiomorphic textures are variably developed and preserved in all but the most severely tectonized and metamorphosed lamprophyres of types (1) and (2).

Despite many efforts over many decades, there still is no classification scheme for the lamprophyric rocks that is entirely satisfactory. The clan as a whole is characterized by a high degree of modal and geochemical variability. Therefore, lamprophyre classifications based on modal composition tend to be burdened by an overabundance of rock names, whereas chemical classifications, though "leaner" and somewhat more logical, are impossible to apply in the field. The treatises by Rock (1987) and Mitchell and Bergman (1991) exhaustively discuss the classification problem and propose useful suggestions. In our view, however, the treatment of lamprophyre classification by Middlemost (1985) is the most cogent yet published. Midddlemost follows the lead of Metais and Chayes (1963), Wimmenauer (1973), and Streckeisen (1980) in erecting a practical threefold subdivision of the lamprophyre clan that is based on modal mineralogy. The ordinary lamprophyres contain feldspars and one or more of the ordinary mafic phases—biotite, amphibole, pyroxene, or olivine. The alkaline lamprophyres are characterized by the presence of feldspathoids as additional primary phases, and the melilitic lamprophyres by the pres-

ence of melilite. The mafic minerals in the latter two categories are typically enriched in titanium and the alkalis relative to their compositions in the ordinary lamprophyres. Accordingly, the lamprophyres within the Soudan-Bigfork area are all ordinary lamprophyres; they will not be subdivided further in this report.

A striking feature of the regional geologic map is the series of aligned, lenticular lamprophyre bodies that extends eastward along and south of latitude 45°75'N., between Idington and Wahlsten (Fig. 3; also Southwick, 1993). Each lens is highly tectonized and metasomatized near its contacts, but is essentially massive in its interior. These lamprophyre bodies appear to have been emplaced along an early fault zone that was reactivated subsequent to their emplacement. Later, the early fault and its contained lamprophyres were subdivided and rotated into several en echelon blocks by northeast-trending left-lateral faults that developed late in the tectonic evolution of the area. The internal parts of these deformed lamprophyre bodies contain syenitic and pyroxenitic phases similar to the rocks found in much less deformed plugs south and west of the Lost Lake swamp (Jirsa and others, 1991; Southwick, 1993, map unit gp). This suggests the possibility of a petrogenetic association between some of the deformed lamprophyres in the Vermilion district (particularly those near Wahlsten) and the plutons of the pyroxenite-syenite-diorite suite. If this is correct, lamprophyres categorized as types (1) or (2) on the basis of tectonic fabric development may overlap in origin. Proof of this connection will ultimately depend on geochronologic evidence.

GEOCHEMISTRY

Organization of the Geochemical Data

The geochemical data discussed in this section are presented in 24 tables in the Appendix, and as electronic datafiles available from the Minnesota Geological Survey. Details on the procedures for obtaining the electronic datafiles are outlined in the introduction to the Appendix tables. To facilitate discussion and the utility of the dataset, and to link the data more firmly to their geologic setting, the tables are organized by rock type, belt, and mappable unit. The logic of this organization is best understood with reference to the geologic map of Figure 3, or the more detailed compilation of Southwick (1993).

Tables Ap(1) through Ap(13) contain analyses of mafic volcanic rocks. Of these, Tables Ap(1) through Ap(8) contain analyses from mappable stratigraphic sequences within the Soudan belt, and Tables Ap(9) through Ap(13) contain analyses from units within the Newton belt. Tables Ap(1) through Ap(3) contain analyses of the Lower member of the Ely Greenstone, the Bear Lake sequence, and mafic metavolcanic rocks that are part of the Soudan Iron-formation Member of the Ely Greenstone. These collectively represent the lower volcanic and iron-formation units of the Soudan belt. Tables Ap(4) and Ap(5) contain analyses of the Upper member of the Ely Greenstone and the Sherry Lake sequence, which together represent the upper volcanic unit of the Soudan belt. Tables Ap(6) through Ap(8) contain data from basalt units that are interstratified with felsic wacke and allied sedimentary rocks of the Lake Vermilion Formation. Analyses of flows near the base of the Lake Vermilion Formation are in Table Ap(6); analyses of isolated mafic flows and flow packets stratigraphically higher in the sedimentary sequence are in Table Ap(7), and analyses of the basalt flows that define the Britt antiform (Fig. 3) are in Table Ap(8).

The basaltic rocks of the Newton belt [Tables Ap(9) through Ap(13)] are organized in terms of the informal sequence nomenclature developed by Jirsa (1990). Each sequence occupies a fault-bounded structural panel of uncertain stratigraphic affinity to adjacent panels. Analyses of rocks from the Thistledew Lake, Joy Lake, Wilson Lake, Cook, and Deer Lake sequences are in Tables Ap(9) through Ap(13), respectively. Tables Ap(14) through Ap(20) contain analyses of sedimentary and volcaniclastic rocks that are predominantly of felsic composition. Tables Ap(14) through Ap(18) contain analyses from sedimentary units in the Soudan belt, Tables Ap(19) and Ap(20) contain data from sedimentary units in the Newton belt.

The analyses of sedimentary rocks of the Soudan belt are grouped with respect to both stratigraphic and structural position. Table Ap(14) contains analyses of rocks from the relatively thin sedimentary units within the piles of basalt that constitute the lower and upper volcanic units. Tables Ap(15) through Ap(18) contain analyses of rocks in the Lake Vermilion Formation. Table Ap(15) contains analyses of rocks in the belt of massive felsic wackes and reworked felsic tuff of the Lake Vermilion Formation that extends along and eastward from the southeastern limb of the Britt antiform (Jirsa and others, 1991; Southwick, 1993). Table Ap(16) contains analyses of sedimentary rocks from the belt of felsic tuff and reworked tuffaceous wacke of the Lake Vermilion Formation that passes through and extends westward from Pike Bay of Lake Vermilion (unit lft of Southwick (1993)). For convenience, this belt of rock is referred to henceforth as the central tuff. Table Ap(17) contains analyses of turbiditic graywacke and pelitic rocks of the Lake Vermilion Formation from the belt of structurally westward- and downward-facing strata that lie south of the central tuff and north of the Britt antiform [see geologic maps of Jirsa and others (1991) and Southwick (1993) for locational details]. Analyses of similar rocks from the graywacke

belt of the Lake Vermilion Formation, north of the central tuff and south of the Mud Creek shear zone are in Table Ap(18).

The sedimentary rocks of the Newton belt are grouped into (1) those located between the Mud Creek shear zone and the Bear River fault [Fig. 3, Table Ap(19)] and (2) those located northwest of the Bear River fault [Fig. 3, Table Ap(20)]. Table Ap(21) contains 11 analyses of iron-formation and allied cherty rocks from throughout the region, irrespective of belt or stratigraphic position. Tables Ap(22), Ap(23), and Ap(24) contain data for hypabyssal mafic intrusions, dacite porphyry intrusions, and lamprophyres respectively. The data for these intrusive rocks are tabulated without regard to belt or stratigraphic position of the enclosing supracrustal rocks.

Geochemistry of the Mafic Volcanic Rocks

Basaltic Sequences in the Soudan Belt

Schulz (1980, 1982) has clearly demonstrated a stratigraphic and temporal change in mafic lava composition between the Lower and Upper members of the Ely Greenstone in the central and eastern parts of the Vermilion district. The Lower member is predominantly calc-alkalic basalt and basaltic andesite, whereas the Upper member is predominantly tholeiitic basalt. The rather sharp transition is at the top of the Soudan Iron-formation Member of the Ely Greenstone, which is locally an unconformity (Sims and Southwick, 1980; Southwick, 1993).

Schulz's basic conclusions are borne out and extended by the data we have assembled in this study. The basaltic rocks of the Lower member of the Ely Greenstone, the Bear Lake sequence, and the Soudan Iron-formation Member of the Ely Greenstone span the range from tholeiitic basalt through basaltic andesite to low-K andesite, and constitute a group that is predominantly calc-alkalic (Figs. 4 and 5). The Zr-Ti-Y discrimination diagram of Pearce and Cann (1973), as modified by Pearce (1996), divides the group among calc-alkalic arc basalt (predominant), volcanic arc tholeiite or ocean-floor basalt, and "within-plate" basalt (least abundant; Fig. 5). Trace-element and rare earth element (REE) abundances normalized against primitive mantle values (Fig. 6) yield a plot with a line that slopes moderately; the rocks are relatively enriched in the large-ion lithophile elements (LILE).

In contrast, basaltic rocks of the Upper member of the Ely Greenstone in the structurally overturned south limb of the Tower-Soudan anticline, together with basaltic rocks of the Sherry Lake sequence in the Sherry Lake anticline are much less diverse and are predominantly tholeiitic (Figs. 7 and 8). All analyses plot in the volcanic arc tholeiite or ocean-floor basalt field on the modified Pearce-Cann diagram (Fig. 8). The primitive-mantle spider diagram for these rocks is nearly flat (Fig. 9). Furthermore, the thin units of basalt that are interstratified with dacitic sedimentary rocks in the Lake Vermilion Formation and the thicker basalt sequence that outlines the Britt antiform are compositionally indistinguishable from the tholeiites of the Upper member of the Ely Greenstone and Sherry Lake sequences (Figs. 10, 11, and 12). The strongly deformed basalt unit that defines the Britt antiform (informally termed the Britt metabasalt) stratigraphically overlies a substantial thickness of Lake Vermilion Formation volcaniclastic and sedimentary rock on the structurally overturned south limb of a major F_1 fold nappe; it is therefore in the upper part of the stratigraphic succession of the Soudan belt.

The essential uniformity of composition among tholeiitic rocks of the Upper member of the Ely Greenstone, the Sherry Lake sequence, the minor mafic units within the Lake Vermilion Formation, and the Britt metabasalt is further evidence that tholeiitic basaltic volcanism overlapped in time and space with calc-alkalic dacitic volcanism and the resedimentation of dacitic detritus during formation of Soudan belt rocks. This conclusion was reached originally from stratigraphic reconstructions (Morey and others, 1970; Sims, 1972b; Ojakangas, 1972a, 1972b).

Basaltic Sequences in the Newton Belt

The structural dismemberment of the Newton belt and the generally poor exposure of rocks within it militate against the use of stratigraphy as the framework for discussing volcanic geochemistry. We do not know the stratigraphic stacking order well enough to use it to identify or interpret temporal changes in basalt composition. Instead, the local sequence terminology of Jirsa (1990; see Table 2) serves as the basis for geochemical characterization.

Calc-alkalic compositions are rare among the mafic rocks of the Newton belt, if not lacking altogether. The basaltic rocks in the Thistledew Lake, Joy Lake, Wilson Lake, and Cook sequences (Figs. 13, 14, and 15) are almost entirely tholeiitic in composition and rather similar in most respects to the Upper member of the Ely Greenstone and its geochemical equivalents in the Soudan belt. Most analyses plot in the volcanic arc tholeiite or ocean-floor basalt field on the modified Pearce-Cann diagram (Fig. 14), but several plot in the within-plate basalt field or outside of it on the low-Y side. The low-Y analyses are not obviously anomalous in other respects; the paucity of Y in these rocks is not readily explained.

The mafic volcanic rocks of the Deer Lake sequence are somewhat more primitive (Figs. 16, 17, and 18); they are closely associated with mafic sills of the Deer Lake Complex, some of which contain substantial volumes of peridotitic differentiates and scattered occurrences of mag-

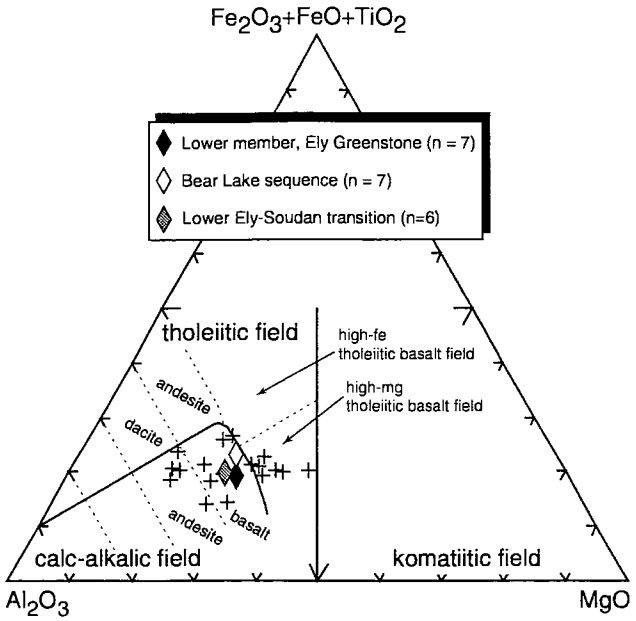

Figure 4. AFTiM diagram (after Jensen, 1976) for basaltic rocks of the lower volcanic unit, Soudan belt. The data are in Appendix Tables Ap(1), Ap(2), and Ap(3). Group means indicated by diamond symbols.

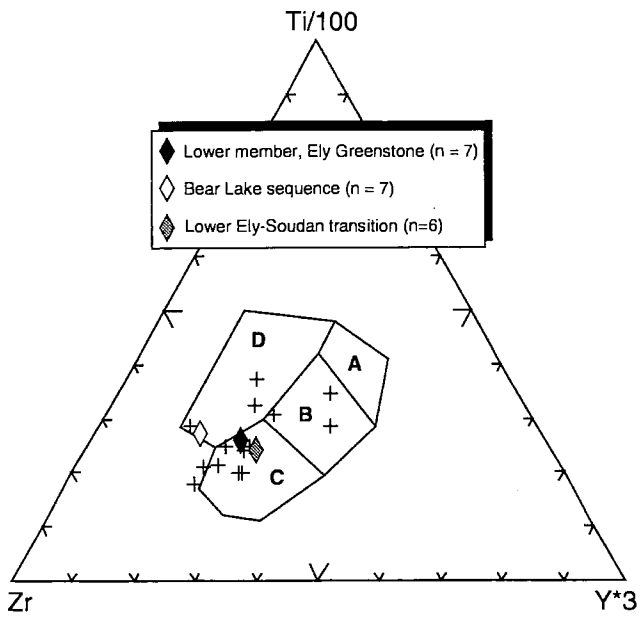

Figure 5. Immobile element plot (after Pearce and Cann, 1973, and Pearce, 1996) for basaltic rocks of the lower volcanic unit, Soudan belt. The data are in Appendix Tables Ap(1), Ap(2), and Ap(3). Field designations: A = low-K tholeiite of volcanic arcs; B = ocean-floor basalt and tholeiitic basalt of volcanic arcs; C = calc-alkali basalt of volcanic arcs; D = within-plate basalt. Group means indicated by diamond symbols.

Figure 6. Spider diagram of mean trace and rare earth element abundance for the basaltic rocks in the lower volcanic unit, Soudan belt. Means are from Appendix Tables Ap(1), Ap(2) and Ap(3). Data normalized against primitive mantle composition of Sun and McDonough (1989).

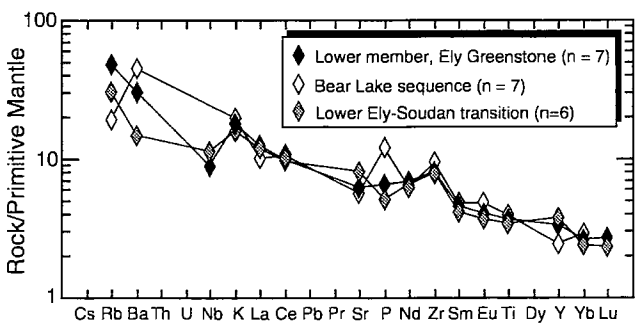

matic Cu-Ni sulfides (Berkley and Himmelberg, 1978; Ripley, 1978). Overall, the mafic flows and associated sills strongly resemble flows and sills in the Newton Lake Formation northeast of Ely, some of which have been interpreted as komatiitic (Green and Schulz, 1977; Schulz, 1982). The chilled-margin compositions of sills in the Deer Lake Complex are discussed below in greater detail.

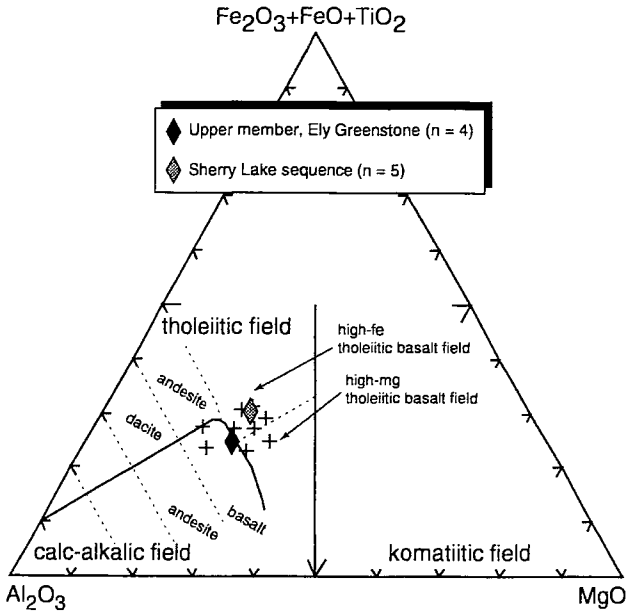

Figure 7. AFTiM diagram (after Jensen, 1976) for basaltic rocks of the upper volcanic unit, Soudan belt. The data are in Appendix Tables Ap(4) and Ap(5). Group means indicated by diamond symbols.

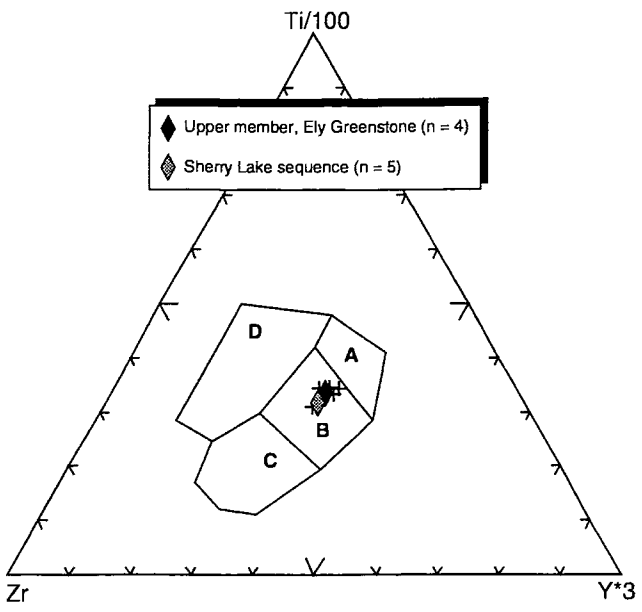

Figure 8. Immobile element plot (after Pearce and Cann, 1973, and Pearce, 1996) for basaltic rocks of the upper volcanic unit, Soudan belt. The data are in Appendix Tables Ap(4) and Ap(5). Field designations: A = low-K tholeiite of volcanic arcs; B = ocean-floor basalt and tholeiitic basalt of volcanic arcs; C = calc-alkali basalt of volcanic arcs; D = within-plate basalt. Group means indicated by diamond symbols.

Figure 9. Spider diagram of mean trace and rare earth element abundance for basaltic rocks in the two sequences that constitute the upper volcanic unit, Soudan belt. Means are from Appendix Tables Ap(4) and Ap(5). Data normalized against primitive mantle composition of Sun and McDonough (1989).

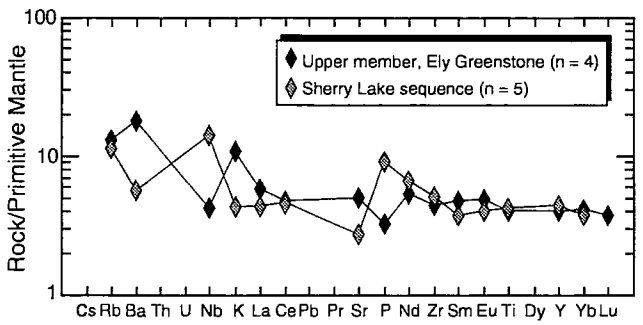

Discussion of the Mafic Volcanic Rocks

Tectonic inferences—It is widely recognized (e.g. Thurston and Chivers, 1990; Williams and others, 1991) that most Archean greenstone belts are composed of one or more depositional cycles of volcanic rocks. Typically, each cycle progresses compositionally from predominantly komatiitic or tholeiitic basalt at the base through calc-alkalic basalt toward the top. In the most fully evolved cycles the calc-alkalic basalt is surmounted by one or more sequences of felsic volcanic rocks that typically grade laterally and vertically into aprons of volcaniclastic sedimentary rocks of predominantly felsic provenance. Laminated iron-formation may appear almost anywhere in the stratigraphy of a cycle, but most commonly it is present in greatest amount in the heterolithic upper parts.

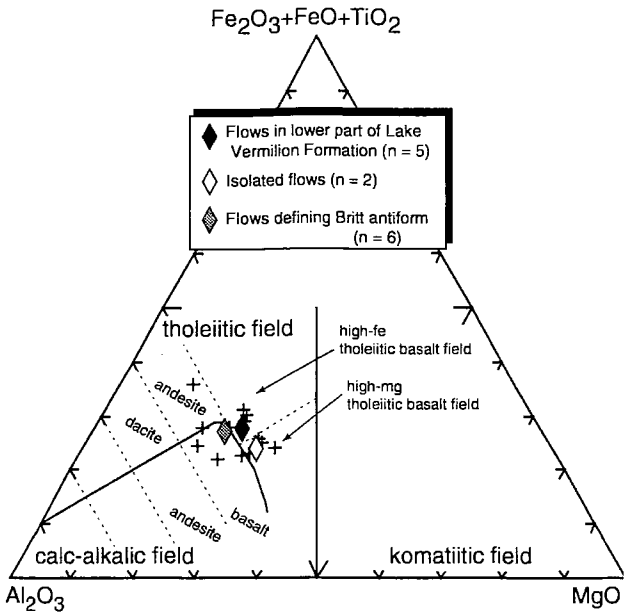

Figure 10. AFTiM diagram (after Jensen, 1976) for basaltic rocks interstratified with sequences of felsic wacke and allied metasedimentary rocks, Soudan belt. Includes flows near the base of the Lake Vermilion Formation, isolated flows higher in the Lake Vermilion section, and flows that define the Britt antiform. The data are in Appendix Tables Ap(6), Ap(7), and Ap(8). Group means indicated by diamond symbols.

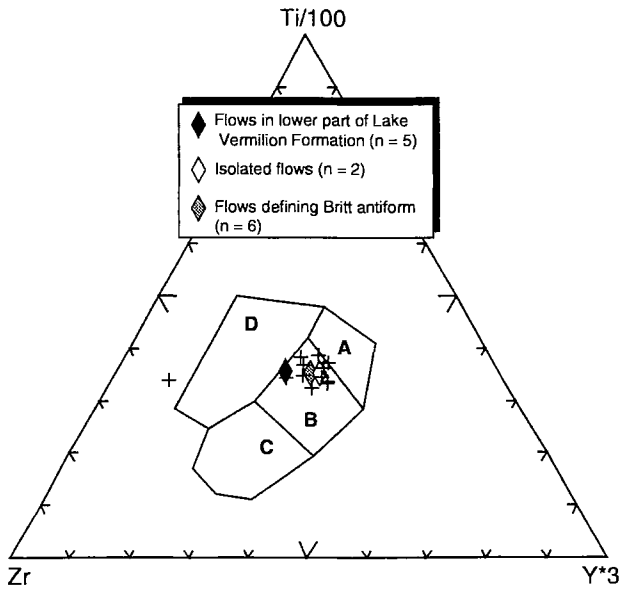

Figure 11. Immobile element plot (after Pearce and Cann, 1973, and Pearce, 1996) for basaltic rocks interstratified with sequences of felsic wacke and allied metasedimentary rocks, Soudan belt. The data are in Appendix Tables Ap(6), Ap(7), and Ap(8). Field designations: A = low-K tholeiite of volcanic arcs; B = ocean-floor basalt and tholeiitic basalt of volcanic arcs; C = calc-alkali basalt of volcanic arcs; D = within-plate basalt. Group means indicated by diamond symbols.

Figure 12. Spider diagram of mean trace and rare earth element abundance for basaltic rocks interstratified with sequences of felsic wacke and allied metasedimentary rocks, Soudan belt. Means from Appendix Tables Ap(6), Ap(7) and Ap(8). Data normalized against primitive mantle composition of Sun and McDonough (1989).

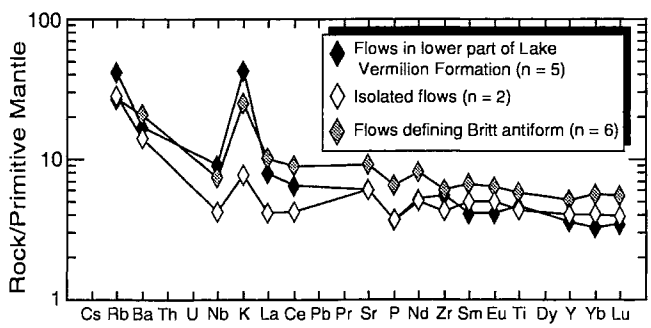

Applying this generalized concept to the Soudan belt, the lower volcanic unit and the overlying iron-formation unit represent roughly the upper half of a typical volcanic cycle. The monolithic, tholeiitic, upper volcanic unit appears to represent the lower or medial portions of a second cycle. Currently accepted reconstructions suggest that the second cycle stratigraphically overlies the first, although precise geochronologic data that would confirm their relative ages are lacking. Because of structural complexities and a general dearth of outcrop, it is impossible to apply the cycle concept to the volcanic rocks of the Newton belt. Fragments of one or several cycles could be present.

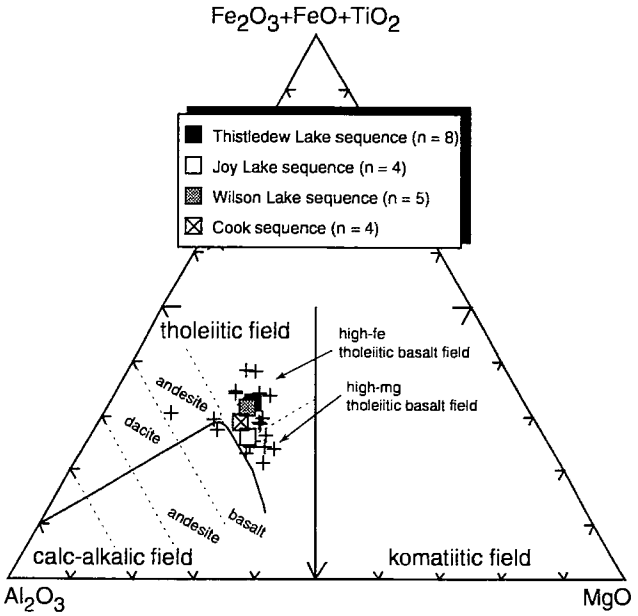

Figure 13. AFTiM diagram (after Jensen, 1976) for basaltic rocks in the Thistledew Lake, Joy Lake, Wilson Lake, and Cook sequences of the Newton belt. The data are in Appendix Tables Ap(9), Ap(10), Ap(11), and Ap(12). Group means indicated by square symbols.

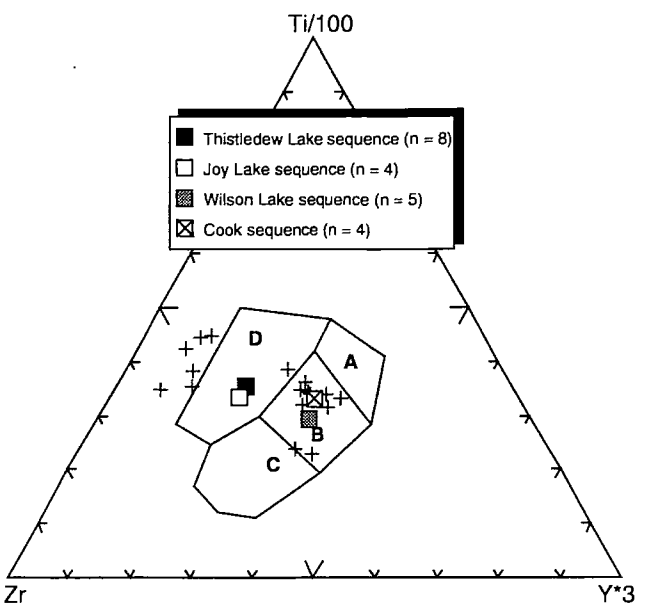

Figure 14. Immobile element plot (after Pearce and Cann, 1973, and Pearce, 1996) for basaltic rocks in the Thistledew Lake, Joy Lake, Wilson Lake, and Cook sequences of the Newton belt. The data are in Appendix Tables Ap(9), Ap(10), Ap(11), and Ap(12). Field designations: A = low-K tholeiite of volcanic arcs; B = ocean-floor basalt and tholeiitic basalt of volcanic arcs; C = calc-alkali basalt of volcanic arcs; D = within-plate basalt. Group means indicated by square symbols.

Figure 15. Spider diagram of mean trace and rare earth element abundance for basaltic rocks in the Thistledew Lake, Joy Lake, Wilson Lake, and Cook sequences of the Newton belt. Means are from Appendix Tables Ap(9), Ap(10), Ap(11) and Ap(12). Data normalized against primitive mantle composition of Sun and McDonough (1989).

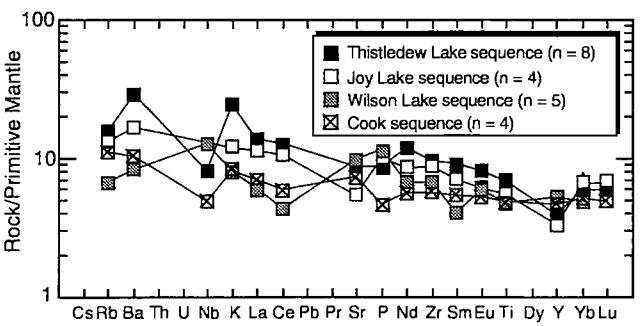

As previously mentioned, the Zr-Ti-Y discrimination diagram suggests an arc-related tectonic setting for the genesis of basaltic rocks in the upper part of the lower volcanic cycle in the Soudan belt (Fig. 5). The uniformly tholeiitic rocks of the upper cycle are ascribed an "ocean floor" origin on the same basis (Figs. 8 and 11). Deductions regarding the tectonic setting that are based on geochemical data support inferences from the physical features and stratigraphic arrangement of the rocks for an island-arc origin of the upper parts of the first volcanic cycle and a ocean-floor origin of the lower parts of the second. The data do not distinguish clearly between ocean floor tholeiitic basalts (Late Archean MORB) and those basalts that formed in back-arc or intra-arc spreading en-

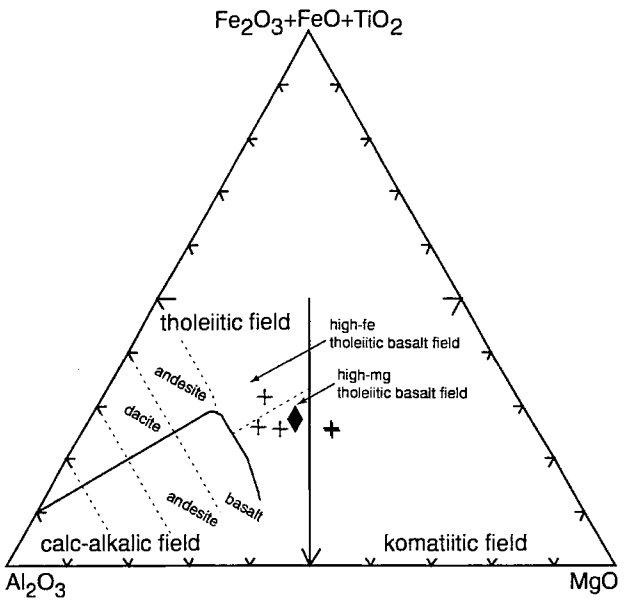

Figure 16. AFTiM diagram (after Jensen, 1976) for basaltic rocks in the Deer Lake sequence of the Newton belt. The data are in Appendix Table Ap(13). Mean indicated by solid diamond.

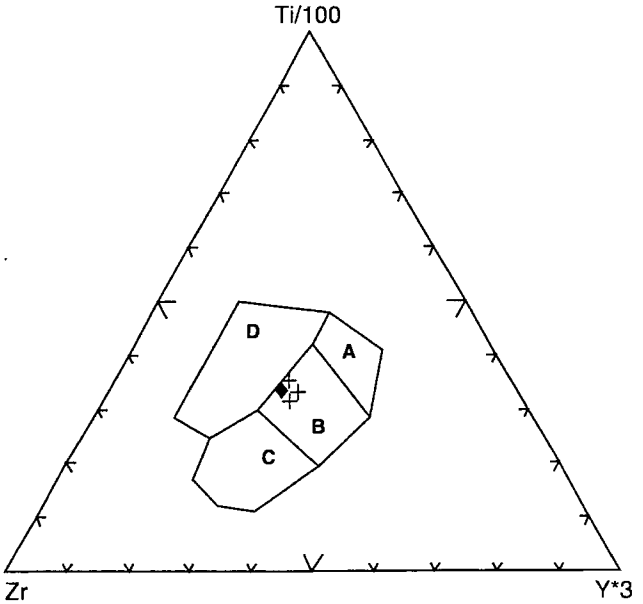

Figure 17. Immobile element plot (after Pearce and Cann, 1973, and Pearce, 1996) for basaltic rocks in the Deer Lake sequence of the Newton belt. The data are in Appendix Table Ap(13). Field designations: A = low-K tholeiite of volcanic arcs; B = ocean-floor basalt and tholeiitic basalt of volcanic arcs; C = calc-alkali basalt of volcanic arcs; D = within-plate basalt. Mean indicated by solid diamond.

Figure 18. Spider diagram of mean trace and rare earth element abundance for basaltic volcanic rocks in the Deer Lake sequence of the Newton belt. Data normalized against the primitive mantle composition of Sun and McDonough (1989). The pronounced positive Nb anomaly is influenced by unusually high Nb values reported for samples 3605 and 3608 [Appendix Table Ap(13)]. Those data were obtained from industry exploration files by Englebert and Hauck (1991) and cannot be independently verified. If they are discarded from the mean, the normalized mean Nb value drops to the more normal position indicated by the star.

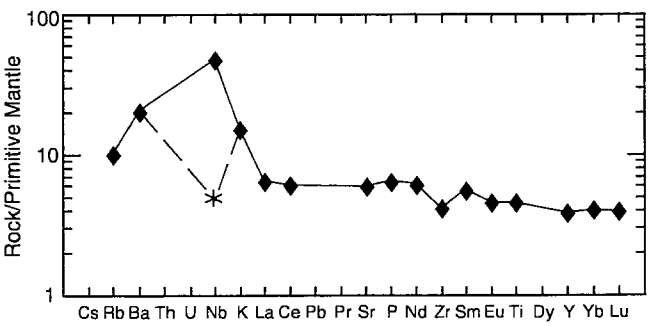

vironments, nor do they distinguish those basalts from tholeiitic rocks that formed in the early stages of development of an oceanic arc. Thus, the second volcanic cycle in the Soudan belt could represent one of several possible Late Archean tectonic settings associated with oceanic convergent margins. The same is true for the tholeiitic rocks in the dismembered fault panels of the Newton belt. However, because the tholeiitic rocks in both belts are intimately associated with significant thicknesses of dacitic volcanic rocks and clastic sedimentary rocks derived from them, we favor an arc-related origin (back-arc or intra-arc) for the tholeiitic sequences of the Soudan-Bigfork area.

Implications for Gold Exploration—Epithermal to mesothermal gold deposits of several types are associated with Cenozoic island-arc volcanotectonic settings in the Circum-Pacific (e.g. Hedenquist, 1987; Sillitoe, 1989). Furthermore, many gold deposits similar in key respects to those of the Circum-Pacific rim occur in Archean greenstone belts in rocks reasonably inferred to be the remnants of arcs or other elements of convergent-margin tectonic regimes (e.g. Kerrich, 1989; Kerrich and Wyman, 1990; Robert, 1996). Although the ultimate source of gold in volcanic-hosted gold deposits has long been a controversial question, one school of thought interprets the gold to have been carried into the upper crust by the magmatic systems from which the volcanic rocks themselves were derived (Sawkins, 1990). Supporting this view is the fact that many volcanic-hosted gold deposits (but not all) occur within volcanic sequences that are intrinsically somewhat enriched in gold. These rocks are thought to have acquired their elevated gold background through processes associated with magma genesis in the upper mantle.

Virtually all economic gold deposits in Archean greenstone belts, and their geologically younger lithotectonic analogs, contain clear evidence of structurally controlled hydrothermal processes having transported and concentrated the metal (Robert, 1996, and references therein). Consequently, much exploration effort is devoted quite properly toward identifying and locating the structural sites where ore-forming hydrothermal systems have operated, or are likely to have operated, during the geological evolution of a regional target terrane. The syngenetic, regional preconcentration of gold seems significant only in the sense that the more gold there is in the neighborhood, the more likely it should be for hydrothermal processes to have generated an economic deposit. An obvious exploration strategy derived from this line of reasoning is to locate and focus upon sequences of volcanic rocks that are somewhat above minimum background tenor in gold.

Analytical data for background gold in unsheared, unaltered mafic volcanic rocks of the Soudan-Bigfork area leave much to be desired, both in the number of available analyses and their analytical quality. Generalizing from the limited gold data presented in the Appendix tables, the mafic sequences of the Soudan belt are not auriferous in any sense (gold tenor is on the order of 1-2 ppb) and appear to be lower in gold than the world-average Archean greenstone (Boyle, 1979; Ho and others, 1990). The Wilson Lake, Cook, and Deer Lake sequences in the Newton belt also carry very low gold values, in the 1-2 ppb range. However, gold values some three to ten times higher than these are reported from rocks of the Thistledew Lake and Joy Lake sequences [Tables Ap(9) and Ap(10)]. These data suggest that given the discouraging gold-exploration history in the Vermilion district *sensu stricto*, together with the apparent low background values for gold in Soudan-belt mafic volcanic rocks, it is time to shift exploration attention. The less well exposed areas of the Newton belt, where there are indications of moderately higher background gold in the basalts of the Thistledew Lake and Joy Lake sequences, warrant further exploration.

Geochemistry of Volcaniclastic and Sedimentary Rocks of Dacitic Provenance, Soudan and Newton Belts

The clastic rocks in the Soudan-Bigfork area range in chemical composition from those essentially identical to volcanic rocks (e.g. rocks classed as reworked tuff and massive dacitic wacke) to those for which the chemical composition deviates substantially from igneous characteristics. Typically, the rocks with compositions that deviate most substantially from igneous compositions are those that were originally fine grained (shale, mudstone, fine ash) or those of coarser texture that originally contained much fine-grained matrix (breccias and conglomerates). The obvious inference is that the finely divided material underwent a greater degree of physical and chemical differentiation in the sedimentary cycle than the coarser material did. Thus, the geochemical attributes of the sedimentary rocks record the combined influences of source-area variability, weathering history, transportation dynamics, and diagenesis. Further geochemical complexities may have arisen during regional deformation and metamorphism.

Geologic mapping shows that slightly-reworked dacitic tuff and closely affiliated dacite-dominated lithic wacke are significantly more abundant at the bedrock surface in the Soudan belt than in the Newton belt. Moreover, these relatively monolithic tuffaceous rocks are distinguishable from the graywacke component of associated graywacke-mudstone couplets (turbidites) on several geochemical criteria, the most direct of which are (1) lower TiO_2 content for the tuffs over a considerable range of SiO_2 values, as shown on a standard Harker diagram (Fig. 19), and (2) higher Na_2O content for the tuffs relative to total FeO and MgO, as shown on a modified AFM diagram (Fig. 20).

Although the tabulated geochemical data do not reveal large compositional differences among the turbiditic graywackes that now are in the different structural panels of the Soudan-Bigfork area, the Newton belt rocks tend as a group to be somewhat poorer in SiO_2 and higher in mafic components than the rocks of the Soudan belt. Broadly speaking, the graywackes of the Newton belt are compositionally more andesitic than their Soudan-belt counterparts. Whether this reflects provenance differences or the effects of chemical differentiation associated with transport and weathering is difficult to determine.

The bulk composition of turbiditic graywacke in the Soudan-Bigfork area resembles that of the more felsic Neogene and Oligocene turbidites in the intra-oceanic Izu-Bonin arc south of Japan (Table 3; Gill and others, 1994). In the Izu-Bonin arc, the composition of turbiditic sediment deposited in intra-arc and forearc basins is linked rather closely to the eruptive evolution of the volcanic arc; the sediments reflect the volcanic trends from basaltic to dacitic activity with the passage of time. Archean volcanism in the Soudan-Bigfork area apparently did not involve the production of much pyroclastic material or its related epiclastic sediments prior to the dacitic stage; andesitic and basaltic tuff and wacke are sparse in the preserved rock record. In contrast, arc-derived basaltic and andesitic wackes are relatively abundant in the Izu-Bonin arc.

In comparison to Izu-Bonin graywacke compositions with similar SiO_2 content (Gill and others, 1994), the Soudan-Bigfork graywackes are relatively enriched in Na, K, Rb, Sr, Ba, and Zr, and depleted in Ca, Ti, Mn, and Y (Fig. 21). The enrichment of the Archean rocks in large-ion lithophile elements (LILE) relative to levels in the indisputably intra-oceanic Izu-Bonin arc suggests that Archean depocenters may have received some contribution from cratonic, continental sources. The average composition of Soudan-belt graywacke is best but imperfectly approximated by a 41:59 mixture of Izu-Bonin dacitic and high-Si andesitic wackes (Table 3; Fig. 21A). The best fit to the average Newton-belt graywacke composition is produced from a 29:71 mixture of Izu-Bonin dacitic and andesitic wackes (Table 3; Fig. 21B). This, together with petrographic evidence of widespread but sparse andesitic clasts in Soudan-Bigfork graywacke (Fig. 22A) suggests that andesitic volcanism may have been more significant than the preserved geologic record in the Soudan-Bigfork area would indicate, especially in the Newton belt.

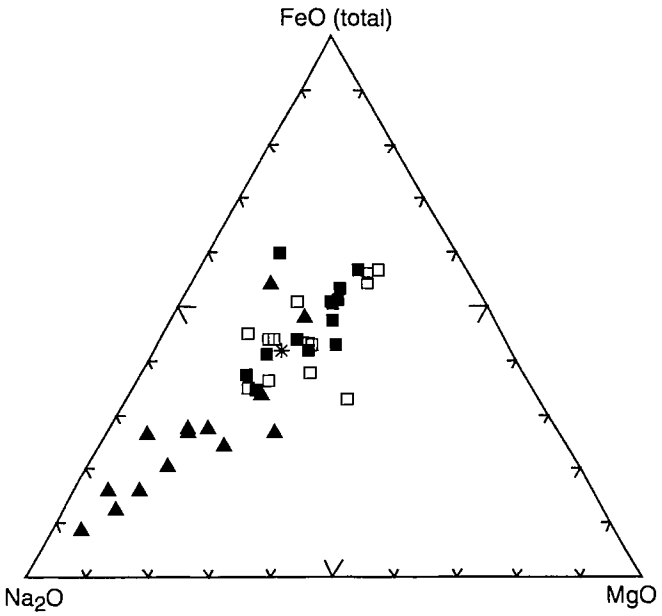

Figure 20. Na_2O - total FeO - MgO plot for metasedimentary rocks of the Soudan-Bigfork area. Same symbols as Figure 19.

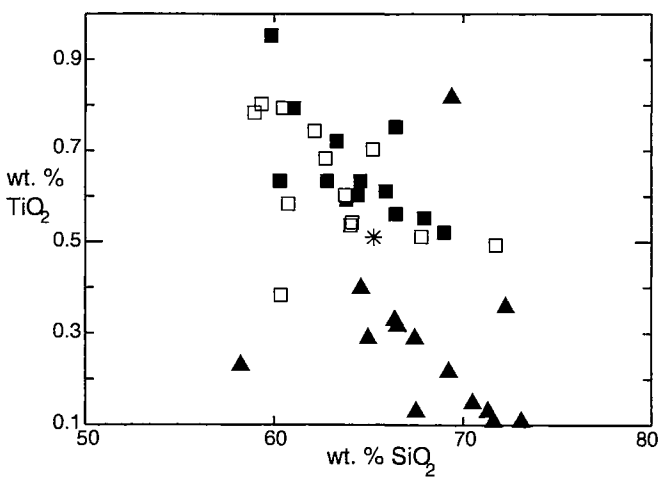

Figure 19. TiO_2 vs. SiO_2 plot for metasedimentary rocks of the Soudan-Bigfork area. Symbols:
□ = metagraywacke of Soudan belt
■ = metagraywacke of Newton belt
▲ = dacite tuff and associated massive dacitic wacke of Soudan belt;
✳ = overall mean metasedimentary rock.

Geochemical Indications of a Heterolithic Sediment Source

Although some contribution from andesitic sources can be inferred, there is unequivocal petrographic evidence that lithic clasts of dacite are the principal framework component in the graywackes and volcaniclastic rocks of the Soudan-Bigfork area (Ojakangas, 1972a, 1972b, 1985). The sediment was clearly derived from a source region in which dacite was a dominant rock type. The framework of most graywacke and associated coarser rocks also includes scattered clasts of iron-formation, ferruginous chert, and andesite (Fig. 22A), as well as rarer clasts of carbonaceous black slate, massive pyrite, and various granitoid rock types (McLimans, 1972; Boerboom and Zartman, 1993). Locally, beds of block breccia and conglomerate contain as much as one-third iron-formation clasts (Fig. 22B) and/or andesitic clasts in addition to the dominant dacite clasts. We conclude from this that the source area was heterolithic, although dominated by dacitic rocks. Further geochemical evidence for source-area heterogeneity is presented below.

Table 3. Mean compositions of turbiditic metasedimentary rocks

[major elements in weight percent oxides; minor elements in parts per million; blank, not calculated]

	Soudan graywacke		Newton graywacke		Soudan tuffs		Izu-Bonin high Si gwke		Izu-Bonin dacitic gwke	
	mean	st. dev	mean	st. dev	mean	st. dev	mean	st. dev	mean	st. dev
	N = 13		N = 13		N = 11		N = 37		N = 57	
SiO_2	61.07	4.01	62.34	2.61	66.50	4.23	60.01	1.85	66.67	1.71
TiO_2	0.59	0.15	0.64	0.12	0.27	0.18	0.77	0.09	0.67	0.09
Al_2O_3	16.66	2.49	15.10	1.16	16.50	1.99	15.05	0.87	13.9	0.61
*Fe_2O_3	1.48	0.00	1.49	0.85	0.99	0.61	8.72	1.07	6.08	0.92
†FeO	4.27	1.28	5.18	1.69	1.48	1.17				
MnO	0.09	0.03	0.11	0.07	0.04	0.03	0.17	0.03	0.21	0.32
MgO	3.14	1.29	3.09	0.86	1.27	0.75	2.94	0.55	1.79	0.39
CaO	3.21	1.66	3.06	1.61	4.09	2.27	7.13	1.49	4.95	0.69
Na_2O	4.11	1.38	3.94	0.95	4.91	1.14	3.00	0.37	3.65	0.31
K_2O	1.60	0.80	1.89	0.40	1.43	0.58	0.73	0.35	0.8	0.22
P_2O_5	0.15	0.02	0.16	0.04	0.10	0.08	0.12	0.04	0.12	0.03
CO_2	1.38	1.04	0.54	0.57	1.08	0.96				
H_2O	1.89	0.98	1.93	1.27	1.03	0.56				
TOTAL	99.64		99.47		99.68		98.64		98.84	
§FeO(t)	5.61		6.52		2.36		7.85	0.96	5.47	0.83
Rb	52.56	34.52	49.80	24.06	46.40	23.44	15	15	11	7
Sr	530.44	227.91	340.80	92.37	686.90	295.57	339	290	226	136
Ba	495.00	167.03	510.36	193.18	478.30	245.88	259	172	347	534
Nb	9.67	2.87	15.50	12.69	8.00	3.32				
Hf			5.27	1.97	4.90	1.56				
Zr	126.22	16.62	156.20	54.16	107.90	56.70	78	18	97	50
Y	11.38	0.92	15.56	16.96	5.62	8.28	33	4	44	25
Cr	241.56	151.18	137.30	63.80	40.11	41.47	26	22		
Ni	88.33	31.19	55.50	27.83	17.00	14.91				
Cu	44.62	22.10	44.41	21.33	12.44	11.98	53	25	20	13
Zn	86.88	16.16	78.67	37.69	43.78	22.62	133	72	159	169
V	160.50	43.37	106.44	28.16	41.78	15.87	189	60	90	39
La	25.49	9.81	25.48	9.32	14.03	10.82				
Ce	51.65	19.24	50.31	16.16	31.23	27.02				
Nd	24.01	8.18	23.30	8.53	13.48	11.91				
Sm	4.32	1.23	4.08	1.66	1.96	1.44				
Eu	1.27	0.28	1.14	0.68	0.62	0.36				
Gd										
Tb	0.47	0.09	0.53	0.41	0.12	0.05				
Yb	1.20	0.23	1.81	1.57	0.54	0.82				
Lu	0.19	0.04	0.27	0.23	0.06	0.00				
Au			0.01	0.01						

* Fe2O3 calculated on basis of stoichiometry

† FeO calculated on basis of stoichiometry

§ total measured iron represented as FeO

Data are presented for graywackes of the Lake Vermilion Formation of the Soudan belt, graywackes of the Newton belt, and dacite tuffs from the Soudan belt. Mean compositions of high-Si andesitic graywacke and dacitic graywacke from the Neogene-Holocene Izu-Bonin arc are presented for comparison. Analyses used for calculating the means for Soudan- and Newton-belt rocks are from Appendix Tables Ap(14) through Ap(20); they represent samples examined and classified petrographically by the authors. Izu-Bonin data are from Gill and others (1994).

Using geochemical criteria developed by Nesbitt and Young (1982) and extended by Camire and others (1993), we have identified a set of graywacke analyses that represents rocks deposited as essentially unweathered lithic detritus. Consequently, these rocks should have retained relatively unambiguous evidence of their source terranes. The selection process derives from the well documented fact that weathering of a feldspathic igneous rock (mainly dacite in this case) primarily involves the conversion of feldspars to clay minerals; this yields a solid product (clay plus residual mineral grains) that is enriched in Al and depleted in Ca, Na, and K relative to fresh rock. Nesbitt and Young (1982) have formalized this relationship as the chemical index of alteration (CIA), defined as:

$$CIA = [Al_2O_3 / (Al_2O_3 + CaO + Na_2O + K_2O)] \times 100$$

Determination of the CIA requires calculation of the oxides from weight-percent whole-rock data as molecular proportions. CaO is the amount of CaO incorporated in the silicate fraction of the rock; i.e. it is a quantity reduced from the total amount by the amount of CaO contained in secondary carbonate minerals. As weathering proceeds and feldspar is converted to clay minerals, the CIA value increases in the solid weathering product toward a theoretical upper limit of 100. Unweathered feldspathic igneous rocks typically have CIA values between 45 and 55.

In clastic sedimentary rocks, high CIA values imply high clay content, which in turn implies weathering in the source area coupled with depositional mechanisms during sedimentation that conserved the residual clay. Low CIA values are typical of glacial tills, which normally contain abundant mechanically pulverized but unweathered rock flour (Nesbitt and Young, 1982). Clastic sediments deposited by any mechanism in which the integrated rates of erosion and mechanical disintegration substantially exceeded the rate of weathering (such as graywackes deposited by rapid erosion and redeposition in tectonically active arc-trench environments) should also yield CIA values near those of fresh feldspathic source rock.

CIA values calculated for all tabulated analyses of sedimentary rock from the Soudan-Bigfork area, plus four unpublished and untabulated partial analyses, are plotted as a histogram (Fig. 23). A CIA value of 56 is taken arbitrarily as the upper cutoff for rocks that effectively lack weathered constituents. CIA values below 45 are recorded for 5 samples, all of which display petrographically visible metasomatic effects (introduced epidote, albite, or

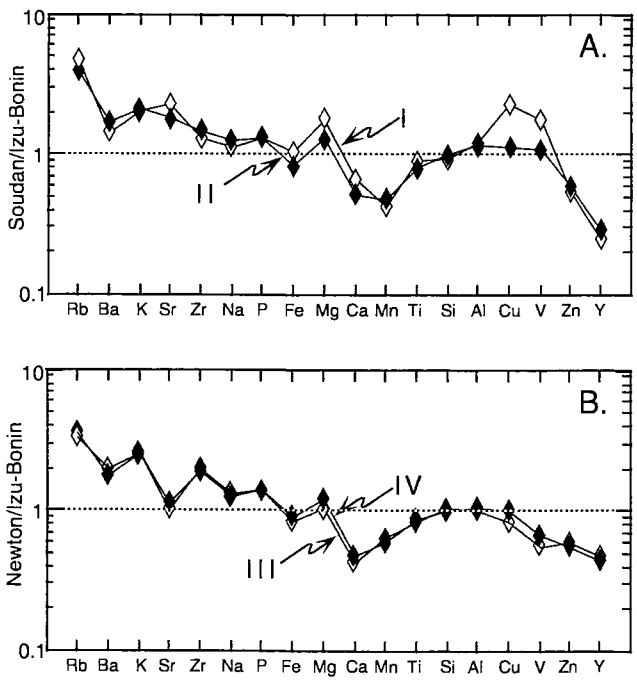

Figure 21. A: Ratio diagram of elemental abundances in the average graywacke of the Soudan belt normalized against (I) an average dacitic wacke from the Izu-Bonin arc and (II) a mixture of 41 percent Izu-Bonin dacitic wacke and 59 percent average Izu-Bonin high-Si andesitic wacke. B: Ratio diagram of elemental abundances in the average graywacke of the Newton belt normalized against (III) an average high-Si andesitic wacke from the Izu-Bonin arc and (IV) a mixture of 29 percent Izu-Bonin dacitic wacke and 71 percent average Izu-Bonin high-Si andesitic wacke. Izu-Bonin data are for Neogene rocks (Gill and others, 1994). The mixtures used to normalize plots II and IV are least-squares best-fits to the major elements in the Soudan- and Newton-belt graywackes, respectively. Elements plotted in an arbitrary order, to enhance plot smoothness and ease of comparison.

A

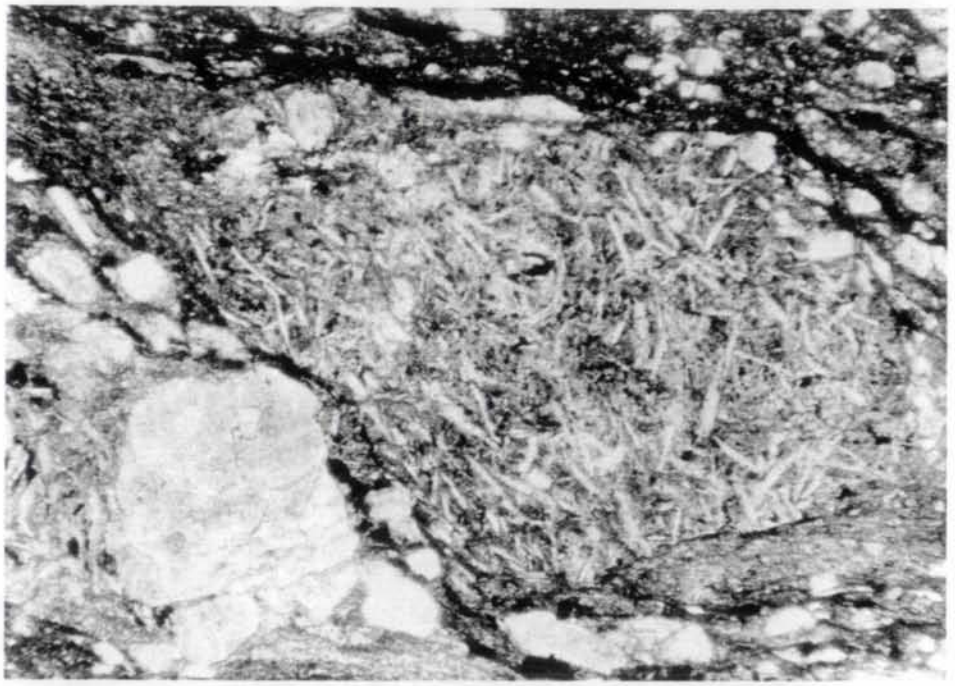

Figure 22A. Photomicrograph of andesite clast in lithic metagraywacke from the Lake Vermilion Formation (sample location: Soudan quadrangle, 62-14-8AABB). About half the clasts in this rock are microporphyritic andesite. Other lithic clasts include quartz-phyric dacite, phyllite, argillite, and abundant unit grains of volcanic quartz.

B

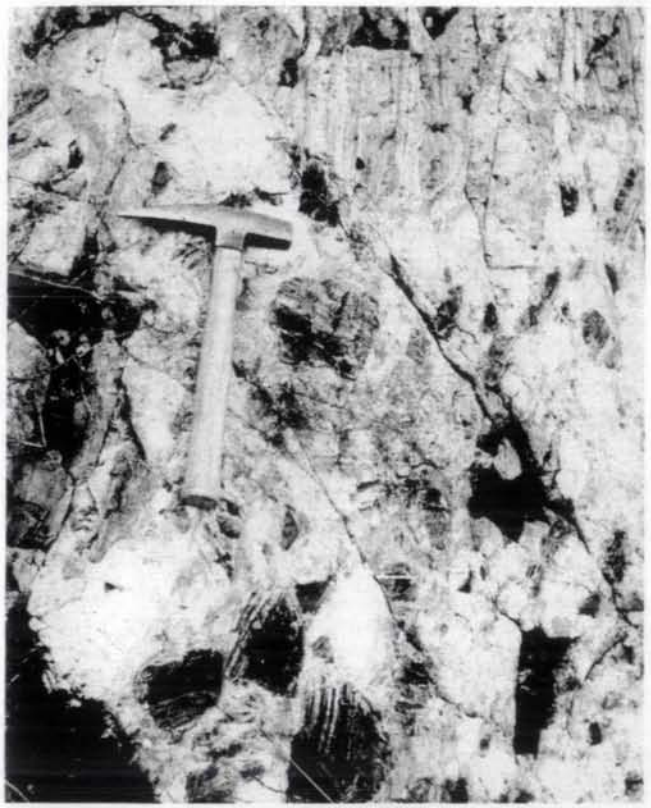

Figure 22B. Field photograph of angular iron-formation clasts in felsic breccia; deposit interpreted as proximal epiclastic sediment. Outcrop located in Soudan quadrangle, 62-14-18 DCCCC. Hammer head is approximately 20 cm long. See page 44 for an explanation of the TRS/ABCD system for describing geographic locations.

chlorite; extensive sericitization); these five analyses are disregarded for the present purpose. Twenty-six sedimentary-rock analyses (60 percent of the sample set) yield CIA values in the range 45 to 56. These are considered to represent essentially clean mechanical mixtures of source-rock constituents.

A related screening approach that utilizes the CIPW chemical norm was developed by Hopson (1964) to address the provenance question for metamorphosed diamictites in the Appalachian Piedmont of Maryland. In general, most unweathered igneous rocks lack normative corundum, whereas clay-bearing sedimentary rocks typically are enriched in alumina relative to other rock-forming chemical constituents and thus contain normative corundum. Hopson (1964) therefore concluded that a metamorphic rock type of debatable origin that contains normative corundum above about 1.5 weight percent could not be derived isochemically from either a normal igneous rock or a sedimentary rock composed only of igneous detritus. A sedimentary protolith that contained some clay would be implied by elevated corundum in the norm. All the Soudan-Bigfork sedimentary rock samples selected as primarily igneous detritus on the basis of CIA contain less than 1.5 percent normative corundum; thus they are co-selected as predominantly igneous mixtures on the basis of the procedurally simpler corundum test.

Theoretically, the bulk chemistry of each of the 26 selected samples of Soudan-Bigfork sedimentary rock should represent a summation of source-rock constituents. Conceptually this may be written in mass balance terms as:

Sedimentary daughter = [Z wt.% source-rock A] + [Y wt.% source-rock B] + [X wt.% source-rock C] + ... [P wt.% source-rock N] + V

where V is a term that incorporates compositional gains or losses due to postdepositional weathering, diagenesis, alteration, or metamorphism, and also the compositional deviations imposed by the physical segregation of material during sedimentation. In a very broad way V is a measure of the chemical "openness" of the system. Only if V is zero and the geochemical characteristics of the source-terrane rock types are known in exceptional detail can the source-rock proportions be calculated quantitatively by iterative solving of the mass-balance equation (Wright and Doherty, 1970). Otherwise, only semiquantitative approximations of source-rock inputs can be derived from the mass-balance approach.

Figure 24A shows the results of mass-balance calculations in which individual graywacke analyses are represented by mixtures of dacite porphyry, the Lower member of the Ely Greenstone, and chert. The data shown are restricted to analyses in which 95 percent or more of the major-element mass of a graywacke can be calculated in terms of the three lithic constituents, and the calculated least-squares residuals are small. These criteria suggest that the uncertainty factor V is relatively small (not zero, however, as that is unattainable), and the calculated weighting of lithic components is therefore interpreted as a valid semiquantitative estimate of source-rock contributions. The basic conclusion is that many Soudan-Bigfork graywackes are primarily mixtures of dacitic detritus (presumably from eruptions more or less coeval with graywacke deposition) and detritus derived from older calc-alkalic basalt and andesite of the lower volcanic unit. Cherty iron-formation appears to have contributed about 1 to 10 percent of the mass of the graywackes analyzed. The chert contribution is regarded as quite uncertain, however, as the selective concentration of quartz phenocrysts in the sediment would have virtually the same geochemical effect as the incorporation of chert clasts.

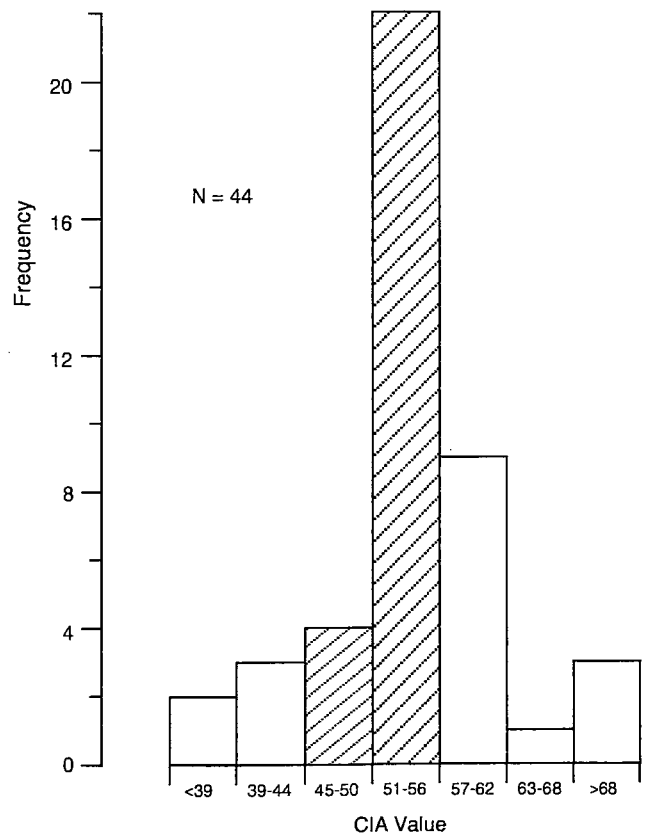

Figure 23. Histogram of CIA values calculated from chemical analyses of lithic wacke and associated metasedimentary rocks of the Soudan-Bigfork area. Twenty-six analyses yielding CIA values in range 45-56 (ruled) are used for estimating graywacke provenance. See text for discussion.

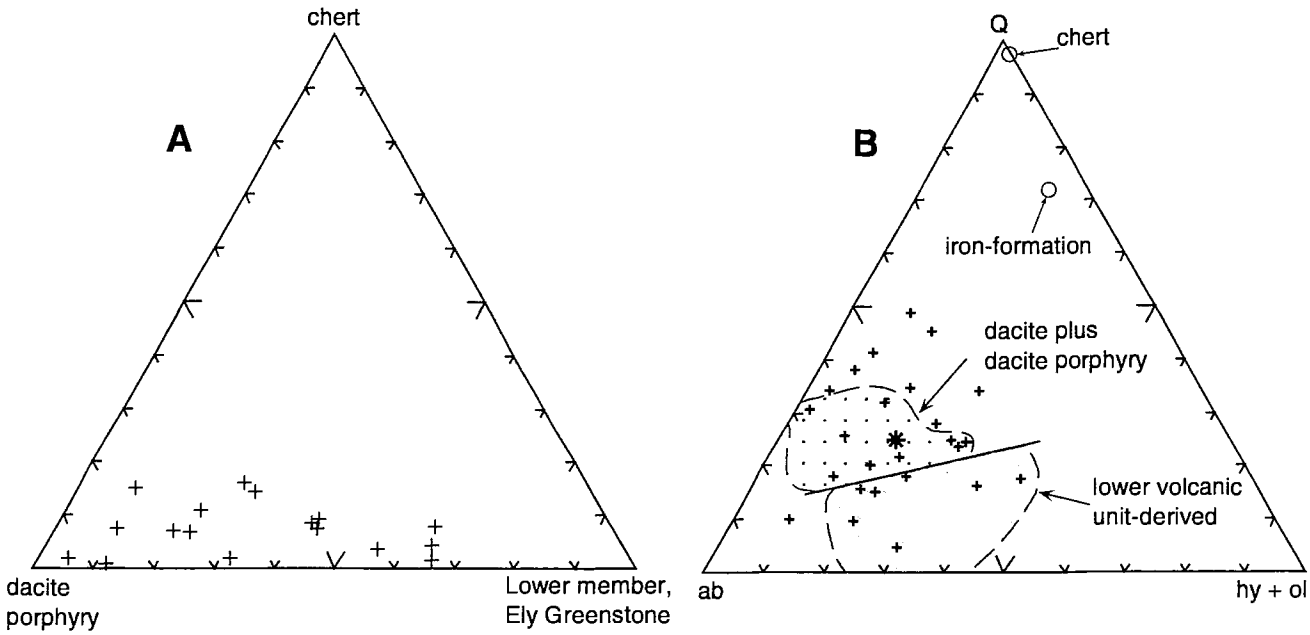

Figure 24A. Plot of selected graywacke analyses calculated as proportions of (1) average dacite porphyry, (2) average basalt in the Lower member of the Ely Greenstone, and (3) weakly ferruginous chert from the Soudan Iron-formation Member of the Ely Greenstone. Proportions calculated by the least-squares method of Wright and Doherty (1970). See text for selection criteria and interpretation. 24B. CIPW normative Q - ab - (hy+ol) plot of graywacke analyses screened to fall in the range of CIA values from 45 to 56. Q = quartz; ab = albite; hy+ol = hypersthene plus olivine. Asterisk is mean of all analyses reported in Appendix Tables Ap(14) through Ap(20). Field for dacite plus dacite porphyry is derived from data in from Appendix Table Ap(23). Field for the lower volcanic unit in the Soudan belt is from data in Appendix Tables Ap(1) through Ap(3). Circle labeled chert represents analysis 110, sample I504; circle labeled iron-formation is the mean iron-formation value; both are from Appendix Table Ap(21). Arbitrary solid line separates fields for dacite porphyry-derived and lower volcanic unit-derived sediments.

Consideration of the geochemical data in the form of CIPW normative mineral compositions leads to a similar set of conclusions. The compositions of source rocks contributing to the graywacke of the Soudan-Bigfork area may be represented approximately by mixtures of normative quartz (Q), albite (ab) and hypersthene plus olivine (hy+ol) (Fig. 24B). The position of a graywacke analysis in normative Q - ab - hy+ol space gives a general sense of the proportions of dacite (ab + Q dominant), basalt or andesite (ab and hy + ol dominant) and cherty iron-formation (Q dominant) that the rock contains among its clastic constituents. The distribution of points in Figure 24B implies that the lower volcanic unit of the Soudan belt, or the equivalent calc-alkalic sequences of basalt and andesite, contributed significant detritus to graywackes of the Soudan-Bigfork region. Altogether, the information presented in Figure 24 augments petrographic observations and conclusions by taking into account the provenance contributions concealed in the fine-grained matrix fraction of the sedimentary rocks.

Geochemistry of Iron-Formation, Soudan and Newton Belts

The iron-formation of the Soudan-Bigfork area is a microlaminated rock in which the individual mm- to cm-thick laminae are composed predominantly of chert, iron oxides, or phyllosilicates. The ratio among these kinds of laminae varies widely from place to place. A fairly common iron-formation rock type is made up mainly of chert laminae and a small fraction of either oxide- or mica-rich laminae. A second common variant consists of alternating chert-rich and oxide-rich laminae in subequal amounts, with little or no micaceous material. A third iron-formation variant consists of about one-third phyllosilicate-rich, thinly bedded schistose layers and about two-thirds laminated to thinly bedded chert-rich and oxide-rich layers, all interleaved on the scale of centimeters to decimeters. Pyritic laminae occur locally and sparingly. Iron-formation sequences that contain abundant phyllosilicate-rich layers (layers of sericite schist, sericite

phyllite, green sericite schist, or green chlorite schist in the local mining terminology) are transitional to phyllitic sequences interpreted to be derived from protoliths of andesitic to dacitic tuff. Thus, the prevailing opinion is that iron-formation sedimentation involved a component of chemical precipitation (responsible for the cherty and iron-rich constituents of the rock) and a component of volcanic ash deposition (responsible for the phyllitic constituents). Most of the ash was probably deposited as air-fall or by bottom currents operating some distance basinward from volcanic source areas.

Geochemically, the chert-oxide component of the iron-formation in the Soudan-Bigfork area is characterized by low contents of Al_2O_3, Na_2O, and K_2O, and very low trace and rare earth element concentrations [Table Ap(21)]. These constituents all increase in abundance with an increase in the proportion of phyllosilicate-rich layers (ash) in the rock. Because of this, it is potentially misleading to compare or interpret iron-formation whole-rock compositions without detailed information on the microstratigraphy and mineral proportions of the analyzed samples. Lacking the requisite detailed sample characterization, absolute abundance data are far less trustworthy for interpretive purposes than elemental ratios, and even ratios must be used with caution.

Bau and Moller (1993) argue that the rare earth element (REE) content of the marine bottom water in Archean oceans was probably controlled by the input from submarine hydrothermal fluids. They further argue that the REE distribution in the Archean bottom water can be described by mixing between low-temperature and high-temperature alteration fluids, that the measurable and consistent fractionation of REE between low-T and high-T alteration fluids observed at modern spreading-centers also prevailed in the Archean, and that detritus-free cherty iron-formation records the REE signature of the Archean water from which it precipitated. Figure 25 shows a mixing line for the normalized ratios Sm/Yb and Eu/Sm between high- and low-T submarine hydrothermal fluids, adapted from Bau and Moller (1993). Data from Soudan-Bigfork iron-formation units plot toward the low-T end member of the mixing graph, which suggests that the rocks were deposited from cool solutions, presumably at some distance from active spreading centers. This inference is consistent with the very low values of Au, Cu, Zn, Pb, and S that occur in these rocks.

Kerswill (1996) provides a useful summary of the attributes of both syngenetic and epigenetic gold deposits hosted by Precambrian iron-formation. He concludes that the presence of abundant sulfide minerals (especially pyrrhotite) is a key indicator for both types. Sulfide minerals are typically disseminated and stratabound as sulfide-facies iron-formation in the syngenetic deposits, and are associated with discordant quartz veins and structural traps of various kinds in the epigenetic deposits. Other geochemical characteristics of both deposit types are elevated amounts of copper and silver, and the virtual absence of lead and zinc. Furthermore, the two deposit types are spatially associated in some mining districts, which reinforces the view that syngenetic and epigenetic ore-forming processes are not accidentally combined.

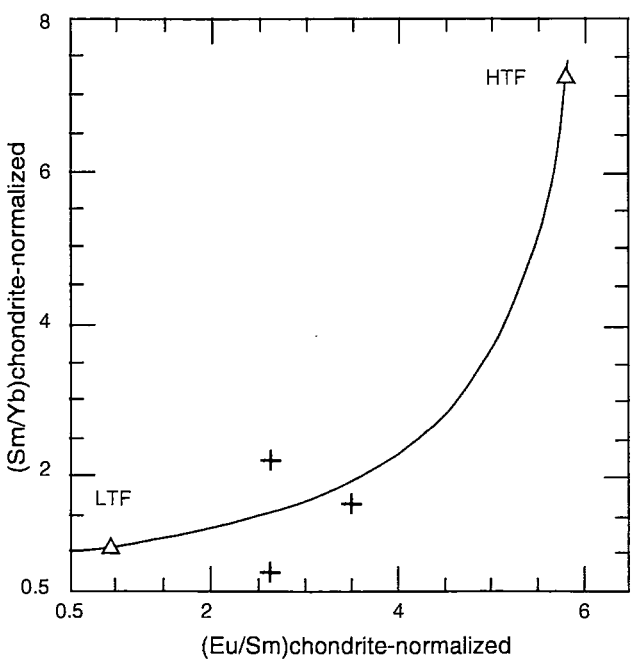

Figure 25. Chondrite-normalized REE graph of a two-component mixing line between the compositions of low-temperature and high-temperature hydrothermal fluids (points LTF and HTF, respectively) that Bau and Moller (1993) interpret as having contributed to the REE budget of Precambrian marine bottom water. Iron-formation data from the Soudan-Bigfork area (+) plot toward the LTF end of the curve. Data normalized to composition of C1 chondrite (Sun and McDonough, 1989).

It follows that the iron-formations of the Soudan-Bigfork area are not intrinsically good candidates for hosting syngenetic, stratabound deposits of gold. Sulfide-facies iron-formation is rare in the area, and the prevalent oxide iron-formation is low in metals, as it is elsewhere in Archean terranes. Indeed, the very presence of oxide iron formation is interpreted by some as a negative indicator for stratiform gold mineralization (Kerswill, 1996). The favorability of the Soudan-Bigfork iron-formations for hosting structurally controlled epigenetic vein deposits of gold remains open and essentially untested. However, the fact that the background metal values in the iron-formation are so low requires that any epigenetic deposit would have to acquire its metals, sulfur, and arsenic from remote and poorly defined sources beyond the host-rock environment.

Geochemistry of Hypabyssal Interior Intrusions

Mafic Subvolcanic Intrusions: The Deer Lake Complex (Newton Belt)

We confine our consideration of the mafic subvolcanic intrusions to the Deer Lake Complex in northern Itasca County. The Deer Lake Complex consists of several differentiated sills that invaded a sequence of possibly coeval volcanic rocks (Deer Lake sequence of Jirsa, 1990) and sedimentary strata assigned to the Joy Lake sequence. Table Ap(22) provides major-element analyses of chilled margins of the differentiated sills; we regard these as most closely approximating the original bulk composition of the sills. Data on the various differentiates of the Deer Lake Complex and of lithologically comparable sills in the Newton Lake Formation are tabulated in Engelbert and Hauck (1991), as are analyses of interior samples from the essentially undifferentiated sills of massive diabase that are associated with volcanic sequences throughout the region.

Though similar, the mean major-element compositions of the chilled margins of sills in the Deer Lake Complex and mafic flows in the wall rocks differ in detail (Table 4). The chilled-margin rocks are weakly enriched in MgO and FeO, and depleted in SiO_2 and Al_2O_3 relative to the mafic flows. These differences are consistent with a comagmatic model for the flows and sills in which the primary control on liquid composition was the fractional crystallization of olivine and pyroxene. Least-squares mixing calculations (Wright and Dougherty, 1970) using mineral data from Ripley and others (1982) as input (Table 4, olivine and pyroxene) show that the major-element composition of the sill margins is closely approximated by the sum of 90.2 percent flows from the Deer Lake Complex, 6.8 percent peridotitic olivine, and 2.7 percent peridotitic clinopyroxene. Essentially, the same result is obtained if the composition of the cumulus peridotite in the sills (Table 4, peridotite layer) is used in place of the mineral compositions in the mixing calculation. In other words, the flows could have been derived from a magma of sill chilled-margin composition that had crystallized about 10 percent of its original mass as intratelluric peridotite by the time of eruption. Because the sills are somewhat more primitive in composition than the flows they intrude, they must represent an independent pulse of less fractionated magma that invaded the volcanic products erupted from a more fractionated, earlier, magmatic pulse.

Berkley and Himmelberg (1978) and Ripley and others (1982) have shown that the sills themselves differentiated through the sequential crystallization and separation of cumulus chromite, olivine, augite, and plagioclase. Furthermore, Ripley (1978, 1979) concluded that a primary sulfide liquid separated from the silicate magma at

Table 4. Mean compositions for mafic and ultramafic rocks of the Deer Lake sequence and Deer Lake Complex

Major elements in weight percent oxides; minor elements in parts per million; blank, not calculated; cpx, clinopyroxene.

	wall-rock flow	Deer Lake Cplx	peridotite layer	olivine	cpx
SiO_2	52.22	51.21	44.08	39.7	53.9
TiO_2	1.01	0.77	0.51	0.12	
Al_2O_3	13.25	11.63	4.53	1.6	
*Fe_2O_3					
†FeO	12.13	12.79	13.26	15.4	6
MnO	0.23	0.23	0.19	0.33	0.28
MgO	9.13	11.50	34.22	44.3	15.7
CaO	8.72	8.57	3.13	0.24	21.3
Na_2O	2.71	2.67	0.06		
K_2O	0.46	0.53	0.01		
P_2O_5	0.15	0.09			
TOTAL	99.00	100.00	99.00	99.97	98.90
¶Mg#	57.31	61.60	82.16	83.69	82.36
Cr (ppm)	493	684	4174	137	3832
Ni (ppm)	114		1179	393	

* Fe2O3 calculated on basis of stoichiometry
† FeO calculated on basis of stoichiometry
§ total measured iron represented as FeO
Mean compositions are calculated volatile-free.
Wall-rock mafic flow mean from Appendix Table Ap(13); Deer Lake Complex chilled sill margin data from Appendix Table Ap(22). Peridotite layer mean is from a peridotite layer within one of the sills; the olivine and clinopyroxene analyses are from the peridotite layer.
Peridotite data from Ripley and others (1982).

an early stage, based on the observation that sulfide phases occur interstitially to plagioclase and pyroxene in rocks of the chilled margin. He also showed that this sulfide liquid changed in composition during overall magmatic differentiation of the sills, progressing from a mixed Cu-Ni-Fe sulfide in the chilled margin, through a Cu-Fe sulfide in clinopyroxenite and augite gabbro horizons, to Fe sulfide in upper gabbro and diorite units. Virtually all of the nickel was stripped from the sulfide liquid as crystallizing Ni-pentlandite at the peridotite stage of differentiation, leaving a Cu-Fe sulfide liquid to crystallize chalcopyrite-bearing assemblages at later stages (Ripley, 1978).

Exploration activity in the 1970's failed to identify economic concentrations of Ni sulfides in the Deer Lake Complex. Ripley (1978, 1979) ascribes the paucity of Ni sulfides to the relatively low MgO content of the parent magma and to iron enrichment during differentiation. The relatively high FeO content of the magma favored the solubility of sulfur in the silicate melt, thus limiting the amount of a separate, nickel-enriched, immiscible sulfide liquid that could form prior to or during crystallization of the sills.

However, since the mid-1980's there has been significant evolution in the techniques of geochemical modeling and the application of modeling results to understanding the behavior of chalcophile elements in magmatic sulfide systems. The detailed petrology-geochemistry approach has been applied beneficially to many specific nickel-copper-cobalt deposits and prospects, and, in recent years, has contributed to major advances in understanding the behavior of the platinum-group elements in

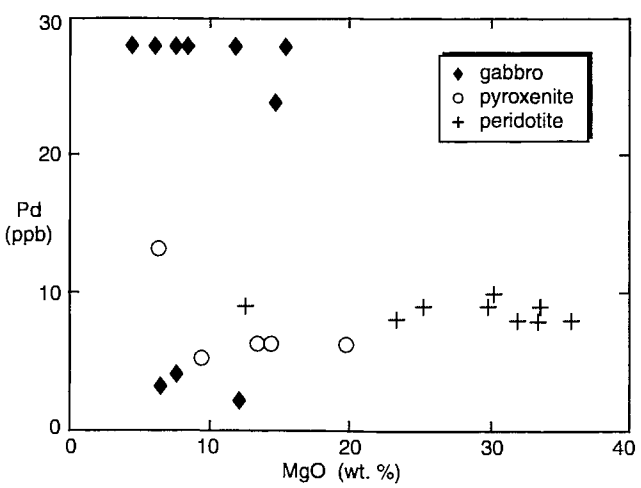

Figure 26. Plot of Pd vs. MgO for interior differentiates of sills that comprise the Deer Lake Complex. Data from Engelbert and Hauck (1991).

mafic magmatic systems (Naldrett, 1989; Naldrett and others, 1990; Li and others, 1992). Most of the key ideas on the controls of Cu, Ni and PGE distribution in mafic complexes, as well as the analytical tools required to apply them, have been developed since the basic petrologic and geochemical work was done on the Deer Lake Complex. Consequently, the Cu, Ni and PGE potential of sills within the Deer Lake Complex has not been evaluated in light of newer, geochemically based concepts and techniques.

Engelbert and Hauck (1991) report palladium values for differentiates of sills in the Deer Lake Complex in the range between 2 and 28 parts per billion. The highest Pd values occur in rocks classed as gabbro that lie in medial or higher positions within the sills. Seventeen of the 24 available Pd analyses for peridotite, pyroxenite and gabbro of the Deer Lake Complex cluster near a mean value of about 8 ppb (Fig. 26), close to the average tenor of unmineralized mafic and ultramafic igneous rocks reported by Crocket (1981). The other seven Pd analyses, all from gabbro, cluster at about 27 ppb. Although these higher values are well within the observed background range for mafic igneous complexes, they may represent a feeble enrichment trend related to igneous differentiation of the magma sourcing the Deer Lake Complex. This possible enrichment could be significant, and should be followed up with further geochemical and petrologic analysis.

Several sill complexes broadly comparable to those of the Deer Lake Complex in terms of scale, bulk major-element composition, and differentiation history are hosts to Cu-Ni-PGE mineralization elsewhere in the Canadian Shield. Examples include the late Archean Lac des Iles Complex in western Ontario (Sutcliffe and others, 1989); certain of the Early Proterozoic Nipissing intrusions in the Huronian region (Lightfoot and Naldrett, 1989; Lightfoot and others, 1993; Lightfoot, 1995); and sills of Early Proterozoic age in the Cape Smith belt (Picard and others, 1996). Despite clear differences in inferred geologic setting, age, and details of composition from these cited examples, the Deer Lake Complex is an attractive target for further PGE exploration because the key processes of magmatic sulfide segregation and concomitant nickel concentration are known to have occurred (Ripley, 1978, 1979; Ripley and others, 1982).

The Deer Lake Complex is also of some potential interest with respect to the genesis of volcanic-hosted massive-sulfide (VMS) ore deposits. Galley (1996) points out that the geochemistry of mafic layered intrusions is pertinent to VMS exploration in four ways: (1) to determine tectonic environment (back-arc or other intra-arc extensional settings being the most favorable for VMS deposition); (2) to assess whether the degree of fractionation in an intrusion was sufficient for the development of a cogenetic volcanic suite of VMS-favorable composition;

(3) to determine whether the intrusion is or is not comagmatic with its host volcanic suite; and (4) to establish whether or not the intrusion shows signs of hydrothermal or deuteric alteration potentially related to the formation of VMS deposits in comagmatic volcanic strata. Although present geological and geochemical data for the Deer Lake Complex appear to indicate that the intrusions are comagmatic with their volcanic host (Galley's favorability criterion 3), they are not sufficient for meaningful evaluation of Galley's criteria 1, 2, and 4.

Nevertheless, the Deer Lake Complex has intriguing similarities in bulk composition and differentiation history to tholeiitic intrusions that are associated with VMS deposits elsewhere in the Superior Province. For example, it is broadly comparable to the Kamiskotia Complex in the Timmins district of Ontario in these respects (Barrie and others, 1991), although its chilled-margin composition is somewhat less evolved and its differentiation trend appears to be somewhat less strongly iron-enriched (Fig. 27). Whether the intrusive rocks of the Deer Lake Complex could or did reach the advanced stages of differentiation achieved by the much larger Kamiskotia intrusion remains to be established through further geologic and petrologic study of the sills and their supracrustal envelope. Modern trace-element, REE, and isotopic studies will be critical components of the required investigation.

In addition, further efforts should be mounted to document the sedimentary and felsic volcanic rock types included in the Joy Lake sequence, which is mapped as intertonguing with the mafic volcanic rocks of the Deer Lake sequence, and locally forms wall rock for the Deer Lake Complex (Jirsa, 1990). If the Joy Lake sequence should be found to contain subunits of strongly evolved felsic material (see following section) that are demonstrably

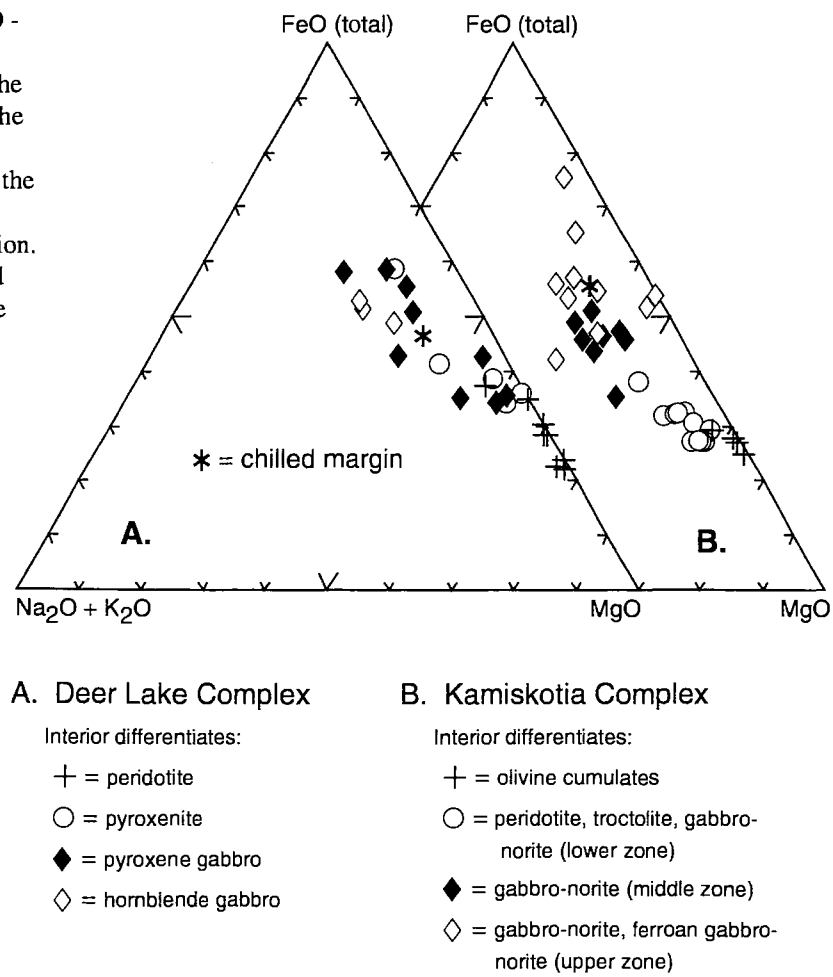

Figure 27. MgO - total FeO - alkalis plot (wt. %) for analyses of rocks from the Deer Lake Complex in the Newton belt (A) and the Kamiskotia Complex in the western Abitibi, Ontario (B). See text for discussion. Data from Engelbert and Hauck (1991) and Barrie and others (1991).

comagmatic with extreme differentiates of sills in the Deer Lake Complex, the general potential for discovery of a VMS ore deposit would be significantly enhanced. Because of spotty bedrock exposure, the critical field data can be obtained only from systematic exploratory drilling that is tied to a multiple-method geophysical program. The program required would entail substantial expenditure.

Felsic Subvolcanic Intrusions: Quartz-Plagioclase Porphyry

The quartz-plagioclase porphyries of the Soudan-Bigfork area are classified modally as dacites because K-felspar is virtually absent. This attribute is borne out chemically [Table Ap(23)] by Na_2O/K_2O ratios in the 3.0-4.0 range; ratios lower than about 3 are obtained only from rocks relatively rich in secondary muscovite and carbonate that apparently underwent mild metasomatic alteration. The SiO_2 content of the porphyries ranges generally between 62 and 68 weight percent (normalized volatile-free basis); a compositional gap between 64 and 66 weight percent SiO_2 broadly divides the quartz-prominent from the plagioclase-prominent porphyries, as classed on the basis of modal phenocryst populations.

Lesher and others (1986) have classified the felsic flows and associated subvolcanic felsic intrusions in the Canadian portion of the southern Superior Province into four geochemical groups, primarily on the basis of trace-element abundances, and have found an empirical relationship between the occurrence of major massive-sulfide accumulations and two of the four felsic host-rock types. The key geochemical attributes of the felsite groups recognized by Lesher and others (1986) are summarized in Table 5, along with the attributes of the felsic porphy-

Table 5. Geochemical characteristics of felsic volcanic sequences and associated hypabyssal intrusives in the Superior Province of Canada as classified by Lesher and others (1986; types F1, F2, F3a, and F3b), and of the Soudan-Bigfork area (this study). See text and Table 6 for interpretation and amplification.

Characteristics	F1	F2	F3a	F3b	Soudan-Bigfork
Slope of chondrite-normalized REE pattern	steep neg.	gentle neg.	flat	flat	steep neg.
**$[La/Yb]_n$	6-34	2-6	1-4	1-5	~20
†Eu anomaly (Eu/Eu*)	0.87-2.0	0.35-1.4	0.37-0.94	0.20-0.61	~1
Zr/Y	9-31	6-11	4-7	2-6	15
§Abundance of HFS elements	low	intermed.	intermed.	high	low
¶Abundance of Sr, ppm	high m=281	intermed. m=106	low m=38	low m=48	high m=500
¶Abundance of Sc, ppm	low m=7.2	intermed. m=9.0	high m=14.4	low m=4.3	low m=7
¶SiO_2 content, wt.%	low m=69.6	high m=73.7	high m=72.8	v. high m=75.4	low m=63.44

** Ratio of chondrite-normalized La to chondrite-normalized Yb.

† Ratio of chondrite-normalized Eu (observed) to chondrite-normalized Eu* that is determined by linear interpolation between the normalized values for adjacent elements Sm, Tb in a standard REE plot.

§ High field-strength elements, typically Y, Zr, U, Th, and the REE.

¶ m is arithmetic mean. Values for Soudan-Bigfork rocks from Appendix Table Ap(23).

Table 6. Mean geochemical data for felsic volcanic sequences and associated hypabyssal intrusions

[major elements in weight percent oxides; minor elements in parts per million; blank, not calculated]

	Superior Province felsite types (Lesher and others, 1986)				Soudan-Bigfork felsite types normalized volatile-free			
	F1	F2	F3a	F3b	qtz. porph.	plag. porph.	dac. flow	grand avg.
	n=10	n=8	n=6	n=8	n=6	n=4	n=4	n=14
SiO_2	69.59	73.72	72.80	75.35	67.32	63.63	62.76	64.92
TiO_2	0.41	0.35	0.40	0.27	0.32	0.41	0.72	0.46
Al_2O_3	15.28	13.62	12.98	12.59	16.33	16.99	16.08	16.44
*Fe_2O_3	4.08	4.91	6.20	3.84	0.94	1.86	1.99	1.56
†FeO	2.29	2.24	4.66	2.96				
MnO	0.07	0.09	0.12	0.07	0.06	0.08	0.11	0.08
MgO	2.03	0.95	1.35	1.47	2.06	2.84	3.40	2.67
CaO	2.46	1.73	1.25	1.12	3.72	4.51	4.30	4.11
Na_2O	4.26	2.48	3.73	2.71	5.16	4.94	3.95	4.75
K_2O	1.81	2.23	1.13	2.56	1.65	2.27	1.87	1.89
P_2O_5	0.07	0.05	0.10	0.04	0.15	0.23	0.17	0.18
CO_2								
H_2O								
TOTAL	100.04	100.15	100.06	100.02	99.00	100.00	100.00	100.00
§FeO(t)	3.68	4.42	5.58	3.46	3.13	3.91	6.45	4.36
Rb	45.1	52.8	23.5	54.0	21.0	33.0	50.5	38.8
Sr	280.8	106.4	38.2	48.1	299.5	1232.0	396.0	524.6
Ba	418.9	358.0	346.7	467.6	278.8	1060.0	556.3	544.9
Sc	7.2	9.0	14.4	4.3	7.0	3.9	10.2	7.0
Nb	13.0	29.0	21.0					
Hf	2.0	7.5	6.5	11.8	2.8	4.5	3.4	3.7
Zr	119.0	330.0	268.0	421.6	92.0	152.5	138.0	135.6
Y	8.8	39.9	52.7	143.8	9.0	9.0	9.0	
Cr	54.8	9.1	8.2	65.5	86.0	51.5	111.5	89.7
Ni	31.3	9.5	66.7	39.1				
Cu	23.7	16.6	55.3	33.8				
Zn	72.3	58.5	38.7	56.3				
V	52.0	81.5	100.7	77.6				
La	20.69	29.64	21.28	52.10	19.00	36.60	20.40	23.93
Ce	42.30	67.62	49.33	128.75	36.85	70.75	41.00	48.31
Nd	18.78	33.12	28.67	72.00	14.95	36.85	24.33	25.23
Sm	3.0:	7.09	7.36	19.46	2.80	5.65	3.17	3.77
Eu	0.974	1.389	1.577	2.739	0.802	1.410	0.810	0.979
Tb	0.344	1.048	1.307	3.894	0.400	0.350	0.375	
Yb	0.982	4.576	6.440	16.613	0.290	1.015	1.310	0.934
Lu	0.156	0.721	0.985	2.462	0.044	0.130	0.270	0.169
Au	0.002	0.005	0.014	0.008				

* Fe2O3 calculated on basis of stoichiometry

† FeO calculated on basis of stoichiometry

§ total measured iron represented as FeO

Felsite types are those distinguished in the Superior Province in Canada (data from Lesher and others, 1986) and the Soudan-Bigfork area (this study). Rock types from the Soudan-Bigfork area include quartz-prominent porphyry (qtz. porph.), plagioclase-prominent porphyry (plag. porph.) and dacite flows (dac. flow); the grand average is the mean calculated from these three rock types. Further compositional detail is presented in Appendix Table Ap(23).

Table 7. General characteristics of the lamprophyre clan (after Rock and others, 1988)

Intrusive occurrence and form:	Minor intrusions that typically contain abundant xenoliths. Commonly associated with breccias, pyroclastic rocks. Complex intrusive shapes are common.
Textural attributes:	Tendency toward panidiomorphism. Lack felsic phenocrysts. Commonly contain pseudohexagonal biotite crystals that show strong color zoning. May contain apatite phenocrysts. Commonly contain felsic, globular segregations ("ocelli") of broadly syenitic, K-rich composition.
Mineralogical (modal) attributes:	Contain abundant biotite, hornblende, or both. Clinopyroxene commonly present. Apatite is typically abundant. May contain primary epidote, chlorite, fluorite, carbonates, sulfates, and volatile-rich phases.
Compositional characteristics of constituent minerals:	Exceptionally high Ti in biotite, amphibole, pyroxene. Exceptionally high Ba in biotite, K-feldspar.
Attributes developed under metamorphism, deformation:	Abundant formation of metamorphic chlorite, biotite, and amphibole. Cleavage and lineation develop well because of abundant phyllosilicates and amphibole. Tend to be mechanically weak; forms boudins and folds readily. Mineral zoning due to wall-rock exchange reactions common along contacts.
Whole-rock chemical attributes:	Strongly elevated K, Ba, Sr, Rb, Th, LREE, P, F, CO_2, H_2O, S, SO_3 (1-3 orders of magnitude above levels in basaltic rocks). Moderate enrichment in Ti, Zr, Nb. MORB-like levels of V, Cr, Co, Ni. Near- to below-MORB levels of Y, HREE.

ries from the Soudan-Bigfork area in Minnesota. Group averages for Canadian and Minnesota felsite types are presented in Table 6. These data clearly show that the Minnesota rocks are most similar to the Canadian felsites of group 1, which are rarely associated with massive sulfide deposits. On this basis, it would seem that the felsic volcanic and subvolcanic rocks of the Soudan-Bigfork area are not the most promising target for massive-sulfide exploration. As a group they are substantially less siliceous, less potassic, and less evolved in other geochemical respects than the felsic rocks in Canada that are associated with major massive sulfide camps.

It is important to recognize, however, that Soudan-belt samples are strongly overrepresented in the porphyry dataset for the Soudan-Bigfork area. Large, poorly exposed tracts of the Newton belt that are interpreted to contain mostly metasedimentary rock types on the basis of geophysical signatures may well contain considerable proportions of felsite. As indicated in the previous section, the "sedimentary" component of the Joy Lake sequence is a logical candidate for serious investigation in this regard.

Lamprophyres

The lamprophyres of the Soudan-Bigfork area are all ordinary lamprophyres that have been altered to varying degrees under deuteric or metamorphic conditions. The analyzed samples [Table Ap(24)] are about equally divided between moderately quartz-normative and moderately olivine-normative compositions; strongly silica-undersaturated and strongly alkaline compositions are not represented. Predictably, the quartz- and olivine-norma-

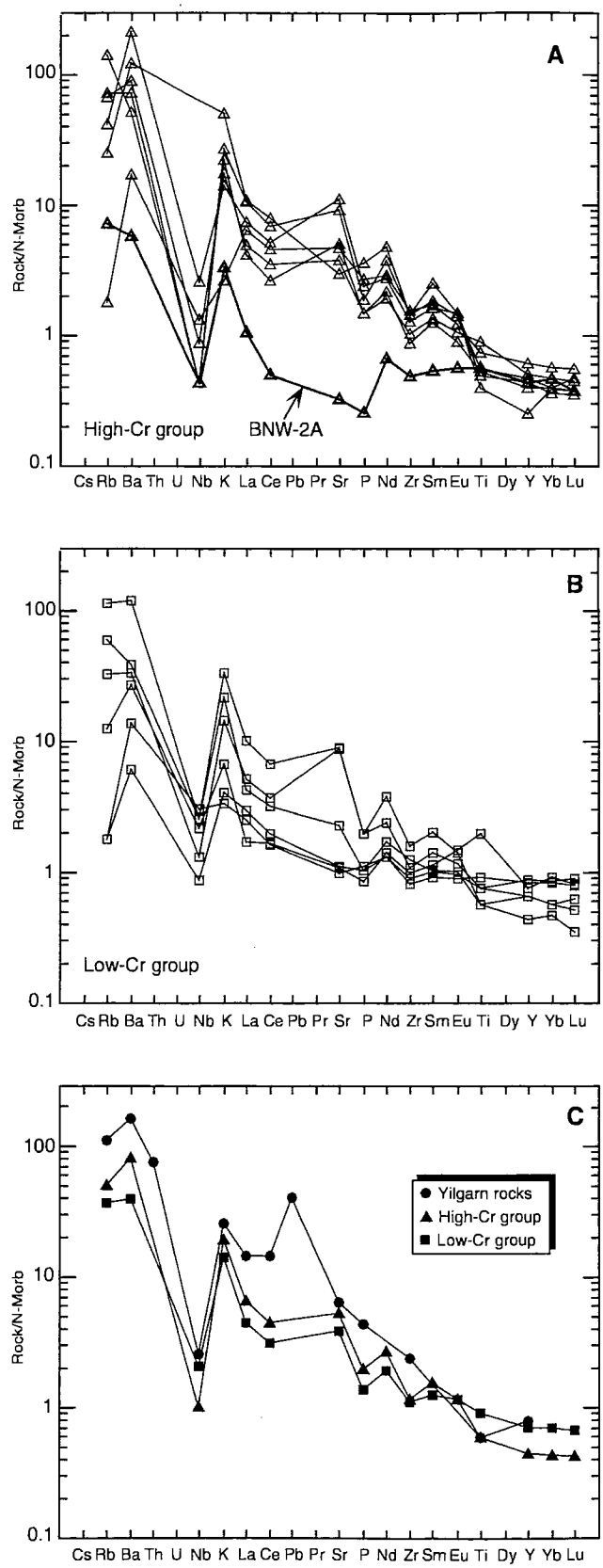

Figure 28. Spider diagrams of Soudan-Bigfork lamprophyre trace and rare earth element abundance; normalized against the composition of normal mid-ocean ridge basalt (N-MORB) as reported in Sun and McDonough (1989). For the purpose of these plots, values for Nb and Nd reported at or below the analytical detection limit are assigned values equal to half the detection limit.
A: High-Cr lamprophyres.
B: Low-Cr lamprophyres.
C: Mean compositions of both lamprophyre groups compared with the mean composition of lamprophyres in the gold camps of the Yilgarn block, Western Australia (Rock and others, 1988). Note that the suite of elements plotted for the Yilgarn rocks differs from the suite plotted for the Minnesota rocks. See Appendix Table Ap(24) for data.

tive subgroups are low and high in Cr abundance, respectively. A Cr content of 450 ppm empirically divides the lamprophyres into low- and high-Cr subtypes. This division is not reflective of modal mineralogy of the samples; i.e., not all rocks in the high-Cr group are enriched in olivine or pyroxenes, minerals into which Cr is strongly partitioned. Many high-Cr rocks are predominantly composed of secondary blue-green hornblende or magnesian actinolite. The secondary amphibole in these rocks is thought to have formed at the expense of olivine and pyroxene under late-magmatic or postmagmatic conditions.

Rock and others (1988) summarize the whole-rock geochemical attributes of the lamprophyre clan in terms of comparisons with mid-ocean ridge basalt (Table 7). Spider diagrams normalized against MORB are therefore a useful means for judging the departure of lamprophyre compositions from the compositions of normal basalt. Both the high-Cr and low-Cr variants of the Soudan-Bigfork lamprophyre population show strong enrichment in the large-ion lithophile elements (LILE), pronounced negative Nb anomalies, and near-normal basaltic levels of the geochemically immobile elements, as compared to MORB (Fig. 28). Furthermore, although there is considerable scatter in the data (Fig. 28A and B), the mean minor- and trace-element abundance patterns of the high-Cr and low-Cr variants are rather similar (Fig. 28C). The high-Cr group is slightly enriched in LILE and depleted in Ti and the heavy rare earths relative to the low-Cr group. The spidergram datasets are internally coherent with the exception of sample BNW-2A, which differs erratically from the rest of the high-Cr population (Fig. 28A, B). This anomalous sample is composed predominantly of pale green magnesian actinolite that has deuterically replaced original pyroxene; the parent rock may have been some sort of pyroxenitic differentiate that is not representative of lamprophyre bulk composition.

Worldwide, the Archean lamprophyres have attracted much recent exploration interest because several of the major gold deposits in Western Australia (Rock and others, 1988) are spatially associated with lamprophyre intrusions. In North America, the conjunction of lamprophyric and trondhjemitic rocks, throughgoing major fault zones, and gold-bearing quartz veins at the Canadian Arrow deposit in Ontario led McNeil and Kerrich (1986) to conclude that deep crustal conduits channelled both deep-seated magmas (i.e., lamprophyres) and magmatic or metamorphic gold-bearing solutions to higher crustal levels. Rock and Groves (1988a, 1988b) concluded that lamprophyric magmas seem to be intrinsically more auriferous than normal magmas, and that lamprophyric magmatism therefore may be a mechanism for delivering gold from deep-crust or mantle sources to the upper crust where it can be further concentrated to economic levels by mesothermal and epithermal processes. Although some lamprophyres are anomalously enriched in gold, many are not, and the erratic distribution of observed gold values in the clan leaves room for divergent interpretations. Rock and others (1988) propose two alternatives: (a) the gold tenor of lamprophyres is naturally erratic, but the relatively infrequent "spikes" of high-background values indicate the site-specific operation of magmatic enrichment processes, or (b) the "natural" condition of lamprophyres is to be enriched in gold; those that are not have lost their gold to secondary removal. The first interpretation is a variant of the "gold is where you find it" aphorism, whereas the second is an optimistic interpretation of geochemical background scatter. Neither view has been fully substantiated.

The lamprophyre–fault zone–gold vein association in Western Australia spurred exploration interest in the lamprophyres near Wahlsten in the Soudan-Bigfork area in the 1980's. The pod-shaped bodies between Wahlsten and Idington, north and east of the hinge of the Britt antiform (Fig. 3) display evidence for fault control and post-emplacement shearing. To date, however, no indications of gold-related mineralization have been identified in these bodies, so far as we know.

Apart from gold content, the lamprophyres of the Soudan-Bigfork area are geochemically similar to the lamprophyres of the Yilgarn block in Australia [Fig. 28C; Table Ap(24)]. Given the experience elsewhere, however, (e.g. Rock and others, 1988), the Minnesota data set may be too small to be a proper test of lamprophyres as potential targets for gold exploration. Further geochemical assessment of the fault-associated lamprophyre megaboudins of the Wahlsten-Idington area, aided by shallow core drilling, would seem to be warranted.

Inferred Tectonic Setting of the Soudan-Bigfork Area

The rock types, rock sequences, and early structural history (i.e., D_1 structures) documented and interpreted for the Soudan-Bigfork area are generally analogous to those observed in Mesozoic to Holocene volcanic arcs of the western Pacific, and strongly suggest a similar tectonic setting for their evolution. The geochemical attributes of the Archean volcanic and sedimentary rocks are also broadly analogous to those of Phanerozoic rocks in the Pacific arcs. Furthermore, the Soudan-Bigfork area is typical of Archean greenstone belts throughout the southern Superior Province. Although it differs in detail from other belts, it possesses the basic geological and geochemical attributes that characterize Archean greenstone belts as a whole. The analogy between greenstone belts and volcanic arcs has been developed in detail by others (e.g., Taira and others, 1992), and the general hypothesis that the southern part of the Superior Province

evolved through Late Archean tectonic accretion of volcanic arcs has won wide acceptance (e.g. Card, 1990; Jackson and Fyon, 1991; Mueller and others, 1996).

Given the amount of deformation and disruption that the rocks of the Soudan-Bigfork area have experienced, and the relative paucity of bedrock exposure, it is virtually impossible to establish the surviving tectonic subenvironments of the original arc complex with any degree of precision. Geological and geochemical attributes suggest that the lower volcanic unit of the Soudan belt was originally fairly close to eruptive centers, in that the volcanic products were mainly calc-alkalic and involved a compositional range characteristic of arc volcanism. Furthermore, the sedimentary facies of associated dacitic wackes and coarser volcaniclastic rocks suggest deposition on submarine slopes near volcanic islands. The upper volcanic unit in the Soudan belt is predominantly tholeiitic basalt that is very similar geochemically to present-day MORB. Whether the upper volcanic unit is Archean MORB, or the product of back-arc spreading, or represents mafic melts erupted in the early stages of arc volcanism, cannot be determined from available data.

The volcanic rocks of the Newton belt are mainly tholeiitic basalt that in part is somewhat more magnesian than typical tholeiites of the Upper member of the Ely Greenstone and Sherry Lake sequences of the Soudan belt. This slightly more primitive character, together with the local presence of differentiated mafic sills, could be interpreted to favor a back-arc origin for some of the Newton-belt rocks. The evidence is not compelling, however, and the back-arc interpretation must be regarded as very tentative. In general, the poorly exposed, heavily faulted Newton belt requires further documentation and reinterpretation; additional data from core drilling would be welcome and potentially illuminating.

The time interval in which Archean subduction and arc accretion occurred in the Soudan-Bigfork area is not well constrained. U-Pb zircon data from the Giants Range batholith bracket D_2 deformation between 2685 and 2669 Ma (Boerboom and Zartman, 1993), but there are no reliable geochronologic data on the depositional ages of prebatholith volcanic or sedimentary rocks. D_2 is bracketed between 2692 and 2681 Ma in the Shebandowan greenstone belt in Ontario, which is essentially on strike with, and nearly connects to, the Vermilion district of Minnesota (Corfu and Stott, 1986; Williams and others, 1991). A felsic sill within the older volcanic succession in the Shebandowan belt is dated reliably at 2733 Ma. This age may or may not be applicable to the volcanic succession in the western Vermilion district or the Soudan-Bigfork area.

INFERENCES PERTINENT TO MINERAL EXPLORATION

The following points relative to mineral potential and mineral exploration strategies have been made piecemeal throughout the foregoing text. We summarize them here for easy reference.

1. In the Soudan belt, the lower volcanic unit is predominantly calc-alkalic basalt that passes upward into calc-alkalic andesite and dacite. Oxide iron-formation is increasingly abundant toward the top of this unit. The upper volcanic unit, and also the thin mafic sequences interstratified or tectonically imbricated with turbidites that are laterally equivalent to (or overlie) the upper volcanic unit, are chiefly tholeiitic flows comparable in composition to modern seafloor and back-arc basalts. The basaltic rocks in all Soudan-belt sequences are characterized by very low background values of gold, typically less than .002 ppm.

2. The sequences of basaltic volcanic rocks in the Newton belt are predominantly tholeiitic. Basaltic volcanic rocks in the Deer Lake sequence are somewhat more geochemically primitive than the rest; a few samples are basaltic komatiites (Fig. 16). Gold background is typically very low in all Newton-belt mafic volcanic rocks except for those in the Thistledew Lake and Joy Lake sequences. Basalts in those two sequences are marginally more auriferous, with background gold values about 3 to 10 times the values found in other Newton-belt basalts.

3. The kilometer-thick sequence of dacite-derived sedimentary rocks (Lake Vermilion Formation) in the Soudan belt bears some resemblance to the thick sedimentary sequences in the Abitibi subprovince in Quebec. Detailed comparisons should be made between the Lake Vermilion Formation and the rocks of Abitibi sedimentary cycles 1 and 3, particularly in terms of the relationships among sedimentation, transcurrent faulting, and veining (Mueller and others, 1996). Geochemically, the sedimentary rocks of the Soudan belt and the rocks of Abitibi cycles 1 and 3 are very similar. If the analogy between rock sequences of the Soudan-Bigfork area and the Abitibi subprovince could be proven, it would enhance the Mud Creek shear zone as an exploration target for sediment-hosted mesothermal gold deposits of the Destor-Porcupine type.

4. Cherty oxide-facies iron-formation units in both the Soudan and Newton belts contain rare earth element abundances that suggest chemical deposition in submarine environments distal from hydrothermal vents (Fig. 25). This accords with the very low background abundances of Cu, Au, Zn, Pb, and S in these rocks [Table Ap(21)]. The sulfide-facies iron-formation that is elsewhere associated with syngenetic and epigenetic gold deposits (Kerswill, 1996) appears to be rare in the Soudan-Bigfork area. Throughout the Soudan and Newton belts, the oxide-facies iron-formation rocks are singularly devoid of trace metals and sulfur, and therefore would not appear to be particularly inviting intrinsic targets for hosting either syngenetic or epigenetic gold deposits. They may, however, have exploration value as guides for locating laterally equivalent, unexposed sulfide-facies rocks.

5. The differentiated gabbro-peridotite sills of the Deer Lake Complex contain subeconomic amounts of Cu-Ni sulfide minerals. The sills are similar in some respects to intrusions elsewhere in the world that contain platinum-group minerals (PGMs). Sills of the Deer Lake Complex merit serious study, using modern geochemical concepts and methods (Naldrett and others, 1990; Lightfoot, 1995) to determine their potential as a target for PGM exploration. In addition, the Deer Lake Complex and its volcanic envelope deserve further consideration as an environment favorable for VMS deposition.

6. The dacite porphyry intrusions and associated dacite flows of the Soudan-Bigfork area have geochemical attributes that place them in the least-favorable category among Superior Province felsites for hosting massive sulfide deposits of economic size and grade (Lesher and others, 1986). As a group, they are less siliceous, less potassic, and less evolved in other geochemical respects than the felsites that host economic massive-sulfide deposits in volcanic belts in Canada. Although the geochemical criteria used to evaluate the potential of felsic rocks for hosting massive-sulfides are not infallible, the paucity of more highly evolved felsite in the Soudan belt may well account for the paucity of VMS discoveries in more than 130 years of exploration effort. The geochemical characteristics of felsic rocks in the Newton belt are not well known, owing to poor exposure and a limited sample base.

7. Lamprophyric rocks in the Soudan-Bigfork area are all "ordinary lamprophyres" in that they contain ordinary rock-forming mafic minerals plus plagioclase and lack feldspathoids, melilite, and exotic trace phases. They are divisible into high-Cr (more than 450 ppm Cr) and low-Cr (less than 450 ppm Cr) subtypes that contain or lack normative olivine, respectively. None of the analyzed lamprophyres contains gold above low background levels [Table Ap(24)]. Nevertheless, some significant lode-gold deposits are closely associated with sheared lamprophyres in other Archean cratons (particularly in Western Australia), which suggests that further attention should be paid to sheared lamprophyre bodies in Minnesota. In that respect, the boudin-like lamprophyre bodies mapped near Wahlsten in the Soudan belt would seem to be inviting exploration targets.

8. The Soudan-Bigfork area possesses many structural and lithologic attributes that in general are associated with metallic ore deposits elsewhere in Archean greenstone belts. The area contains a diversity of volcanic rock types broadly characteristic of a convergent-margin tectonic environment (volcanic arcs and related tectonic elements) and has a deformational history that includes multiple folding and faulting events, which has produced structural conditions generally favorable for the localization of epithermal and mesothermal deposits. In detail, however, the volcanic rocks of the Soudan belt possess geochemical attributes that are not particularly favorable for the development of significant ore deposits. The belt lacks the magnesian tholeiites and komatiites frequently associated with productive lode-gold camps, and contains abundant, thick sections of normal ocean-floor tholeiite and arc-related calc-alkalic basalts that are impoverished in intrinsic tenor of gold. Moreover, the felsites of the belt are not of optimum composition for hosting significant VMS deposits, as summarized in item 6 above. The Newton belt, on the other hand, does contain more primitive mafic sequences that are marginally more auriferous than mafic sequences in the Soudan belt. The geochemical potential of the felsic rocks of the Newton belt for hosting VMS deposits is not well defined and thus could be considerable. On this basis it would appear that exploration in the heavily faulted, poorly exposed Newton belt might prove rewarding, despite the inherent difficulties presented by relatively thick overburden.

ACKNOWLEDGMENTS

The authors acknowledge with thanks the assistance of Steven Hauck with database structure and other technical input, and the scrupulous editorial work of Kate Pound.

REFERENCES CITED

Arth, J.G., and Hanson, G.N., 1975, Geochemistry and origin of the early Precambrian crust of northeastern Minnesota: Geochimica et Cosmochimica Acta, v. 39, p. 325-362.

Barley, M.E., and Groves, D.I., 1992, Supercontinent cycles and the distribution of metal deposits through time: Geology, v. 20, p. 291-294.

Barnes, S.J., Lesher, C.M., and Keays, R.R., 1995, Geochemistry of mineralised and barren komatiites from the Perseverance nickel deposit, Western Australia: Lithos, v. 34, p. 209-234.

Barrie, C.T., Gorton, M.P., Naldrett, A.J., and Hart, T.R., 1991, Geochemical constraints on the petrogenesis of the Kamiskotia gabbroic complex and related basalts, western Abitibi subprovince, Ontario, Canada: Precambrian Research, v. 50, p. 173-199.

Bau, M., and Moller, P., 1993, Rare earth element systematics of the chemically precipitated component in Early Precambrian iron formations and the evolution of the terrestrial atmosphere-hydrosphere-lithosphere system: Geochimica et Cosmochimica Acta, v. 57, p. 2239-2249.

Berkley, J.L., 1972, The geology of the Deer Lake Gabbro-Peridotite Complex, Itasca County, Minnesota: M.A. thesis, University of Missouri, Colombia, 107 p.

Berkley, J.L., and Himmelberg, G.R., 1978, Cumulus mineralogy and petrology of the Deer Lake Complex, Itasca County, Minnesota, Part A *of* Geology of the Deer Lake Complex, Itasca County, Minnesota: Minnesota Geological Survey Report of Investigations 20, p. A1-18.

Boerboom, T.J., and Zartman, R.E., 1993, Geology, geochemistry, and geochronology of the central Giants Range batholith, northeastern Minnesota: Canadian Journal of Earth Sciences, v. 30, p. 2510-2522.

Boyle, R.W., 1979, The geochemistry of gold and its deposits: Geological Survey of Canada Bulletin 280, 584 p.

Camire, G.E., La Fleche, M.R., and Ludden, J.N., 1993, Archean metasedimentary rocks from the northwestern Pontiac Subprovince of the Canadian Shield: Chemical characterization, weathering and modelling of the source areas: Precambrian Geology, v. 62, p. 285-305.

Card, K.D., 1990, A review of the Superior Province of the Canadian Shield, a product of Archean accretion: Precambrian Research, v. 48, p. 99-156.

Card, K.D., Poulsen, K.H., and Robert, F., 1989, The Archean Superior Province of the Canadian Shield and its lode gold deposits, *in* Keays, R.R., Ramsay, W.R.H., and Groves, D.I., eds., The geology of gold deposits: The perspective in 1988: Economic Geology Monograph 6, p. 19-36.

Chown, E.H., Daigneault, R., Mueller, W., and Mortensen, J., 1992, Tectonic evolution of the northern volcanic zone, Abitibi belt, Quebec: Canadian Journal of Earth Sciences, v. 29, p. 2211-2225.

Clements, J.M., 1903, The Vermilion iron-bearing district of Minnesota: U.S. Geological Survey Monograph 45, 463 p.

Clift, P.D., 1995, Volcaniclastic sedimentation and volcanism during the rifting of western Pacific backarc basins, *in* Taylor, B., and Natland, J., eds., Active margins and marginal basins of the western Pacific: American Geophysical Union Geophysical Monograph 88, p. 67-96.

Corfu, F., and Stott, G.M., 1986, U-Pb ages for late magmatism and regional deformation in the Shebandowan belt, Superior Province, Canada: Canadian Journal of Earth Sciences, v. 23, p. 1075-1082.

Crocket, J.H., 1981, Geochemistry of the platinum group elements, *in* Cabri, L.J., ed., Platinum group elements: Mineralogy, geology, recovery: Canadian Institute of Mining and Metallurgy Special Volume 23, p. 47-64.

DiTullio, L., and Bryne, T., 1990, Deformation paths in the shallow levels of an accretionary prism: The Eocene Shimanto belt of southwest Japan: Geological Society of America Bulletin, v. 102, p. 1420-1438.

Englebert, J.A., and Hauck, S.A., eds., 1991, Bedrock geochemistry of Archean rocks in northern Minnesota: University of Minnesota, Natural Resources Research Institute Technical Report NRRI/TR-91/12, 200 p., 6 floppy diskettes in pockets, separate portfolio containing 17 folded maps.

Galley, A.G., 1996, Geochemical characteristics of subvolcanic intrusions associated with Precambrian massive sulphide districts, *in* Wyman, D.A., ed., Trace element geochemistry of volcanic rocks: Applications for massive sulphide exploration: Geological Association of Canada Short Course Notes, v. 12. p. 239-278.

Gill, J.B., Hiscott, R.N., and Vidal, P., 1994, Turbidite geochemistry and evolution of the Izu-Bonin arc and continents: Lithos, v. 33, p. 135-168.

Green, J.C., 1970, Lower Precambrian rocks of the Gabbro Lake quadrangle, northeastern Minnesota: Minnesota Geological Survey Special Publication Series SP-13, 96 p.

Green, J.C., and Schulz, K.J., 1977, Iron-rich basaltic komatiites in the early Precambrian Vermilion District, Minnesota: Canadian Journal of Earth Sciences, v. 14, p. 2181-2192.

Grunsky, E.C., Easton, R.M., Thurston, P.C., and Jensen, L.S., 1992, Characterization and statistical classification of Archean volcanic rocks of the Superior Province using major-element geochemistry, *in* Thurston, P.C., Williams, H.R., Sutcliffe, R.H., and Stott, G. M., eds., Geology of Ontario: Ontario Geological Survey Special Volume 4, Part 2, p. 1397-1438.

Hedenquist, J.W., 1987, Mineralization associated with volcanic-related hydrothermal systems in the Circum-Pacific basin, *in* Horn, M.K., ed., Transactions of the fourth Circum-Pacific energy and mineral resources conference [Singapore]: Circum-Pacific Council for Energy and Mineral Resources, American Association of Petroleum Geologists, p. 513-524.

Ho, S.E., Groves, D.I., and Bennett, J.M., eds., 1990, Gold deposits of the Archean Yilgarn Block, Western Australia: Nature, genesis and exploration guides: Perth, University of Western Australia, Geology Department (Key Centre) and University Extension Publication 20, 407 p.

Hopson, C.A., 1964, The crystalline rocks of Howard and Montgomery Counties *in* The geology of Howard and Montgomery Counties: Baltimore, Maryland Geological Survey, p. 27-215.

Hudleston, P.J., 1976, Early deformational history of Archean rocks in the Vermilion district, northeastern Minnesota: Canadian Journal of Earth Sciences, v. 13, p. 579-592.

Hudleston, P.J., Schultz-Ela, D., and Southwick, D.L., 1988, Transpression in an Archean greenstone belt, northern Minnesota: Canadian Journal of Earth Sciences, v. 25, p. 1060-1068.

Jackson, S.L., and Fyon, J.A., 1991, The western Abitibi subprovince in Ontario, *in* Thurston, P.C., Williams, H.R., Sutcliffe, R.H., and Stott, G. M., eds., Geology of Ontario: Ontario Geological Survey Special Volume 4, Part 1, p. 405-482.

Jahn, Bor-Ming, Shih, Chi-Yu, and Murthy, V.R., 1974, Trace element geochemistry of Archean volcanic rocks: Geochimica et Cosmochimica Acta, v. 38, p. 611-627.

Jensen, L.A., 1976, A new cation plot for classifying subalkalic volcanic rocks: Ontario Division of Mines Miscellaneous Paper 66, 22 p.

Jirsa, M.A., 1988, Geologic map of the Sherry Lake quadrangle, Itasca County, Minnesota: Minnesota Geological Survey Miscellaneous Map Series M-64, scale 1:24,000.

Jirsa, M.A., 1990, Bedrock geologic map of northeastern Itasca County, Minnesota: Minnesota Geological Survey Miscellaneous Map Series M-68, scale 1:48,000.

Jirsa, M.A., 1998, Bedrock geologic map of the Midway area, St. Louis County, Minnesota: Minnesota Geological Survey Miscellaneous Map Series M-86, scale 1:12,000.

Jirsa, M.A., and Boerboom, T.J., 1990, Bedrock geologic map of parts of Koochiching, Itasca, and Beltrami Counties, north-central Minnesota: Minnesota Geological Survey Miscellaneous Map Series M-67, scale 1:250,000.

Jirsa, M.A., Boerboom, T.J., Chandler, V.W., and McSwiggen, P.L., 1991, Bedrock geologic map of the Cook to Side Lake area, St. Louis and Itasca Counties, Minnesota: Minnesota Geological Survey Miscellaneous Map Series M-75, scale 1:48,000.

Jirsa, M.A., Boerboom, T.J., and Morey, G.B., 1998, Bedrock geologic map of the Virginia Horn, Mesabi Iron Range, St. Louis County, Minnesota: Minnesota Geological Survey Miscellaneous Map Series M-85, scale 1:48,000.

Jirsa, M.A., Southwick, D.L., and Boerboom, T.J., 1992, Structural evolution of Archean rocks in the western Wawa subprovince, Minnesota: Refolding of pre-cleavage nappes during D_2 transpression: Canadian Journal of Earth Sciences, v. 29, p. 2146-2155.

Kerrich, R., 1989, Geodynamic setting and hydraulic regimes: Shear zone hosted mesothermal gold deposits, *in* Bursnall, J.T., ed., Mineralization and shear zones: Geological Association of Canada Short Course Notes v. 6, p. 89-128.

Kerrich, R., and Wyman, D.A., 1990, Geodynamic setting of mesothermal gold deposits: An association with accretionary tectonic regimes: Geology, v. 18, p. 882-885.

Kerrich, R., and Wyman, D.A., 1996, The trace element systematics of igneous rocks in mineral exploration: An overview, *in* Wyman, D.A., ed., Trace element geochemistry of volcanic rocks: Applications for massive sulphide exploration: Geological Association of Canada Short Course Notes, v. 12, p. 1-50.

Kerswill, J.A., 1996, Iron-formation-hosted stratabound gold, *in* Eckstrand, O.R., Sinclair, W.D., and Thorpe, R.I., eds., Geology of Canadian mineral deposit types: Geological Society of America, The geology of North America, v. P-1, p. 367-382.

Kimura, G., Koga, K., and Fujioka, K., 1989, Deformed soft sediments at the junction between the Mariana and Yap trenches: Journal of Structural Geology, v. 11, p. 463-472.

Knipe, R.J., 1986, Microstructural evolution of vein arrays in Deep Sea Drilling Project cores from the Japan Trench, Leg 57, *in* Moore, J.C., ed., Structural fabrics in deep sea drilling project core from forearcs: Geological Society of American Memoir 166, p. 75-87.

La Fleche, M.R., and Camire, G., 1996, Geochemistry and provenance of metasedimentary rocks from the Archean Golden Pond sequence (Casa Berardi mining district, Abitibi subprovince): Canadian Journal of Earth Sciences, v. 33, p. 676-690.

La Fleche, M.R., Dupuy, C., and Dostal, J., 1992, Tholeiitic volcanic rocks of the late Archean Blake River Group, southern Abitibi greenstone belt: Origin and geodynamic implications: Canadian Journal of Earth Sciences, v. 29, p. 1448-1458.

Lesher, C.M., Goodwin, A.M., Campbell, I.H., and Gorton, M.P., 1986, Trace-element geochemistry of ore-associated and barren felsic metavolcanic rocks in the Superior Province, Canada: Canadian Journal of Earth Sciences, v. 23, p. 222-237.

Lesher, C.M., and Stone, W.E., 1996, Exploration geochemistry of komatiites, *in* Wyman, D.A., ed., Trace element geochemistry of volcanic rocks: Applications for massive sulphide exploration: Geological Association of Canada Short Course Notes, v. 12, p. 153-204.

Li, C., Naldrett, A.J., Coats, C.J.A., and Johannssen, P., 1992, Platinum, palladium, gold, and copper-rich stringers at the Strathcona mine, Sudbury: Their enrichment by fractionation of a sulfide liquid: Economic Geology, v. 87, p. 1584-1598.

Lightfoot, P.C., 1995, Geochemistry of the Nipissing Gabbro: Source and mineral potential: Canadian Mineralogist, v. 33, p. 934-935.

Lightfoot, P.C., DeSouza, H., and Doherty, W., 1993, Differentiation and source of the Nipissing Diabase intrusions, Ontario, Canada: Canadian Journal of Earth Sciences, v. 30, p. 1123-1140.

Lightfoot, P.C., and Naldrett, A.J., 1989, Assimilation and crystallization in basic magma chambers: Trace-element and Nd-isotopic variations in the Kerns sill, Nipissing diabase province, Ontario: Canadian Journal of Earth Sciences, v. 26, p. 737-754.

MacKay, M.E., and Moore, G.F., 1990, Variation in deformation of the south Panama accretionary prism: Response to oblique subduction and trench sediment variation: Tectonics, v. 9, p. 683-698.

Marsaglia, K.M., Boggs, S., Jr., Clift, P.D., Seyedolali, A., and Smith, R., 1995, Sedimentation in western Pacific backarc basins: New insights from recent ODP drilling, *in* Taylor, B., and Natland, J., eds., Active margins and marginal basins of the western Pacific: American Geophysical Union Geophysical Monograph 88, p. 291-314.

McLimans. R.K., 1972, Granite-bearing conglomerates in the Knife Lake Group, Vermilion District, *in* Sims, P.K., and Morey, G.B., eds., Geology of Minnesota: A centennial volume: Minnesota Geological Survey, p. 91-97.

McNeil, A.M., and Kerrich, R., 1986, Archean lamprophyre dykes and gold mineralization, Matheson, Ontario: The conjunction of LILE-enriched magmas, deep crustal structures and Au concentration: Canadian Journal of Earth Sciences, v. 23, p. 324-343.

Metais, D., and Chayes, F., 1963, Varieties of lamprophyre: Annual Report of the Geophysical Laboratory, Carnegie Institute Yearbook 62, p. 156-157.

Middlemost, E.A.K., 1985, Magmas and magmatic rocks: New York, N.Y., Longman, 266 p.

Mitchell, A.H.G., and Garson, M.S., 1981, Mineral deposits and global tectonic settings: San Diego, California, Academic Press, 405 p.

Mitchell, R.H., and Bergman, S.C., 1991, Petrology of lamproites: New York, N.Y., Plenum Press, 447 p.

Morey, G.B., 1996, Geologic map of Minnesota, bedrock geology: Minnesota Geological Survey State Map Series S-20, digital version 2, scale 1:1,000,000.

Morey, G.B., Green, J.C., Ojakangas, R.W., and Sims, P.K., 1970, Stratigraphy of the Lower Precambrian rocks in the Vermilion District, northeastern Minnesota: Minnesota Geological Survey Report of Investigations 14, 33 p.

Mueller, W.U., Daigneault, R., Mortensen, J.K., and Chown, E.H., 1996, Archean terrane docking: Upper crust collision tectonics, Abitibi greenstone belt, Quebec, Canada: Tectonophysics, v. 265, p. 127-150.

Mueller, W.U., and Donaldson, J.A., 1992, Development of sedimentary basins in the Archean Abitibi belt, Canada: An overview: Canadian Journal of Earth Sciences, v. 29, p. 2249-2265.

Naldrett, A.J., 1989, Magmatic sulfide deposits: Oxford, England, Oxford University Press, 186 p.

Naldrett, A.J., Brugmann, G.E., and Wilson, 1990, Models for the concentration of PGE in layered intrusions: Canadian Mineralogist, v. 28, p. 389-408.

Nesbitt, H.W., and Young, G.M., 1982, Early Proterozoic climates and plate motions inferred from major element chemistry of lutites: Nature, v. 299, p. 715-717.

Ojakangas, R.W., 1972a, Archean volcanogenic graywackes of the Vermilion District, Northeastern Minnesota: Geological Society of America Bulletin, v. 83, p. 429-442.

Ojakangas, R.W., 1972b, Graywackes and related rocks of the Knife Lake Group and Lake Vermilion Formation, Vermilion District, *in* Sims, P.K., and Morey, G.B., eds., Geology of Minnesota: A centennial volume: Minnesota Geological Survey, p. 82-90.

Ojakangas, R.W., 1985, Review of Archean clastic sedimentation, Canadian Shield: Major felsic volcanic contribution to turbidite and alluvial fan-fluvial facies associations, *in* Ayres, L.D., Thurston, P.C., Card, K.D., and Weber, W., eds., Evolution of Archean supracrustal sequences: Geological Association of Canada Special Paper 28, p. 23-47.

Ontario Geological Survey, 1992, Chart A - Archean tectonic assemblages, plutonic suites and events in Ontario: Ontario Geological Survey Map 2579.

Pearce, J.A., 1996, A user's guide to basalt discrimination diagrams, *in* Wyman, D.A., ed., Trace element geochemistry of volcanic rocks: Applications for massive sulphide exploration: Geological Association of Canada Short Course Notes, v. 12. p. 79-113.

Pearce, J.A., and Cann, J.R., 1973, Tectonic setting of basic volcanic rocks determined using trace element analyses: Earth and Planetary Science Letters, v. 19, p. 290-300.

Picard, C., Amosse, J., Piboule, M., and Giovenazzo, D., 1996, Physical and chemical constraints on platinum-group element behavior during crystallization of a basaltic komatiite liquid: Example of the Proterozoic Delta sill, New Quebec, Canada: Economic Geology, v. 90, p. 2287-2302.

Platt, J.P., 1990, Thrust mechanics in highly overpressured accretionary wedges: Journal of Geophysical Research, v. 95, p. 9025-9034.

Poulsen, K.H., 1996, Lode gold, *in* Eckstrand, O.R., Sinclair, W.D., and Thorpe, R.I., eds., Geology of Canadian mineral deposit types: Geological Society of America, The geology of North America, v. P-1, p. 323-328.

Ramsey, J.G., and Huber, M.I., 1987, The techniques of modern structural geology. Volume 2: Folds and fractures: London, Academic Press, p. 309-700.

Ripley, E.M., 1978, Sulfide minerals in the layered sills of the Deer Lake Complex, Itasca County, Minnesota, Part B *of* Geology of the Deer Lake Complex, Itasca County, Minnesota: Minnesota Geological Survey Report of Investigations 20, p. B1- B32.

Ripley, E.M., 1979, Sulfide petrology of basal chilled margins in layered sills of the Archean Deer Lake Complex, Minnesota: Contributions to Mineralogy and Petrology, v. 69, p. 345-354.

Ripley, E.M., Rao, B.V., and Berkley, J.L., 1982, Mineralogical and chemical variations within layered sills of the Deer Lake Complex, Minnesota: Contributions to Mineralogy and Petrology, v. 80, p. 230-239.

Robert, F., 1996, Quartz-carbonate vein gold, *in* Eckstrand, O.R., Sinclair, W.D., and Thorpe, R.I., eds., Geology of Canadian mineral deposit types: Geological Society of America, The geology of North America, v. P-1, p. 350-366.

Rock, N.M.S., 1987, The nature and origin of lamprophyres: an overview, *in* Fytton, J.G., and Upton, B.G.J., eds., Alkaline igneous rocks: Geological Society of London Special Publication 30, p. 191-226.

Rock, N.M.S., and Groves, D.I., 1988a, Do lamprophyres carry gold as well as diamonds?: Nature, v. 332, p. 253-255.

Rock, N.M.S., and Groves, D.I., 1988b, Can lamprophyres resolve the genetic controversy over mesothermal gold deposits?: Geology, v. 16, p. 538-541.

Rock, N.M.S., Hallberg, J.A., Groves, D.I., and Mather, P.J., 1988, Archaean lamprophyres in the goldfields of the Yilgarn block, Western Australia: New indications of their widespread distribution and significance, *in* Ho, S.E., and Groves, D. I., eds., Advances in understanding Precambrian gold deposits, volume II: Perth, University of Western Australia, Geology Department and University Extension Publication 12, p. 245-275.

Sawkins, F.J., 1990, Metal deposits in relation to plate tectonics (2nd ed.): New York, N.Y., Springer-Verlag, 461 p.

Schultz-Ela, D.D., and Hudleston, P.J., 1991, Strain in an Archean greenstone belt of Minnesota: Tectonophysics, v. 190, p. 233-268.

Schulz, K.J., 1980, The magmatic evolution of the Vermilion greenstone belt, NE Minnesota: Precambrian Research, v. 11, p. 215-245.

Schulz, K.J., 1982, Magnesian basalts from the Archean terrains of Minnesota, *in* Arndt, N.T., and Nisbet, E.G., eds., Komatiites: London, Allen and Unwin, p. 171-186.

Sillitoe, R.H., 1989, Gold deposits in western Pacific island arcs; the magmatic connection, *in* Keays, R.R., Ramsay, W.R.H., and Groves, D.I., eds., The geology of gold deposits: The perspective in 1988: Economic Geology Monograph 6, p. 274-291.

Sims, P.K., 1972a, Vermilion district and adjacent areas, *in* Sims, P.K., and Morey, G.B., eds., Geology of Minnesota: A centennial volume: Minnesota Geological Survey, p. 49-62.

Sims, P.K., 1972b, Metavolcanic and associated synvolcanic rocks in Vermilion district, *in* Sims, P.K., and Morey, G.B., eds., Geology of Minnesota: A centennial volume: Minnesota Geological Survey, p. 63-75.

Sims, P.K., and Southwick, D.L., 1980, Geologic map of the Soudan quadrangle, St. Louis County, Minnesota: U.S. Geological Survey Geologic Quadrangle Map GQ-1540, scale 1:24,000.

Sims, P.K., and Southwick, D.L., 1985, Geologic map of Archean rocks, western Vermilion district, northern Minnesota: U.S. Geological Survey Miscellaneous Investigations Map I-1527, scale 1:48,000.

Southwick, D.L., comp., 1993, Geologic map of Archean bedrock, Soudan-Bigfork area, northern Minnesota: Minnesota Geological Survey Miscellaneous Map Series M-77, scale 1:100,000.

Southwick, D.L., Schulz, K.J., Ojakangas, R.W., Bauer, R.L., Shirey, S.B., and Hanson, G.N., 1993, Greenstone-granite terrane, *in* The Lake Superior region and Trans-Hudson orogen, chap. 2 *of* Reed, J.C., Jr., and others, eds., Precambrian: Conterminous U.S.: Geological Society of America, The Geology of North America, v. C-2, p. 18–30.

Stolz, A.J., 1995, Geochemistry of the Mount Windsor volcanics: Implications for the tectonic setting of Cambro-Ordovician volcanic-hosted massive sulfide mineralization in northeastern Australia: Economic Geology, v. 90, p. 1080-1097.

Streckeisen, A.L., 1980, Classification and nomenclature of volcanic rocks, lamprophyres, carbonatites and melilitic rocks, IUGS Subcommission on the Systematics of Igneous Rocks: Geologische Rundschau, v. 69, p. 194-207.

Sun, S.S., and McDonough, W.F., 1989, Chemical and isotopic systematics of oceanic basalts: Implications for mantle composition and processes, *in* Saunders, A.D., and Norry, M.J., eds., Magmatism in the ocean basins: Geological Society [London] Special Publication 42, p. 313-345.

Sutcliffe, R.H., Sweeny, J.M., and Edgar, A. D., 1989, The Lac des Iles Complex, Ontario: Petrology and platinum-group-elements mineralization in an Archean mafic intrusion: Canadian Journal of Earth Sciences, v. 26, p. 1408-1427.

Swinden, H.S., Jenner, G.A., Kean, B.F., and Evans, D.T.W., 1989, Volcanic rock geochemistry as a guide for massive sulphide exploration in central Newfoundland: Newfoundland Department of Mines, Geological Survey Branch Current Research Report 89-1, p. 201-219.

Taira, A., Pickering, K.T., Windley, B.F., and Soh, W., 1992, Accretion of Japanese Island arcs and implications for the origin of Archean greenstone belts: Tectonics, v. 11, p. 1224-1244.

Thurston, P.C., and Chivers, K.M., 1990, Secular variation in greenstone belt development, emphasizing the Superior Province, Canada: Precambrian Research, v. 46, p. 21-58.

Welsh,, J.L., Englebert, J.A., and Hauck, S.A., 1991, General geology, structure, and geochemistry of Archean rocks of the Virginia Horn area, northeastern Minnesota, *in* Englebert, J.A., and Hauck, S.A., eds., Bedrock geochemistry of Archean rocks in northern Minnesota: University of Minnesota, Natural Resources Research Institute Technical Report NRRI/TR-91/12, Part 4, p. 100-137.

Williams, H.R., Stott, G.M., Heather, K.B., Muir, T.L., and Sage, R.P., 1991, Wawa subprovince, *in* Thurston, P.C., Williams, H.R., Sutcliffe, R.H., and Stott, G. M., eds., Geology of Ontario: Ontario Geological Survey Special Volume 4, Part 1, p. 485-539.

Wimmenauer, W., 1973, Lamprophyre, Semilamprophyre, und anchibasaltische Ganggesteine: Fortschritte der Mineralogie, B. 51, H. 1, p. 3-67.

Wright, T.L., and Doherty, P.C., 1970, A linear programming and least squares computer method for solving petrologic mixing problems: Geological Society of America Bulletin, v. 81, p. 1995-2008.

APPENDIX

Introduction to the Appendix Tables

Analyses presented in the appendix tables were obtained from several different laboratories over a span of years. For most samples, details of the methods used, the location of the laboratory and the name of the original analyst are available. For the rest, only the analytical data survives. The following outline of analysts and methods supplies most of the basic facts, but is not an exhaustive list of methods used. The number preceding each entry corresponds to the "analyst number" provided in the footnotes for each appendix table. Further details about a particular analysis can be obtained by contacting the authors. In the appendix tables, individual analyses are numbered sequentially (1 through 156). Each number corresponds with a footnote that contains the original sample number, a brief sample description, and the sample location.

The appendix tables present the major elements as weight-percent oxides in standard format. Where the total for the major oxides falls below 96 wt. percent, it is italicized. The concentration of minor elements, trace elements and rare earth elements is reported in parts per million (ppm) by weight. The H_2O entry is total water (i.e. H_2O+ plus H_2O) if both were reported in the original analysis. Where original analyses reported volatiles as "loss on ignition" (LOI), the H_2O entry is presented as LOI.

Analysts and Analytical Methods

(1) XRAL Laboratories, Don Mills, Ontario, Canada
Major elements: X-ray fluorescence spectrometry (XRF); wet chemistry for FeO, H_2O, CO_2
Minor and trace elements: Inductively coupled plasma spectrometry (ICP); direct current plasma spectrometry (DCP); induced nuclear neutron activation (INNA), as appropriate to the element and the technology available at the date of analysis
Rare earth elements: ICP, INNA

(2) U.S. Geological Survey Rock Analysis Laboratories, Reston, Virginia
Major elements: XRF, wet chemistry
Minor and trace elements: ICP, INNA
Rare earth elements: INNA

(3) Scott E. Robinson, Department of Geology, University of North Dakota, Grand Forks, North Dakota
Major elements: XRF
Minor and trace elements: XRF

(4) K. Ramlal, Department of Geology, University of Manitoba, Winnipeg, Manitoba, Canada
Major elements: XRF, wet chemistry

(5) P. O'Day, Department of Geology, Cornell University, Ithaca, New York
Major elements: XRF, wet chemistry
Minor and trace elements: INNA
Rare earth elements: INNA

(6) J.G Arth, Jr., Department of Earth and Space Sciences, State University of New York at Stony Brook, Stony Brook, New York

Major elements: Atomic absorption (AA), XRF, wet chemistry
Minor and trace elements: XRF, isotope dilution/ mass spectrometry
Rare earth elements: Isotope dilution/mass spectrometry

(7) Chemex, Inc., Sparks, Nevada

Major elements: XRF, wet chemistry
Minor and trace elements: ICP, INNA
Rare earth elements: ICP, INNA

(8) Acme Laboratories, Inc., Vancouver, British Columbia, Canada

Major elements: XRF, wet chemistry
Minor and trace elements: ICP, INNA
Rare earth elements: ICP, INNA

(9) R. Knurr, Geochemistry Laboratory, Department of Geology and Geophysics, University of Minnesota, Minneapolis, Minnesota

Major elements: Direct current argon plasma/optical emission spectrometry (DCAP/OES), wet chemistry
Minor and trace elements: DCAP/OES
Rare earth elements: DCAP/OES

System used to Describe Sample Locations

Sample locations are given in the TRS/ABCD system routinely used by the Minnesota Geological Survey for locating data points of all types throughout the state. The system is a shorthand variant of the familiar Public Land Survey System, or township-range-section system, that has been employed for legal land descriptions since the early days of statehood. In Minnesota, almost all townships are measured north of a zero standard parallel and west of a zero standard meridian. The exceptions, in extreme northeastern Minnesota, amount to only a few square miles. Thus a township is legally described as T. (Y) N., R. (X) W. This may be specified in an abbreviated form as Y-X. The traditional quarter system of subdividing townships is cumbersome in several respects and is replaced by a notation in which A=NE1/4, B=NW1/4, C=SW1/4, and D=SE1/4. These apply to all levels of subdivision and are listed in order from the largest to the smallest quadrant pertaining to a location. Thus, a location described traditionally as the NW1/4 of the NW1/4 of the SW1/4 of the NE1/4 of section 11, T. 61 N., R. 25 W. becomes 61-25-11ACBB in the TRS/ABCD notation. This system is used in the appendix-table footnotes.

Electronic Datafiles

The appendix tables are available separately as electronic files. The data can be obtained on floppy disc at a nominal additional cost through the Map and Publications Office of the Minnesota Geological Survey. Alternatively, they may be downloaded through the Minnesota Geological Survey website, http://geolab.geo.umn.edu/mgs. Please see the website or contact the MGS Map and Publications Office for downloading and ordering information.

Table Ap(1). Basaltic rocks, Lower member, Ely Greenstone, Soudan belt

[major elements in weight percent oxides; minor elements in parts per million; —, no data; blank, not calculated]

Sample	1	2	3	4	5	6	7	mean	std. dev.
SiO_2	57.8	54.6	52.1	49.8	50.4	57.3	51.5	53.36	3.25
TiO_2	0.54	0.74	0.75	0.93	0.92	0.83	0.79	0.79	0.13
Al_2O_3	17.2	15.6	14.8	16.3	16.8	17.6	16.3	16.37	0.95
*Fe_2O_3	1.43	0.66	2.13	2.13	1.9	1	1.8	1.58	0.57
†FeO	3.7	5.5	6.2	7.1	7.7	6.4	6.6	6.17	1.29
MnO	0.06	0.19	0.15	0.18	0.14	0.2	0.14	0.15	0.05
MgO	5.61	5.02	6.77	7.95	9.5	3.6	8.2	6.66	2.05
CaO	4.49	4.75	8.47	7.42	4.3	3	3.8	5.18	2.00
Na_2O	4.99	5.11	3.22	2.27	3.8	5.8	2.9	4.01	1.31
K_2O	0.37	0.45	0.12	1.89	0.36	0.4	0.12	0.53	0.61
P_2O_5	0.13	0.15	0.14	0.13	0.17	0.1	0.17	0.14	0.02
CO_2	0.16	2.89	0.98	0.06	0.15	1.1	2.4	1.11	1.14
H_2O	2.5	3.1	2.8	1.6	4.85	3.22	5.25	3.33	1.29
Total	98.98	98.76	98.63	97.76	100.99	100.55	99.97	99.38	
§FeO(t)	4.99	6.09	8.12	9.02	9.41	7.30	8.22	7.59	
¶Mg#	66.74	59.51	59.81	61.14	64.30	46.80	64.03	61.03	
Rb	5	8	<2	74	5	8	83	31	37
Sr	130	193	116	270	87	66	49	130	78
Ba	143	247	40	313	141	116	467	210	144
Nb	4	10	5	6	<10	<10	<10	6	3
Hf	2.3	3	1.6	1.7	—	—	—	2	1
Zr	85	124	61	62	110	68	127	91	29
Y	12	15	11	11	20	15	22	15	4
Cr	150	54	220	260	—	—	—	171	90
Ni	63	42	88	119	134	169	124	106	44
Cu	69	61	58	57	74	55	37	59	12
Zn	63	211	76	78	96	159	119	115	53
V	143	150	229	276	—	—	—	200	64
La	10	13.2	5.3	5.7	—	—	—	8.55	3.76
Ce	20.6	26.5	10.5	11	—	—	—	17.15	7.78
Nd	10.1	13.3	6.5	7.1	—	—	—	9.25	3.13
Sm	2	2.8	1.6	1.6	—	—	—	2.00	0.57
Eu	0.63	0.74	0.64	0.65	—	—	—	0.67	0.05
Gd	2	2.9	1.7	1.8	—	—	—	2.10	0.55
Tb	0.3	0.5	0.3	0.5	—	—	—	0.40	0.12
Yb	1.1	1.5	1.3	1.2	—	—	—	1.28	0.17
Lu	0.16	0.23	0.2	0.2	—	—	—	0.20	0.03
Au	<.001	0.002	0.002	<.001	—	—	—	0.002	

* Fe_2O_3 calculated on basis of stoichiometry ; † FeO calculated on basis of stoichiometry; § Total measured iron represented as FeO; ¶ Mg# is mol ratio 100Mg/(Mg+Fe) in which Fe is total Fe reported as FeO.

1 - DS-S-511B: Basaltic andesite or andesite, pillowed. Soudan quadrangle, 62-14-29ABBA. Analyst (1).
2 - GB-S-24B: Metabasalt, pillowed, strongly deformed. Soudan quadrangle, 62-15-25BDAB. Analyst (1).
3 - DS-S-779: Metabasalt, massive. Soudan quadrangle, 62-14-19CBBD. Analyst (1).
4 - GB-E-16: Metabasalt, massive, amphibolite grade, near contact with Giants Range batholith, Eagles Nest quadrangle, 62-14-36DDCB. Analyst (1).
5 - S-795: Metabasalt, pillowed, moderately deformed. Soudan quadrangle, 62-14-30DCB. Analyst (2).
6 - S-796: Metabasalt, pillowed, strongly deformed. Soudan quadrangle, 62-14-29CBDD. Analyst (2).
7 - S-82-35: Metabasalt, pillowed, moderately deformed. Soudan quadrangle, 62-15-35BCDD. Analyst (2).

Table Ap(2). Metabasalt and allied rocks, Bear Lake sequence, Soudan belt

[major elements in weight percent oxides; minor elements in parts per million; —, no data; totals below 96 wt. percent are italicized]

Sample	8	9	10	11	12	mean	std. dev.
SiO_2	55.30	57.85	44.73	45.92	53.43	51.45	5.82
TiO_2	0.62	1.03	1.11	0.47	1.06	0.86	0.29
Al_2O_3	15.81	15.14	18.35	14.95	15.16	15.88	1.42
*Fe_2O_3	1.32	1.00	2.55	2.38	1.71	1.79	0.67
†FeO	5.51	6.08	10.18	7.63	7.94	7.47	1.83
MnO	0.13	0.14	0.20	0.17	0.14	0.16	0.03
MgO	3.58	4.43	6.72	11.04	5.07	6.17	2.96
CaO	6.68	6.69	7.39	9.96	7.40	7.62	1.35
Na_2O	5.40	4.56	2.97	1.72	3.14	3.56	1.44
K_2O	1.57	0.31	0.41	0.38	0.29	0.59	0.55
P_2O_5	0.25	0.29	0.32	0.19	0.27	0.26	0.05
CO_2	0.35	—	—	0.00	0.09	0.15	0.18
H_2O	0.74	0.20	0.40	0.50	0.80	0.53	0.25
Total	97.26	97.72	*95.33*	*95.31*	96.50	96.49	
§FeO(t)	6.70	6.98	12.48	9.77	9.48	9.08	
¶Mg#	48.82	53.12	49.01	66.84	48.83	54.79	
Rb	30	5	8	10	8	12	10
Sr	245	130	210	22	200	161	88
Ba	1230	79	58	59	120	309	515
Nb	<20	<20	<20	<20	<20	–	
Hf	2.8	3	2	1	1.9	2	1
Zr	130	123	83	<20	84	105	25
Y	<20	11	<20	<20	<20	11	
Cr	80	146	149	465	160	200	151
Ni	50	76	147	334	89	139	115
Cu	10	56	50	84	38	48	27
Zn	29	124	95	57	87	78	36
V	90	151	197	154	133	145	39
La	9	12	5	2	6	6.80	3.83
Ce	26	30	13	5	19	18.60	10.01
Nd	9	<5	8	<5	8	8.33	0.58
Sm	2.2	3.05	2.3	1.0	2.0	2.11	0.74
Eu	1	0.95	0.8	0.4	0.8	0.79	0.24
Gd	—	—	—	—	—	—	
Tb	<1	<1	<1	<1	<1	—	
Yb	0.8	2	1.9	1.5	0.9	1.42	0.55
Lu	<1.0	<1.0	<1.0	<1.0	<1.0	—	
Au	<.001	<.001	<.001	<.001	<.001	—	

* Fe_2O_3 calculated on basis of stoichiometry; † FeO calculated on basis of stoichiometry;
§ Total measured iron represented as FeO; ¶ Mg# is mol ratio 100Mg/(Mg+Fe) in which Fe is total Fe reported as FeO.

8 - I209AX: Basaltic andesite flow. Sherry Lake quadrangle, 60-23-10CAA. Analyst (7).
9 - I217B: Andesite flow. Horsehead Lake quadrangle, 60-23-22CBC. Analyst (7).
10 - 1020EX: Basaltic andesite flow. Sherry Lake quadrangle, 60-23-22ACB. Analyst (7).
11 - I220X: Metabasalt, pillowed. Horsehead Lake quadrangle, 60-23-28DAA. Analyst (7).
12 - I329B: Basaltic andesite flow, plagioclase-phyric. Horsehead Lake quadrangle, 60-24-13DAB. Analyst (7).

Table Ap(3). Metabasalt and allied rocks from the transition between the Lower member and the Soudan Iron-formation Member of the Ely Greenstone, Soudan belt

[major elements in weight percent oxides; minor elements in parts per million; —, no data; blank, not calculated]

Sample	13	14	15	16	17	18	mean	std. dev.
SiO_2	52.1	53.9	49.3	54.8	51.9	56.5	53.08	2.53
TiO_2	0.71	0.46	0.49	0.93	1.2	0.64	0.74	0.28
Al_2O_3	17.4	15.1	14.6	16.9	20.2	13.5	16.28	2.41
*Fe_2O_3	2.24	1.05	3.74	3.1	0.9	1.3	2.06	1.17
†FeO	5.9	3.9	5.1	5.6	6.2	7.4	5.68	1.17
MnO	0.13	0.12	0.16	0.22	0.12	0.16	0.15	0.04
MgO	6.29	5.93	8.78	3.5	4.3	6.8	5.93	1.87
CaO	6.08	6.1	12.4	9.3	4.7	4.4	7.16	3.10
Na_2O	3.51	5.45	1.96	3.7	5.2	3	3.80	1.33
K_2O	0.79	0.09	0.81	0.59	0.5	0.11	0.48	0.32
P_2O_5	0.15	0.11	0.05	0.09	0.14	0.14	0.11	0.04
CO_2	0.53	4.29	0.12	0.14	1.4	2	1.41	1.59
H_2O	3.1	2.9	1.5	1.06	3.54	4.29	2.73	1.23
Total	98.93	99.4	99.01	99.93	100.3	100.24	99.61	
§FeO(t)	7.92	4.85	8.47	8.39	7.01	8.57	7.53	
¶Mg#	58.64	68.59	64.92	42.67	52.25	58.60	58.43	
Rb	21	<2	34	11	10	<2	19	11
Sr	190	141	184	128	294	86	171	72
Ba	237	85	64	114	80	41	104	70
Nb	5	8	<2	<10	11	<10	8	3
Hf	2.6	5.4	0.8	—	—	—	3	2
Zr	90	95	26	66	150	101	88	41
Y	13	11	10	25	26	18	17	7
Cr	200	190	510	—	—	—	300	182
Ni	132	94	88	145	126	139	121	24
Cu	4	47	108	94	66	43	60	38
Zn	85	52	63	92	127	76	83	26
V	192	106	222	—	—	—	173	60
La	9.8	12.3	2.4	—	—	—	8.17	5.15
Ce	20.3	25.4	4.6	—	—	—	16.77	10.84
Nd	11.7	10.9	4	—	—	—	8.87	4.23
Sm	2.4	2.1	1	—	—	—	1.83	0.74
Eu	0.78	0.64	0.41	—	—	—	0.61	0.19
Gd	2.2	1.9	1.4	—	—	—	1.83	0.40
Tb	0.4	0.3	0.3	—	—	—	0.33	0.06
Yb	1.3	1.1	1.1	—	—	—	1.17	0.12
Lu	0.17	0.17	0.16	—	—	—	0.17	0.01
Au	<.001	<.001	<.001	—	—	—	<.001	

* Fe_2O_3 calculated on basis of stoichiometry; † FeO calculated on basis of stoichiometry; § Total measured iron represented as FeO; ¶ Mg# is mol ratio 100Mg/(Mg+Fe) in which Fe is total Fe reported as FeO.

13 - GB-S-4A: Metadiabase. Tower quadrangle, 62-15-33ACAD. Analyst (1).

14 - GB-S-16A: Metabasalt, highly schistose zone in pillowed sequence. Soudan quadrangle, 62-15-27DBCC. Analyst (1).

15 - DS-S-460: Metadiabase. Soudan quadrangle, 61-14-18BBAC. Analyst (1).

16 - S-398: Metabasalt, pillowed, moderately deformed. Soudan quadrangle, 61-14-7CDCB. Analyst (2).

17 - S-424: Massive flow or sill of plagioclase-phyric basaltic andesite. Soudan quadrangle, 61-15-4ADAD. Analyst (2).

18 - S-792: Metabasalt, pillowed, moderately deformed. Soudan quadrangle, 62-15-32CCDB. Analyst (2).

Table Ap(4). Metabasalt and metadiabase, Upper member, Ely Greenstone, Soudan belt

[major elements in weight percent oxides; minor elements in parts per million; —, no data; blank, not calculated]

Sample	19	20	21	22	mean	std.dev.
SiO_2	50.7	49.7	52.4	47.9	50.18	1.88
TiO_2	0.83	0.96	0.84	0.89	0.88	0.06
Al_2O_3	14.9	15.5	15.5	15.3	15.30	0.28
*Fe_2O_3	1.93	1.31	1.74	2.3	1.82	0.41
†FeO	7.2	8.9	6.9	9	8.00	1.10
MnO	0.23	0.22	0.21	0.2	0.22	0.01
MgO	6.53	4.04	4.57	8.1	5.81	1.86
CaO	10	7.63	12.8	10.3	10.18	2.11
Na_2O	3.12	3.93	1.8	1.8	2.66	1.05
K_2O	0.32	0.32	0.28	0.35	0.32	0.03
P_2O_5	0.06	0.07	0.06	0.08	0.07	0.01
CO_2	0.94	3.61	1.01	0.05	1.40	1.54
H_2O	2.2	3	1.1	2.76	2.27	0.85
Total	98.96	99.19	99.21	99.03	99.11	
§FeO(t)	8.94	10.08	8.47	11.07	9.64	
¶Mg#	56.59	41.70	49.06	56.63	51.82	
Rb	4	4	<2	17	8	8
Sr	106	96	96	125	106	14
Ba	186	104	124	79	123	46
Nb	<2	2	4	<10	3	1
Hf	1.4	2.1	1.7	—	2	0
Zr	44	53	42	60	50	8
Y	17	19	18	20	19	1
Cr	280	250	310	—	280	30
Ni	114	124	129	132	125	8
Cu	73	96	102	87	90	13
Zn	96	107	79	79	90	14
V	297	354	333	—	328	29
La	4	4	3.8	—	3.93	0.12
Ce	7.1	9.6	8.7	—	8.47	1.27
Nd	6.8	8.1	7.1	—	7.33	0.68
Sm	1.9	2.3	2.1	—	2.10	0.20
Eu	0.73	0.78	0.94	—	0.82	0.11
Gd	2.8	2.9	2.8	—	2.83	0.06
Tb	0.5	0.6	0.5	—	0.53	0.06
Yb	1.7	2.2	2.2	—	2.03	0.29
Lu	0.3	0.3	0.24	—	0.28	0.03
Au	<.001	<.001	<.001	—	<.001	

* Fe_2O_3 calculated on basis of stoichiometry; † FeO calculated on basis of stoichiometry;
§ Total measured iron represented as FeO; ¶ Mg# is mol ratio 100Mg/(Mg+Fe) in which Fe is total Fe reported as FeO.

19 - PK-T-78: Metabasalt, pillowed, moderately deformed. Tower quadrangle, 61-15-6ABDC. Analyst (1).
20 - DS-T-143: Metabasalt, pillowed, moderately deformed. Tower quadrangle, 61-15-8ABBD. Analyst (1).
21 - DS-S-806: Metabasalt, pillowed, moderately deformed. Soudan quadrangle, 61-15-15ABDC. Analyst (1).
22 - S-420: Metadiabase; thick, massive flow unit. Soudan quadrangle, 61-15-10ACCC. Analyst (2).

Table Ap(5). Metabasalt, Sherry Lake sequence, Soudan belt

[major elements in weight percent oxides; minor elements in parts per million; —, no data; blank, not calculated]

Sample	23	24	25	26	27	meanstd. dev.	
SiO_2	46.45	48.50	50.01	47.81	48.30	48.21	1.28
TiO_2	0.89	0.82	0.92	1.00	0.92	0.91	0.07
Al_2O_3	14.85	15.27	14.91	13.56	14.60	14.64	0.65
*Fe_2O_3	2.80	2.64	1.87	—	—	2.44	0.50
†FeO	10.37	8.62	9.68	12.49	12.78	10.79	1.80
MnO	0.27	0.21	0.19	0.35	0.24	0.25	0.06
MgO	5.75	5.68	6.78	5.87	7.37	6.29	0.75
CaO	11.95	12.58	10.58	12.96	11.60	11.93	0.92
Na_2O	1.74	1.72	1.97	1.06	1.86	1.67	0.36
K_2O	0.15	0.12	0.14	0.13	0.11	0.13	0.01
P_2O_5	0.29	0.28	0.18	0.14	0.09	0.20	0.09
CO_2	0.37	0.58	—	—	0.13	0.36	0.23
H_2O	0.17	0.26	0.20	2.8	0.60	0.81	1.13
TOTAL	96.02	97.28	97.43	98.17	98.6	98.62	
§FeO(t)	12.89	11.00	11.35	12.49	12.78	12.10	
¶Mg#	44.29	47.95	51.58	45.61	50.71	48.03	
Rb	3	3	2.5	—	20	7	9
Sr	67	38	37.5	58	90	58	22
Ba	55.5	40	30.5	9	60	39	21
Nb	<20	<20	<20	—	10	10	
Hf	1.25	1	1.5	—	—	1	0
Zr	62	63	55	—	50	58	6
Y	<20	<20	<20	—	20	20	
Cr	290.5	320	350	14	160	227	139
Ni	126.5	105	87.5	21	—	85	46
Cu	144	120	117	153	—	134	18
Zn	96	64	75	67	—	76	14
V	255	210	250	39	—	189	102
La	2.5	3	3.5	3	—	3.00	0.41
Ce	9	8	8	—	—	8.33	0.58
Nd	9	<5	<5	—	—	9.00	
Sm	1.7	1.5	1.8	—	—	1.67	0.15
Eu	0.75	0.6	0.7	—	—	0.68	0.08
Gd	—	—	—	—	—		
Tb	<1	<1	1	—	—	1.00	
Yb	2	1.6	1.9	—	—	1.83	0.21
Lu	<1.0	<1.0	<1.0	—	—		
Au	0.0045	0.003	0.0025	—	—	0.003	0.00

* Fe_2O_3 calculated on basis of stoichiometry; † FeO calculated on basis of stoichiometry;
§ Total measured iron represented as FeO; ¶ Mg# is mol ratio 100Mg/(Mg+Fe) in which Fe is total Fe reported as FeO.

23 - I012X: Metabasalt, pillowed. Sherry Lake quadrangle, 60-22-8AAA. Analyst (7).
24 - I011X: Metabasalt, pillowed. Sherry Lake quadrangle, 60-22-8AAD. Analyst (7).
25 - I098X: Metabasalt, pillowed. Sherry Lake quadrangle, 60-23-25BAD. Analyst (7).
26 - SOC-1-2: Metabasalt, massive. Sherry Lake quadrangle, 60-23-25CBB. Analyst (?).
27 - NEI-54: Metabasalt, pillowed. Sherry Lake quadrangle, 61-22-34AC. Analyst (1).

Table Ap(6). Metabasalt from lower portion of the Lake Vermilion Formation, Soudan belt

[major elements in weight percent oxides; minor elements in parts per million; —, no data; blank, not calculated; totals below 96 wt. percent italicized]

Sample	28	29	30	31	32	mean	std. dev.
SiO_2	48.3	47.7	48.02	44.77	46.86	47.13	1.43
TiO_2	1	0.85	1.09	1	1.05	1.00	0.09
Al_2O_3	15.2	16.4	12.53	13.72	12.96	14.16	1.61
*Fe_2O_3	2.74	1.84	2.29	2.18	2.49	2.31	0.34
†FeO	9.6	6.7	8.24	7.83	8.97	8.27	1.11
MnO	0.3	0.11	0.29	0.2	0.24	0.23	0.08
MgO	5.98	5.46	5.02	6.46	5	5.58	0.63
CaO	9.22	5.96	16.45	13.34	14.28	11.85	4.21
Na_2O	1.49	2.4	2.79	4.72	4.68	3.22	1.43
K_2O	0.27	2.26	—	—	—	1.26	1.41
P_2O_5	0.11	0.12	0.05	0.06	0.06	0.08	0.03
CO_2	0.75	4.32	—	—	—	2.32	2.52
H_2O	3.3	4	—	—	—	3.65	0.49
Total	98.26	98.12	96.77	*94.28*	96.59	101.06	
§FeO(t)	12.07	8.36	10.30	9.79	11.21	10.35	
¶Mg#	46.93	53.83	46.51	54.07	44.31	49.06	
Rb	4	48	—	—	—	26	31
Sr	88	58	172	79	247	129	79
Ba	87	314	58	34	97	118	112
Nb	6	7	—	—	—	7	1
Hf	1.9	2.2	—	—	—	2	0
Zr	54	86	54	63	47	61	15
Y	22	5	17	17	20	16	7
Cr	310	250	328	377	230	299	60
Ni	141	142	32	28	33	75	61
Cu	111	78	—	—	—	95	23
Zn	131	93	—	—	—	112	27
V	345	190	1594	1937	1666	1146	814
La	4	6.7	—	—	—	5.35	1.91
Ce	8.9	14.1	—	—	—	11.50	3.68
Nd	7.1	7.1	—	—	—	7.10	0.00
Sm	2.1	1.6	—	—	—	1.85	0.35
Eu	0.82	0.55	—	—	—	0.69	0.19
Gd	3	1.3	—	—	—	2.15	1.20
Tb	0.6	0.1	—	—	—	0.35	0.35
Yb	2.3	0.9	—	—	—	1.60	0.99
Lu	0.38	0.13	—	—	—	0.26	0.18
Au	0.002	0.003	—	—	—	0.0025	

* Fe_2O_3 calculated on basis of stoichiometry; † FeO calculated on basis of stoichiometry;
§ Total measured iron represented as FeO; ¶ Mg# is mol ratio 100Mg/(Mg+Fe) in which Fe is total Fe reported as FeO.

28 - DS-S-77: Metabasalt, poorly pillowed, moderately deformed. Soudan quadrangle, 62-14-18DDCB. Analyst (1).
29 - DS-S-258: Metabasalt, schistose, intensely deformed. Soudan quadrangle, 62-15-23ABCA. Analyst (1).
30 - ST-40: Metabasalt, pillowed, moderately deformed. Soudan quadrangle, 62-14-16CDBA. Analyst (3).
31 - ST-60: Metabasalt, pillowed, moderately deformed. Soudan quadrangle, 62-14-18CDBD. Analyst (3).
32 - SFV219-3: Mafic metavolcanic rock; primary features obscure. Soudan quadrangle, 62-15-24BABD. Analyst (3).

Table Ap(7). Thin metabasalt units in the Lake Vermilion Formation, Soudan belt

[major elements in weight percent oxides; minor elements in parts per million; —, no data; blank, not calculated]

Sample	33	34	mean
SiO_2	53.2	50.3	51.75
TiO_2	0.88	0.97	0.93
Al_2O_3	15.1	14.8	14.95
*Fe_2O_3	1.75	1.39	1.57
†FeO	7.5	9.1	8.30
MnO	0.19	0.22	0.21
MgO	6.6	7.08	6.84
CaO	10.2	10.6	10.40
Na_2O	2.83	2.28	2.56
K_2O	0.25	0.21	0.23
P_2O_5	0.08	0.07	0.08
CO_2	0.05	0.16	0.11
H_2O	1.1	1.1	1.10
Total	99.73	98.28	99.03
§FeO(t)	9.08	10.35	9.71
¶Mg#	56.48	54.96	55.68
Rb	18	<2	
Sr	125	130	128
Ba	112	84	98
Nb	<10	3	
Hf	—	1.9	
Zr	43	51	47
Y	17	20	19
Cr	303	290	297
Ni	—	103	
Cu	—	79	
Zn	—	104	
V	—	363	
La	2.7	3	2.85
Ce	7.3	7.7	7.50
Nd	6.8	6.7	6.75
Sm	2	2.4	2.20
Eu	0.83	0.83	0.83
Gd	—	3.1	
Tb	0.5	0.6	0.55
Yb	1.8	2.2	2.00
Lu	0.27	0.3	0.29

* Fe_2O_3 calculated on basis of stoichiometry;
† FeO calculated on basis of stoichiometry;
§ Total measured iron represented as FeO;
¶ Mg# is mol ratio 100Mg/(Mg+Fe) in which Fe is total Fe reported as FeO.

33 - T-195: Metabasalt, massive. Tower quadrangle, 61-16-11CAAD. Analyst (1).
34 - C052X: Metabasalt. Linden Grove quadrangle, 61-19-8DCA. Analyst (1).

Table Ap(8). Metabasalt from the Britt antiform, Soudan belt

[major elements in weight percent oxides; minor elements in parts per million; blank, not calculated]

Sample	35	36	37	38	39	40	mean	std. dev.
SiO_2	50.6	51.4	53	51.2	47.9	51.9	51.00	1.72
TiO_2	2.02	0.75	1.96	1.04	0.71	0.93	1.24	0.60
Al_2O_3	15.1	16.1	14.2	15.5	14.8	15.7	15.23	0.68
*Fe_2O_3	3.86	5.19	2.16	2.09	2.46	3.59	3.23	1.22
†FeO	9.4	4.3	7.4	6.8	8.4	7.1	7.23	1.73
MnO	0.38	0.28	0.23	0.2	0.18	0.28	0.26	0.07
MgO	2.82	4.1	4.88	6.43	8.19	3.99	5.07	1.94
CaO	9.45	11.3	8.8	11.1	11.9	11.6	10.69	1.26
Na_2O	2.99	3.83	3.19	3.01	1.72	2.35	2.85	0.73
K_2O	1.06	0.78	0.83	0.57	0.57	0.67	0.75	0.19
P_2O_5	0.2	0.06	0.27	0.13	0.06	0.11	0.14	0.08
CO_2	0.08	0.05	0.01	0.02	0.03	0.04	0.04	0.02
H_2O	0.9	0.9	1	1	1.3	1	1.02	0.15
Total	98.86	99.04	97.93	99.09	98.22	99.26	98.75	
§FeO(t)	12.87	8.97	9.34	8.68	10.61	10.33	10.14	
¶Mg#	28.10	44.92	48.23	56.93	57.92	40.80	47.15	
Rb	17	21	24	10	21	10	17	6
Sr	149	337	215	161	133	142	190	78
Ba	249	110	252	73	74	102	143	84
Nb	3	4	10	4	<2	<2	5	3
Hf	3.9	1.8	4.5	1.8	0.8	1.7	2	1
Zr	105	43	120	55	32	49	67	36
Y	34	14	42	19	12	20	24	12
Cr	94	310	100	240	290	250	214	94
Ni	41	140	43	96	137	113	95	44
Cu	16	91	13	18	97	165	67	62
Zn	155	84	116	114	84	114	111	26
V	435	300	438	340	283	341	356	66
La	11.4	2.8	10.6	9	2.5	5	6.88	3.95
Ce	23.7	6.2	29.3	19	5.2	11	15.73	9.82
Nd	16.5	5.2	20	12	4.3	7.4	10.90	6.38
Sm	4.4	1.6	5.3	2.9	1.3	2.1	2.93	1.61
Eu	1.59	0.67	1.68	1.01	0.55	0.85	1.06	0.47
Gd	5.8	2.3	8.9	3.2	1.7	2.9	4.13	2.73
Tb	1	0.4	1.1	0.5	0.3	0.5	0.63	0.33
Yb	3.7	1.8	4.4	2.4	1.7	2.7	2.78	1.07
Lu	0.55	0.31	0.66	0.31	0.21	0.4	0.41	0.17

* Fe_2O_3 calculated on basis of stoichiometry; † FeO calculated on basis of stoichiometry;
§ Total measured iron represented as FeO; ¶ Mg# is : mol ratio 100Mg/(Mg+Fe) in which Fe is total Fe reported as FeO.

35 - DS-BNW-8: Metabasalt, pillowed, hornblende-bearing, lineated. Biwabik NW quadrangle, 61-17-26DAAD. Analyst (1).
36 - DS-BNW-13: Metabasalt, pillowed, strongly lineated. Biwabik NW quadrangle, 61-17-26DCCA. Analyst (1).
37 - C576A: Metabasalt, hornblende-bearing, lineated. Britt quadrangle, 60-17-8CAAA. Analyst (1).
38 - C589A: Metabasalt, glomeroporphyritic. Britt quadrangle, 60-17-4DCBD. Analyst (1).
39 - C637A: Metabasalt. Britt quadrangle, 61-17-30BACD. Analyst (1).
40 - C710B: Metabasalt. Britt quadrangle, 60-17-18BDAB. Analyst (1).

Table Ap(9). Metabasalt and allied rocks, Thistledew Lake sequence, Newton belt

[major elements in weight percent oxides; minor elements in parts per million; —, no data; blank, not calculated]

Sample	41	42	43	44	45	46	47	48	mean	std. dev.
SiO_2	52.47	52.50	55.10	48.97	49.25	49.80	47.10	49.40	50.57	2.57
TiO_2	1.97	1.85	1.61	1.87	2.01	0.96	0.90	0.72	1.49	0.54
Al_2O_3	12.66	12.86	11.70	14.10	12.89	15.60	15.80	15.00	13.83	1.52
*Fe_2O_3	3.44	2.16	5.32	1.83	2.86	1.82	1.49	1.23	2.52	1.34
†FeO	11.4	9.7	10.6	10.5	12.8	7.9	10.9	9.6	10.43	1.44
MnO	0.21	0.21	0.34	0.18	0.26	0.17	0.18	0.18	0.22	0.06
MgO	4.68	4.38	2.64	5.51	5.31	6.74	8.05	8.22	5.69	1.90
CaO	5.20	6.52	5.92	9.77	7.82	11.20	5.48	8.89	7.60	2.19
Na_2O	3.11	2.77	3.71	3.01	3.17	2.80	3.96	2.23	3.10	0.55
K_2O	1.31	0.61	0.50	0.45	1.11	0.64	0.79	0.54	0.74	0.31
P_2O_5	0.20	0.20	0.63	0.17	0.18	0.09	0.03	0.06	0.19	0.19
CO_2	<0.01	0.12	0.02	0.04	0.06	0.09	0.11	0.07	0.07	0.04
H_2O	1.92	2.13	0.80	1.52	0.44	1.50	2.40	2.30	1.63	0.71
Total	98.57	96.01	98.89	97.92	98.16	99.31	97.19	98.44	98.08	
§FeO(t)	14.50	11.64	15.39	12.15	15.37	9.54	12.24	10.71	12.69	
¶Mg#	36.55	40.16	23.44	44.73	38.13	55.77	53.99	57.80	44.45	
Rb	5	4	6	3	16	20	13	11	10	6
Sr	256	145	211	336	155	136	115	100	182	81
Ba	305	237	233	88	343	80	182	120	199	98
Nb	—	—	9	—	—	7	5	2	6	3
Hf	4.6	5.0	4.8	3.3	3.8	2	1.5	1.1	3	2
Zr	156	163	162	116	118	52	54	39	108	52
Y	12	13	54	8	10	20	16	10	18	15
Cr	13	28	55	28	44	250	100	160	85	82
Ni	14	62	5	30	39	50	55	71	41	23
Cu	61	83	16.4	62	96	110.0	167.0	109.0	88	44
Zn	65	130	141.0	60	64	72.8	111.0	133.0	97	35
V	320	290	48	60	140	281	329	272	218	116
La	13.0	12.0	23.8	6.6	8.6	4.6	3.5	3.5	9.45	6.85
Ce	30	30	56.5	17	22	9.6	8.7	7.3	22.64	16.42
Nd	21	20	40.8	12	15	8.0	7.0	5.5	16.16	11.51
Sm	4.4	5.3	9.2	3.4	4.2	2.4	2.0	1.3	4.03	2.48
Eu	1.16	1.61	3.40	1.12	1.28	0.92	0.61	0.63	1.34	0.90
Gd										
Tb	0.9	1.1	1.7	0.6	0.8	0.5	0.5	0.3	0.80	0.44
Yb	3.48	4.34	5.5	2.27	2.94	2.1	1.8	1.0	2.93	1.46
Lu	0.55	0.63	0.88	0.33	0.47	0.29	0.28	0.12	0.44	0.24
Au	0.013	0.009	0.002	0.007	0.131	0.002	0.005	0.001	0.021	0.045

* Fe_2O_3 calculated on basis of stoichiometry; † FeO calculated on basis of stoichiometry; § Total measured iron represented as FeO; ¶ Mg# is mol ratio 100Mg/(Mg+Fe) in which Fe is total Fe reported as FeO.

41 - I399X: Metabasalt, pillowed. Deer Lake East quadrangle, 61-23-4ADC. Analyst (1).
42 - I370X: Metabasalt, pillowed. Deer Lake East quadrangle, 61-23-8DB. Analyst (1).
43 - I505C: Metabasalt, pillowed. Deer Lake West quadrangle, 61-24-8BBAC. Analyst (1).
44 - I409X: Basaltic andesite flow. Deer Lake East quadrangle, 61-24-24DBA. Analyst (1).
45 - I410: Metabasalt, pillowed. Deer Lake East quadrangle, 61-24-24BAB. Analyst (1).
46 - I566: Metabasalt, pillowed. Effie SE quadrangle, 61-25-20CBDD. Analyst (1).
47 - I532X: Metabasalt, pillowed. Coon Lake quadrangle, 61-25-30BABC. Analyst (1).
48 - I529: Metabasalt, pillowed. Coon Lake quadrangle, 61-26-36DCBB. Analyst (1).

Table Ap(10). Metabasalt and allied rocks, Joy Lake sequence, Newton belt

[major elements in weight percent oxides; minor elements in parts per million; —, no data; blank, not calculated]

Sample	49	50	51	52	mean	std. dev.
SiO_2	49.50	53.89	50.50	58.41	53.08	4.02
TiO_2	1.16	1.54	0.71	1.33	1.19	0.35
Al_2O_3	14.30	14.90	16.10	14.41	14.93	0.82
*Fe_2O_3	2.68	1.21	2.48	3.60	2.49	0.98
†FeO	10.1	8.0	7.4	7.1	8.15	1.35
MnO	0.20	0.20	0.19	0.10	0.17	0.05
MgO	6.85	6.66	8.15	4.08	6.44	1.70
CaO	10.10	9.66	5.61	2.76	7.03	3.49
Na_2O	1.87	2.29	3.75	4.69	3.15	1.31
K_2O	0.32	0.19	0.74	0.18	0.36	0.26
P_2O_5	0.12	0.22	0.32	0.22	0.22	0.08
CO_2	0.01	<0.01	0.22	0.12	0.12	0.11
H_2O	1.60	2.30	3.3	1.79	2.25	0.76
Total	98.81	101.06	99.47	98.79	99.58	
§FeO(t)	12.51	9.09	9.63	10.34	10.39	
¶Mg#	49.42	56.66	60.15	41.31	52.49	
Rb	2	5	28	2	8	13
Sr	80	136	92	144	113	32
Ba	53	39	302	66	115	125
Nb	2	—	<10	—	—	
Hf	2.4	3.1	—	3.6	3	1
Zr	70	108	73	133	96	30
Y	27	6	21	6	15	11
Cr	130	32	177	20	90	76
Ni	84	22	—	28	45	34
Cu	131.0	37	—	42	70	53
Zn	124.0	19	—	65	69	53
V	345	50	—	190	195	148
La	5.7	6.5	—	11.0	7.73	2.86
Ce	12.7	17	—	26	18.57	6.79
Nd	9.5	12	—	13	11.50	1.80
Sm	2.7	3.5	—	3.0	3.07	0.40
Eu	0.95	1.07	—	1.02	1.01	0.06
Gd	—	—	—	—	—	
Tb	0.6	0.9	—	0.6	0.70	0.17
Yb	3.0	3.90	—	2.65	3.18	0.64
Lu	0.44	0.60	—	0.42	0.49	0.10
Au	—	0.008	—	0.009	0.009	0.001

* Fe_2O_3 calculated on basis of stoichiometry; † FeO calculated on basis of stoichiometry; § Total measured iron represented as FeO; ¶ Mg# is mol ratio 100Mg/(Mg+Fe) in which Fe is total Fe reported as FeO.

49 - PK-IT-4: Metabasalt, pillowed. Silverdale quadrangle, 62-22-2AADA. Analyst (1).
50 - I388AX: Basaltic andesite flow. Deer Lake West quadrangle, 62-24-17BDA. Analyst (1).
51 - KIB-13: Metabasalt, pillowed, from drill core. Effie SE quadrangle, 62-25-33BBBBBC. Analyst (1).
52 - DL42B: Metabasalt, anomalously enriched in magnetite. Effie SE quadrangle, 61-25-3CAC. Analyst (1).

Table Ap(11). Metabasalt, Wilson Lake sequence, Newton belt

[major elements in weight percent oxides; minor elements in parts per million; —, no data; blank, not calculated; totals below 96 wt. percent italicized]

Sample	53	54	55	56	57	mean	std. dev.
SiO_2	50.20	48.80	46.51	50.48	47.42	48.68	1.72
TiO_2	1.33	1.42	0.71	0.98	0.76	1.04	0.32
Al_2O_3	12.70	13.33	15.34	14.81	15.39	14.31	1.23
*Fe_2O_3	—	2.58	2.48	4.19	9.18	4.61	3.15
†FeO	13.68	11.70	8.61	8.69	2.46	9.03	4.25
MnO	0.26	0.25	0.19	0.22	0.13	0.21	0.05
MgO	6.37	6.01	7.79	6.91	2.29	5.87	2.11
CaO	6.37	9.30	10.30	10.67	18.26	10.98	4.41
Na_2O	3.80	2.43	1.61	1.66	0.10	1.92	1.35
K_2O	0.42	0.30	0.14	0.27	0.06	0.24	0.14
P_2O_5	0.22	0.33	0.25	0.24	0.23	0.25	0.04
CO_2	—	0.11	0.00	<0.01	0.01	0.04	0.06
H_2O	1.5	0.62	0.46	0.40	0.30	0.66	0.49
Total	96.85	97.18	*94.39*	99.52	96.59	97.84	
§FeO(t)	13.68	14.02	10.84	12.46	10.72	13.17	
¶Mg#	45.38	43.33	56.18	49.73	27.59	44.30	
Rb	—	6	3	5	3	4	2
Sr	—	44	26	64	690	206	323
Ba	130	65	26	50	20	58	44
Nb	9.0	<20	<20	<20	<20	9	
Hf	5	2	1	1.5	1.2	2	2
Zr	124	78	<20	51	48	75	35
Y	—	24	<20	<20	<20	24	
Cr	—	84	239	200	160	171	66
Ni	—	55	129	93	48	81	37
Cu	44	132	120	105	26	85	47
Zn	—	91	66	90	30	69	29
V	—	371	237	230	196	259	77
La	12	4	1	2	2	4.20	4.49
Ce	—	15	5	6	5	7.75	4.86
Nd	—	9	<5	<5	<5	9.00	
Sm	—	2.8	1.4	1.6	1.4	1.80	0.67
Eu	2.0	1.0	0.6	0.8	0.6	1.00	0.58
Gd	—	—	—	—	—	—	
Tb	1	<1	<1	<1	<1	1.00	
Yb	—	3.8	2.4	1.6	1.7	2.37	1.01
Lu	—	<1.0	<1.0	<1.0	<1.0	—	
Au	—	0.002	<.001	<.001	<.001	<0.001	

* Fe_2O_3 calculated on basis of stoichiometry; † FeO calculated on basis of stoichiometry; § Total measured iron represented as FeO; ¶ Mg# is mol ratio 100Mg/(Mg+Fe) in which Fe is total Fe reported as FeO.

53 - 3005: Metabasalt, pillowed. Horsehead Lake quadrangle, 61-23-28DC. Analyst (?).
54 - I306X: Metabasalt, pillowed. Horsehead Lake quadrangle, 61-23-32ADC. Analyst (7).
55 - I308X: Metabasalt, pillowed. Horsehead Lake quadrangle, 61-23-33CBB. Analyst (7).
56 - I291A: Metabasalt, pillowed. Horsehead Lake quadrangle, 61-24-36DBD. Analyst (7).
57 - I295B: Metabasalt, pillowed. Horsehead Lake quadrangle, 61-24-36DDA. Analyst (7).

Table Ap(12). Metabasalt, Cook sequence, Newton belt

[major elements in weight percent oxides;
minor elements in parts per million; —, no data; blank, not calculated]

Sample	58	59	60	61	mean	std. dev.
SiO_2	48.9	47	50.6	49.1	48.90	1.48
TiO_2	1.42	0.81	1.04	0.96	1.06	0.26
Al_2O_3	14	15.3	15.8	14	14.78	0.92
*Fe_2O_3	4.1	3.23	4.31	2.09	3.43	1.01
†FeO	9.9	7.8	6.9	10	8.65	1.55
MnO	0.24	0.2	0.22	0.23	0.22	0.02
MgO	4.8	6.93	4.83	6.52	5.77	1.12
CaO	9.79	12	11.5	11	11.07	0.95
Na_2O	3.66	1.8	2.02	2.16	2.41	0.85
K_2O	0.31	0.16	0.19	0.31	0.24	0.08
P_2O_5	0.15	0.06	0.08	0.11	0.10	0.04
CO_2	0.26	0.58	0.08	0.48	0.35	0.22
H_2O	1.3	2.6	2.04	1.1	1.76	0.69
Total	98.83	98.47	99.61	98.06	98.74	
§FeO(t)	13.59	10.71	10.78	11.88	11.74	
¶Mg#	38.66	53.59	44.43	49.47	46.72	
Rb	<2	<2	12	2	7	7
Sr	300	143	106	76	156	10
Ba	58	55	73	98	71	20
Nb	3	<2	<10	4	4	1
Hf	2.9	1.5	—	—	2	1
Zr	84	47	69	50	63	17
Y	27	15	21	22	21	5
Cr	140	350	300	150	235	106
Ni	64	123	—	87	91	30
Cu	63	130	—	141	111	42
Zn	102	86	—	123	104	19
V	439	266	—	320	342	89
La	6.2	3.9	—	4.4	4.83	1.21
Ce	14.4	7.9	—	9	10.43	3.48
Nd	10.6	5.6	—	6.8	7.67	2.61
Sm	3.3	1.8	—	2.1	2.40	0.79
Eu	1.16	0.66	—	0.78	0.87	0.26
Gd	4.1	2.4	—	4.1	3.53	0.98
Tb	0.7	0.4	—	0.5	0.53	0.15
Yb	3.3	1.8	—	2.5	2.53	0.75
Lu	0.44	0.24	—	0.39	0.36	0.10
Au	<.001	<.001	—	<.001	<.001	

* Fe_2O_3 calculated on basis of stoichiometry; † FeO calculated on basis of stoichiometry;
§ Total measured iron represented as FeO; ¶ Mg# is mol ratio 100Mg/(Mg+Fe) in which Fe is total Fe reported as FeO.

58 - C017X: Metabasalt, pillowed to massive thin flow. Meadow Brook quadrangle, 62-20-9CAAB. Analyst (1).
59 - C037X: Metabasalt, pillowed thin flow. Gheen quadrangle, 63-19-34CCCB. Analyst (1).
60 - CD-22-36: Metabasalt, pillowed. Cook quadrangle, 62-18-20ACDC. Analyst (1).
61 - C067X: Metabasalt, pillowed, actinolite- and chlorite-bearing. Cook quadrangle, 62-19-26BADA. Analyst (1).

Table Ap(13). Metabasalt, Deer Lake sequence, Newton belt

[major elements in weight percent oxides; minor elements in parts per million; —, no data; blank, not calculated]

Sample	62	63	64	65	66	mean	std. dev.
SiO_2	52.90	53.50	48.30	50.30	49.60	50.92	2.21
TiO_2	0.86	1.11	0.69	0.71	1.54	0.98	0.35
Al_2O_3	14.10	13.90	11.50	11.40	13.70	12.92	1.35
*Fe_2O_3	—	—	1.19	1.72	2.19	1.70	0.50
†FeO	10.26	10.62	10.0	9.7	10.9	10.31	0.55
MnO	0.29	0.16	0.19	0.21	0.27	0.22	0.05
MgO	7.03	8.41	11.10	10.90	7.05	8.90	2.00
CaO	10.40	8.58	9.26	8.91	5.36	8.50	1.89
Na_2O	2.55	2.33	1.69	2.32	4.31	2.64	0.99
K_2O	0.11	0.64	0.86	0.34	0.31	0.45	0.30
P_2O_5	0.27	0.16	0.07	0.08	0.15	0.14	0.08
CO_2	—	—	0.62	0.04	0.03	0.23	0.34
H_2O	0.55	0.85	2.80	1.90	2.90	2.11	0.95
Total	99.32	100.26	98.27	98.53	98.31	100.02	
§FeO(t)	10.26	10.62	11.07	11.25	12.87	11.83	
¶Mg#	55.01	58.56	64.15	63.36	49.43	57.29	
Rb	—	—	14	3	2	6	7
Sr	—	—	81	127	164	124	42
Ba	—	—	197	113	118	143	47
Nb	86	76	2	2	6	34	43
Hf	—	—	1.8	1.5	3.2	2	1
Zr	20	20	45	51	95	46	31
Y	—	—	13	14	25	17	7
Cr	—	—	670	690	120	493	323
Ni	—	—	135	153	54	114	53
Cu	—	—	55.6	93.3	152.0	100	49
Zn	—	—	56.0	86.1	57.4	67	17
V	—	—	259	260	352	290	53
La	—	—	4.5	3.7	5.2	4.47	0.75
Ce	—	—	9.4	8.4	14.0	10.60	2.99
Nd	—	—	7.3	6.2	11.8	8.43	2.97
Sm	—	—	2.1	1.6	3.7	2.47	1.10
Eu	—	—	0.72	0.60	0.97	0.76	0.19
Gd	—	—	—	—	—	—	
Tb	—	—	0.4	0.4	0.8	0.53	0.23
Yb	—	—	1.4	1.3	3.3	2.00	1.13
Lu	—	—	0.22	0.18	0.47	0.29	0.16
Au	—	—	0.0018	0.0015	0.0032	0.0022	0.0009

* Fe_2O_3 calculated on basis of stoichiometry; † FeO calculated on basis of stoichiometry; § Total measured iron represented as FeO; ¶ Mg# is mol ratio 100Mg/(Mg+Fe) in which Fe is total Fe reported as FeO.

62 - 3605: Metabasalt, pillowed. Deer Lake West quadrangle, 61-25-12DA. Analyst (?).
63 - 3608: Metabasalt, pillowed. Deer Lake West quadrangle, 61-25-12DA. Analyst (?).
64 - I554: Metabasalt, spinifex-textured. Effie SE quadrangle, 61-25-17DBBC. Analyst (1).
65 - I567: Metabasalt, spinifex-textured. Effie SE quadrangle, 61-25-20DBCD. Analyst (1).
66 - I543BX: Metabasalt, pillowed. Effie SE quadrangle, 61-26-25ADBA. Analyst (1).

Table Ap(14). Felsic volcaniclastic rocks within dominantly mafic sequences of the Soudan belt

[major elements in weight percent oxides; minor elements in parts per million; —, no data]

Sample	67	68
SiO_2	62.81	68.90
TiO_2	0.39	0.82
Al_2O_3	15.84	13.57
*Fe_2O_3	1.65	1.67
†FeO	2.45	3.64
MnO	0.05	0.06
MgO	2.58	1.26
CaO	3.42	4.28
Na_2O	5.21	3.13
K_2O	2.45	1.73
P_2O_5	0.34	0.14
CO_2	<0.01	—
H_2O	0.14	0.35
Total	97.33	99.55
§FeO(t)	3.93	5.15
Rb	95	36
Sr	995	117
Ba	910	323
Nb	<20	<20
Hf	3.8	6
Zr	141	238
Y	<20	26
Cr	115	106
Ni	44	14
Cu	30	28
Zn	53	85
V	54	56
La	35	19
Ce	88	50
Nd	41	16
Sm	4.4	3.8
Eu	1.2	1.1
Gd	—	—
Tb	<1	<1
Yb	0.5	2.7
Lu	<1.0	<1.0
Au	<.001	<.001

*Fe_2O_3 calculated on basis of stoichiometry;
†FeO calculated on basis of stoichiometry;
§Total measured iron represented as FeO.

67 - I006Y: Dacite crystal tuff; in felsic unit within the Sherry Lake sequence. Sherry Lake quadrangle, 60-22-9AAA. Analyst (7).

68 - I217DX: Felsic tuff; felsic unit in Bear Lake sequence. Horsehead Lake quadrangle, 60-23-22CBC. Analyst (7).

Table Ap(15). Metasedimentary rocks of the Lake Vermilion Formation, south of Wahlsten fault, Soudan belt

[major elements in weight percent oxides; minor elements in parts per million]

Sample	69	70
SiO_2	71.6	66
TiO_2	0.36	0.28
Al_2O_3	14.9	16.1
*Fe_2O_3	0.54	0.92
†FeO	1.5	1.4
MnO	0.02	0.06
MgO	0.98	1.9
CaO	3.08	4.04
Na_2O	4.46	5.04
K_2O	1.51	1.9
P_2O_5	0.03	0.13
CO_2	0.01	0.95
H_2O	0.6	0.9
Total	99.59	99.62
§FeO(t)	1.99	2.23
Rb	53	60
Sr	373	980
Ba	356	851
Nb	10	7
Zr	133	134
Y	4	4
Cr	15	37
Ni	2	24
Cu	5	5
Zn	57	47
V	55	50
La	13.2	26
Ce	26.2	50.8
Nd	9.8	21.3
Sm	1.5	3
Eu	0.58	0.84
Tb	0.1	0.2
Yb	0.4	0.4
Lu	<0.05	0.06

* Fe_2O_3 calculated on basis of stoichiometry;
† FeO calculated on basis of stoichiometry;
§ Total measured iron represented as FeO.

69 - DS-BNW-17: Massive felsic wacke. Biwabik NW quadrangle, 61-17-35BDDA. Analyst (1).

70 - DS-BNE-91: Massive felsic wacke. Biwabik NE quadrangle, 61-16-26CDBD. Analyst (1).

Table Ap(16). Felsic tuff and reworked tuffaceous wacke of the central tuff (unit lft of Southwick, 1993), Lake Vermilion Formation, Soudan belt

[major elements in weight percent oxides; minor elements in parts per million; —, no data]

Sample	71	72	73	74	75	76	77
SiO_2	68.1	65.3	69.6	63.6	56.7	71	70.1
TiO_2	0.22	0.13	0.15	0.31	0.22	0.11	0.13
Al_2O_3	18.9	18.4	17.21	14.26	20.2	16.9	15.7
*Fe_2O_3	0.35	0.11	1.45	1.44	2	0.38	0.55
†FeO	1.4	0.7	0.68	3.96	0.2	0.3	0.7
MnO	<.01	0.02	0.03	0.12	0.03	0.02	0.04
MgO	0.81	0.56	0.52	2.38	2.06	0.35	0.82
CaO	2.71	4.75	3.3	4.62	11.6	2.62	3.81
Na_2O	3.7	5.04	5.01	3.33	3.47	6.22	5.49
K_2O	2.04	1.63	0.64	1.36	0.74	1.13	0.84
P_2O_5	0.05	0.05	0.04	0.09	0.15	0.04	0.05
CO_2	0.04	2.21	0.09	2.23	0.05	<.01	0.66
H_2O	1.3	1.1	1.19	2.18	0.7	0.6	1.11
Total	99.62	100	99.91	99.88	98.12	99.67	100
§FeO(t)	1.72	0.80	1.99	5.26	2.00	0.64	1.20
Rb	65	31	—	—	15	27	30
Sr	622	941	—	—	992	558	636
Ba	637	313	—	—	284	241	313
Nb	6	4	—	—	9	<2	14
Zr	91	67	—	—	62	58	53
Y	2	3	—	—	2	2	<10
Cr	14	8	—	—	35	5	—
Ni	11	4	—	—	36	3	—
Cu	3	3	—	—	5	6	—
Zn	61	19	—	—	26	27	—
V	32	23	—	—	51	12	—
La	4.5	5.3	—	—	13	4	—
Ce	10.4	8	—	—	26.1	7.3	—
Nd	4.5	4.6	—	—	13	3.3	—
Sm	0.8	0.7	—	—	1.7	0.4	—
Eu	0.31	0.23	—	—	0.56	0.24	—
Tb	<0.1	<0.1	—	—	0.1	<.1	—
Yb	0.2	0.1	—	—	0.2	0.2	—
Lu	<0.05	<0.5	—	—	0.06	<.05	—

* Fe_2O_3 calculated on basis of stoichiometry; † FeO calculated on basis of stoichiometry;
§ Total measured iron represented as FeO.

71 - RO-T-65: Lithic metagraywacke, dacitic. Tower quadrangle, 61-16-1ADDB. Analyst (1).
72 - RO-T-102: Lithic metagraywacke, dacitic. Tower quadrangle, 62-15-30DCCA. Analyst (1).
73 - RO-T-24: Lithic metagraywacke, dacitic. Tower quadrangle, 61-16-1ACAA. Analyst (4).
74 - PK-T-79: Dacitic tuff-breccia, slightly reworked. Tower quadrangle, 61-15-6BADC. Analyst (4).
75 - C212A: Felsic tuff, slightly reworked, from thick massive bed. Sassas Creek quadrangle, 62-18-26CCAA. Analyst (1).
76 - C301A: Crystal tuff. Cook quadrangle, 61-18-8DBC. Analyst (1).
77 - CD-20-77: Feldspathic tuff-wacke. Cook quadrangle, 62-18-31CDCC. Analyst (1).

Table Ap(17). Graywacke, slate and pelitic schist units of the Lake Vermilion Formation, between the central tuff and the Wahlsten fault, Soudan belt

[major elements in weight percent oxides; minor elements in parts per million; —, no data]

Sample	78	79	80	81	82	83	84
SiO_2	61.4	65.7	59.1	70.45	57.5	62.8	57.3
TiO_2	0.58	0.49	0.56	0.48	0.36	0.67	0.77
Al_2O_3	15.1	15.4	14.1	12.79	16.82	14.9	21.3
*Fe_2O_3	0.88	0.52	1.32	0.86	1.22	1.88	3.56
†FeO	4.4	2.8	4.4	2.96	4.4	4.9	4
MnO	0.1	0.07	0.09	0.06	0.13	0.11	0.09
MgO	3.87	1.82	6.22	1.19	2.28	2.46	3.72
CaO	4.15	3.95	4.96	4.55	6.08	2.43	1.13
Na_2O	4.82	4.31	5.3	3.39	4.76	3.91	1.78
K_2O	0.68	1.61	0.99	1.18	1.53	1.92	2.66
P_2O_5	0.17	0.15	0.18	0.15	0.12	0.19	0.15
CO_2	1.02	1.02	0.24	1.13	2.49	0.14	<.01
H_2O	2.1	1.5	0.16	0.84	2.03	1.7	1.2
Total	99.27	99.34	97.62	100.03	99.72	98.01	97.66
§FeO (t)	5.19	3.27	5.59	3.73	5.50	6.59	7.20
Rb	13	47	17	—	—	66	97
Sr	706	873	530	—	—	511	229
Ba	349	588	281	—	—	611	603
Nb	10	14	6	—	—	9	12
Zr	146	139	113	—	—	111	143
Y	12	11	11	—	—	13	10
Cr	170	95	330	—	—	610	200
Ni	65	49	129	—	—	132	76
Cu	38	34	44	—	—	65	28
Zn	88	71	70	—	—	77	101
V	114	104	130	—	—	185	192
La	33	29.5	22.4	—	—	22.7	37.3
Ce	68.9	62	46.3	—	—	45.6	70.8
Nd	32.1	27.1	22.6	—	—	23.8	32
Sm	5.6	4.8	4.3	—	—	4.2	5.1
Eu	1.61	1.48	1.43	—	—	1.17	1.52
Tb	0.5	0.4	0.5	—	—	0.5	0.5
Yb	1	1	1	—	—	1.3	1
Lu	0.18	0.13	0.17	—	—	0.22	0.14

* Fe_2O_3 calculated on basis of stoichiometry; † FeO calculated on basis of stoichiometry; § Total measured iron represented as FeO; ¶ Mg# is mol ratio 100Mg/(Mg+Fe) in which Fe is total Fe reported as FeO.

78 - DS-T-148: Lithic metagraywacke. Tower quadrangle, 61-15-8DAAB. Analyst (1).

79 - DS-S-807: Metagraywacke, fine-grained. Soudan quadrangle, 61-15-15ACDA. Analyst (1).

80 - RO-T-864G: Metagraywacke. Tower quadrangle, 61-15-20CBAB. Analyst (1).

81 - RO-T-3A: Metagraywacke, near base of graded bed. Tower quadrangle, 61-16-2AADC. Analyst (4).

82 - RO-T-3(sl): Slaty mudstone near top of graded bed. Tower quadrangle, 61-16-2AADC. Analyst (4).

83 - M193: Metagraywacke. Sassas Creek quadrangle, 61-17-16DCBC. Analyst (1).

84 - C539-2: Staurolite schist. Dark Lake quadrangle, 61-19-31CDBC. Analyst (1).

Table Ap(18). Metasedimentary rocks north of central tuff unit, Lake Vermilion Formation, Soudan belt

[major elements in weight percent oxides; minor elements in parts per million; —, no data]

Sample	85	86	87	88	89	90	91	92	93
SiO_2	63.1	56.4	63.65	70.5	61.05	59.63	62.6	57.1	60.3
TiO_2	0.28	0.74	0.32	0.11	0.51	0.71	0.53	0.75	0.65
Al_2O_3	18.5	15.4	16.56	14.02	15.77	18.75	16.9	20.8	17.8
*Fe_2O_3	1.39	0.81	0.93	0.41	1.29	—	1.46	3.39	0.97
†FeO	0.8	5.8	2.12	0.84	4.04	6.95	3.5	4.4	4.9
MnO	0.01	0.13	0.03	0.03	0.1	0.08	0.08	0.08	0.08
MgO	1.33	3.73	1.77	0.43	2.25	3.68	2.93	3.73	3.42
CaO	2.61	4.77	3.24	3.15	4.26	0.96	2.06	1.34	2.06
Na_2O	6.65	4.88	6.09	5.87	4.39	2.17	5.6	2.14	4.28
K_2O	2.22	0.42	0.91	0.96	1.33	2.88	1.71	2.84	1.43
P_2O_5	0.11	0.1	0.14	0.02	0.12	—	0.15	0.15	0.14
CO_2	1.39	3.04	1.99	2.2	1.73	—	<.01	<.01	<.01
H_2O	1.2	2.9	1.92	1.12	2.83	4.23	2.08	1.6	2.3
Total	99.59	99.12	99.67	99.66	99.67	100.04	99.6	98.32	98.33
§FeO(t)	2.05	6.53	2.96	1.21	5.20	6.95	4.78	7.45	5.77
Rb	52	9	—	—	—	—	54	101	69
Sr	655	454	—	—	—	—	821	298	352
Ba	555	206	—	—	—	543	679	658	432
Nb	6	6	—	—	—	—	13	9	8
Zr	102	104	—	—	—	—	109	137	134
Y	2	11	—	—	—	—	<10	11	12
Cr	26	190	—	—	—	219	—	170	190
Ni	15	89	—	—	—	121	—	68	66
Cu	27	89	—	—	—	—	—	21	38
Zn	19	118	—	—	—	—	—	82	88
V	43	228	—	—	—	—	—	184	147
La	6.3	8.6	—	—	—	28.68	—	34.5	12.7
Ce	14.3	17.5	—	—	—	60.94	—	66.6	26.2
Nd	7.8	9.5	—	—	—	23.6	—	32.2	13.2
Sm	1.3	2.3	—	—	—	5.1	—	5.2	2.3
Eu	0.51	0.79	—	—	—	0.95	—	1.43	1.09
Tb	0.1	0.3	—	—	—	0.6	—	0.5	0.4
Yb	0.2	1.4	—	—	—	1.59	—	1.1	1.4
Lu	<0.05	0.22	—	—	—	0.27	—	0.19	0.21

* Fe_2O_3 calculated on basis of stoichiometry; † FeO calculated on basis of stoichiometry; § Total measured iron represented as FeO.

85 - RO-T-596: Resedimented dacitic tuff-agglomerate. Tower quadrangle, 62-15-16BBDB. Analyst (1).

86 - PK-S-21: Lithic wacke, edge of Mud Creek shear zone. Soudan quadrangle, 62-14-8AABB. Analyst (1).

87 - RO-T-711: Resedimented quartz-plagioclase tuff. Tower quadrangle, 62-15-21CCCA. Analyst (4).

88 - RO-T-727: Felsic tuff. Tower quadrangle, 62-15-20DBAC. Analyst (4).

89 - RO-T-728: Lithic metagraywacke. Tower quadrangle, 62-15-20DBDA. Analyst (4).

90 - DS-S-168sl: Slaty laminated mudstone. Soudan quadrangle, 62-14-18BBAA. Analyst (5).

91 - CD-6B-193: Tuffaceous, argillaceous metagraywacke, fine-grained. Bear River quadrangle, 61-21-4ADAD. Analyst (1).

92 - C235: Staurolite schist. Linden Grove quadrangle, 61-19-18BCCD. Analyst (1).

93 - M053: Metagraywacke, fine-grained, biotite-bearing. Linden Grove quadrangle, 61-19-9CADC. Analyst (1).

Table Ap(19). Metasedimentary rocks between the Mud Creek shear zone and the Bear River fault, Newton belt

[major elements in weight percent oxides; minor elements in parts per million; —, no data]

Sample	94	95	96	97	98	99	100
SiO_2	63.7	63.55	63.65	61.59	64.7	68.1	62.5
TiO_2	0.54	0.59	0.72	0.57	0.52	0.51	0.61
Al_2O_3	15.6	15.91	13.92	15.84	15.6	14.7	16.6
*Fe_2O_3	1.27	1.33	1.34	—	0.87	0.91	2.27
†FeO	3.2	3.68	4.24	5.84	3.9	3.5	4.1
MnO	0.06	0.05	0.07	0.1	0.04	0.07	0.1
MgO	2.61	2.31	2.78	2.92	2.85	2.02	3.04
CaO	1.67	1.56	2.82	3.48	1.26	2.66	1.76
Na_2O	5.66	5.88	4.19	2.65	3.66	4.17	3.01
K_2O	1.31	1.26	1.89	2.47	1.63	1.85	2.49
P_2O_5	0.15	0.19	0.11	—	0.12	0.12	0.17
CO_2	0.61	1.02	1.4	—	0.01	<.01	—
H_2O	2.1	2.23	2.63	5.14	2.5	0.7	2.93
Total	98.48	99.56	99.76	100.6	97.66	99.31	99.58
§FeO(t)	4.34	4.88	5.45	5.84	4.68	4.32	6.14
Rb	40	—	—	—	47	82	86
Sr	396	—	—	—	303	369	381
Ba	454	—	—	548	544	477	909
Nb	7	—	—	—	4	26	35
Zr	133	—	—	—	122	123	144
Y	6	—	—	—	11	<10	15
Cr	130	—	—	164	120	—	120
Ni	59	—	—	104	44	—	70
Cu	41	—	—	—	32	—	53
Zn	79	—	—	—	49	—	85
V	99	—	—	—	108	—	116
La	22.2	—	—	10.98	22.4	—	29.5
Ce	45.8	—	—	25.49	44.1	—	52
Nd	20.2	—	—	11.3	19.3	—	21
Sm	3.3	—	—	2.5	3.2	—	3.82
Eu	0.82	—	—	0.71	1.03	—	0.92
Tb	0.3	—	—	0.34	0.4	—	0.4
Yb	0.8	—	—	1.26	1	—	1.37
Lu	0.13	—	—	0.21	0.15	—	0.2

* Fe_2O_3 calculated on basis of stoichiometry; † FeO calculated on basis of stoichiometry; § Total measured iron represented as FeO.

94 - RO-T-493: Fine-grained tuffaceous metasiltstone. Sioux Pine Island quadrangle, 62-16-3CDDB. Analyst (1).

95 - RO-T-493R: Same as RO-T-493. Analyst (4).

96 - RO-T-493AR: Fine- to medium-grained metagraywacke. Same location as RO-T-493. Analyst (4).

97 - DS-S-707: Slaty laminated mudstone. Soudan quadrangle, 62-15-10BBAA. Analyst (5).

98 - C230: Fine-grained schistose wacke. Linden Grove quadrangle, 62-19-21BCCB. Analyst (1).

99 - CD-2-79: Schistose metagraywacke. Bear River quadrangle, 62-22-12DCAD. Analyst (1).

100 - CD-37-114: Schistose metagraywacke. Bear River quadrangle, 62-22-14BBBC. Analyst (7).

Table Ap(20). Metasedimentary rocks northwest of the Bear River fault, Newton belt

[major elements in weight percent oxides; minor elements in parts per million; —, no data]

Sample	101	102	103	104	105	106
SiO_2	58.50	61.07	63.00	61.60	58.87	59.56
TiO_2	0.93	0.61	0.58	0.70	0.61	0.77
Al_2O_3	12.10	15.91	15.75	15.20	14.48	14.72
*Fe_2O_3	3.84	0.83	1.02	1.04	1.79	1.32
†FeO	5.9	5.7	4.8	6.3	9.1	7.1
MnO	0.30	0.11	0.10	0.11	0.14	0.15
MgO	1.83	3.62	3.90	3.48	4.97	3.85
CaO	7.45	3.74	3.55	3.14	2.56	4.15
Na_2O	4.45	3.56	3.73	3.52	3.28	3.45
K_2O	2.14	1.81	1.94	1.89	1.57	2.35
P_2O_5	0.17	0.18	0.19	0.15	0.15	0.24
CO_2	0.20	<0.01	<0.01	0.02	<0.01	<0.01
H_2O	0.70	1.33	0.40	2.00	1.47	0.91
Total	98.51	98.47	98.96	99.15	98.99	98.57
§FeO(t)	9.36	6.45	5.72	7.23	10.71	8.29
Rb	40	30	63	69	23	18
Sr	249	375	453	389	129	364
Ba	363	529	603	369	148	670
Nb	16	—	—	5	—	—
Hf	6.6	3.3	3.6	6.5	3.7	7.9
Zr	197	118	117	212	120	276
Y	60	8	8	15	8	9
Cr	75	135	150	260	24	195
Ni	8	60	68	69	15	58
Cu	53.4	46	34	81.3	3	56
Zn	157.0	66	60	109.0	25	78
V	104	130	110	141	40	110
La	25.1	24.0	30.0	39.6	13.0	38.0
Ce	59.1	48	56	73.6	27	72
Nd	37.5	21	22	29.7	15	36
Sm	8.2	3.4	4.0	4.8	2.6	5.0
Eu	3.00	0.79	0.78	1.21	0.85	1.24
Gd						
Tb	1.7	0.4	0.4	0.5	0.4	0.5
Yb	6.2	1.35	1.29	1.6	1.52	1.68
Lu	0.91	0.19	0.20	0.22	0.24	0.27
Au	0.002	0.007	0.02	<.001	0.011	0.015

* Fe_2O_3 calculated on basis of stoichiometry; † FeO calculated on basis of stoichiometry;
§ Total measured iron represented as FeO.

101 - I505B: Dacitic crystal tuff; Thistledew Lake sequence. Deer Lake West quadrangle, 61-24-8BBAC. Analyst (1).
102 - DL14X: Felsic tuff or wacke; Joy Lake sequence. Deer Lake West quadrangle, 61-25-1DDBC. Analyst (1).
103 - DL53X: Felsic tuff or wacke; Joy Lake sequence. Effie SE quadrangle, 61-25-15BBB. Analyst (1).
104 - I525AX: Volcanogenic graywacke; Joy Lake sequence. Togo quadrangle, 62-22-10DBCC. Analyst (1).
105 - I387CX: Graywacke; Joy Lake sequence. Deer Lake West quadrangle, 62-24-16BBB. Analyst (1).
106 - I389X: Dacitic tuff; Joy Lake sequence. Deer Lake West sequence, 62-24-17AD. Analyst (1).

Table Ap(21). Iron-formation and related cherty rocks, Soudan-Bigfork area

[major elements in weight percent oxides; minor elements in parts per million; —, no data; blank, not calculated; *Fe_2O_3 calculated on basis of stoichiometry; †FeO calculated on basis of stoichiometry; §Total measured iron represented as FeO]

Sample	107	108	109	110	111	112	113	114	115	116	117	mean	std. dev.
SiO_2	45.86	53.43	56.14	91.30	82.90	50.80	65.50	61.20	77.62	62.66	87.91	66.85	15.68
TiO_2	<0.01	<0.01	<0.01	0.03	0.08	0.85	0.16	0.62	0.03	0.13	0.12	0.25	0.31
Al_2O_3	0.19	0.11	0.17	0.24	0.94	16.80	18.40	12.20	2.17	2.91	3.04	5.20	7.04
*Fe_2O_3	42.55	28.80	15.42	3.91	9.92	1.18	1.06	1.48	17.35	32.25	5.33	—	
†FeO	6.92	12.00	15.60	1.5	—	6.60	3.10	13.20	—	—	—	21.45	
MnO	0.01	0.03	2.23	0.03	0.43	0.15	0.06	0.14	0.03	0.02	0.02	0.29	0.66
MgO	0.09	1.44	2.95	0.22	1.06	7.08	1.72	2.52	0.62	1.17	1.00	1.81	1.96
CaO	0.16	1.54	3.37	0.27	0.01	5.37	1.79	1.60	0.20	0.13	0.08	1.32	1.71
Na_2O	0.03	0.02	<0.01	0.03	0.14	5.01	0.87	0.05	0.01	0.03	0.06	0.63	1.56
K_2O	0.01	0.01	0.02	0.02	0.01	0.08	2.46	1.15	0.10	0.31	0.10	0.39	0.76
P_2O_5	0.33	0.34	0.15	0.01	0.06	0.18	1.20	1.07	0.08	0.10	0.05	0.32	0.42
LOI	1.62	0.74	0.71	0.62	4.5	1.23	0.02	0.03	—	—	—	1.18	1.44
CO_2	0.03	<0.01	0.05	0.01	—	0.03	0.02	0.03	—	—	—	0.03	0.01
H_2O +	0.01	0.08	0.17	0.40	—	3.00	2.70	3.70	—	—	—	1.44	1.62
H_2O -	0.04	0.03	0.08	—	—	—	—	—	—	—	—	0.05	0.03
S	0.005	0.009	1.740	0.06	—	0.05	0.03	0.04	0.66	0.08	1.38	0.41	0.64
Total	97.86	98.58	98.80	98.65	100.05	98.41	99.09	99.03	98.87	99.79	99.09	101.62	
§FeO(t)	45.22	37.92	29.48	5.02	8.93	7.66	4.05	14.53	15.62	29.03	4.80	21.45	14.61
Rb	1	2	2	<2	—	10.0	100	60	400	380	140	122	160
Sr	6	10	9	<10	2	170	250	<10	10	10	10	53	91
Ba	30	30	60	75	4	130	400	200	10	50	20	92	118
Nb	<20	<20	<20	4	—	30	10	20	10	10	10	13	9
Hf	<0.5	<0.5	<0.5	<0.5	—	—	—	—	—	—	—	—	
Zr	21	<20	<20	4	—	80	<10	70	10	20	40	35	30
Y	<20	<20	<20	<1	—	20	20	10	12	7	38	18	11
Cr	33	35	42	190	68	—	—	—	185	200	225	122	85
Ni	3	2	5	6	11	—	—	—	5	30	10	9	9
Cu	8	23	46	29.6	6	122.0	11.9	21.5	—	—	—	34	38
Zn	9	18	210	8.9	90	37.2	34.5	93.6	65	65	60	63	57
V	<1	<1	<1	11	13	—	—	—	25	35	17	20	10
La	1	1	2	0.4	2	—	—	—	3	3	13	3.17	4.08
Ce	2	3	4	0.7	—	—	—	—	5	10	30	7.81	10.22
Nd	<5	<5	<5	0.4	—	—	—	—	—	—	—	0.40	
Sm	0.2	0.3	0.2	<0.1	—	—	—	—	—	—	—	0.23	0.06
Eu	0.2	0.4	0.2	<0.05	—	—	—	—	—	—	—	0.27	0.12
Gd													
Tb	<1	<1	<1	<1	—	—	—	—	—	—	—	—	
Yb	0.1	0.2	0.3	<0.1	—	—	—	—	—	—	—	0.20	0.10
Lu	<1.0	<1.0	<1.0	<0.05	—	—	—	—	—	—	—	—	
Au	<.001	0.002	0.005	0.002	—	0.006	0.001	<.005	0.001	0.001	0.001	0.0024	0.0020
Pb	5	5	5	9	6	1.15	0.72	2.58	20	24	16	9	8

107 - I092X: Magnetite-chert iron-formation, laminated. Upper part of Bear Lake sequence. Sherry Lake quadrangle, 60-23-23BDA. Analyst (7).

108 - I154X: Iron-formation, laminated to thin-bedded; layers are chert-magnetite and actinolite-chlorite. Upper part of Bear Lake sequence. Sherry Lake quadrangle, 60-23 36DCA. Analyst (7).

109 - I008Z: Iron-formation, laminated; layers consist of chert, magnetite, and chlorite in varying amounts. Local facies within Wilson Lake sequence. Horsehead Lake quadrangle, 60-24-2ACA. Analyst (7).

110 - I504: Iron-formation, lean, very cherty. Upper part of Bear Lake sequence. Sherry Lake quadrangle, 60-23-36DDBB. Analyst (1).

111 - HER-2-3: Interbedded ferruginous chert and metatuff, Bear Lake sequence. Drill core sample. Sherry Lake quadrangle, 61-22-32BAB. Analyst (8).

112 - 14512: Iron-formation, Soudan member of Ely Greenstone. Soudan Mine, No. 8 shaft, 2700 ft level. Soudan quadrangle, 62-15-27BB. Analyst (1).

113 - 14994: Iron-formation, Soudan member of Ely Greenstone. Soudan Mine, No. 8 shaft, 2700 ft level. Soudan quadrangle, 62-15-27BB. Analyst (1).

114 - 14966: Iron-formation, Soudan member of Ely Greenstone. Soudan Mine, No. 8 shaft, 2700 ft level. Soudan quadrangle, 62-15-27BB. Analyst (1).

115 - 20827: Chert-rich jasper, Soudan member of Ely Greenstone. Soudan quadrangle, 62-15-27. Analyst (?).

116 - 20829: Jasper, Soudan member of Ely Greenstone. Soudan quadrangle, 62-15-27. Analyst (?).

117 - 20838: Silica-cemented chert breccia, Soudan member of Ely Greenstone. Soudan quadrangle, 62-15-27. Analyst (?).

Table Ap(22). Chilled sill margins from mafic sills, Deer Lake Complex, Newton belt

[major elements in weight percent oxides; minor elements in parts per million; —, no data; blank, not calculated]

Sample	118	119	120	121	122	123	124	mean	std. dev.
SiO_2	49.7	50.3	44.1	50	58.6	46.2	49.4	49.76	4.53
TiO_2	0.76	0.88	0.47	0.92	0.9	0.65	0.64	0.75	0.17
Al_2O_3	10.1	14.1	8.5	13.6	12.6	9.3	10.9	11.30	2.17
*Fe_2O_3	—	—	0.67	—	0.71	0.34	—	0.57	0.20
†FeO	12.8	13.3	11.3	14	7.9	11.6	12.5	11.91	2.00
MnO	0.32	0.17	0.18	0.37	0.13	0.18	0.23	0.23	0.09
MgO	10.5	6.93	19.7	6.5	6.2	17.2	11.2	11.18	5.39
CaO	9.08	7.16	8.6	7.98	6.8	8.5	10.2	8.33	1.15
Na_2O	3.2	3.6	0.35	4.6	4.6	0.6	1.23	2.60	1.84
K_2O	0.35	0.66	0.06	0.78	0.27	0.64	0.83	0.51	0.29
P_2O_5	—	—	0.1	—	0.08	0.08	—	0.09	0.01
CO_2	—	—	0.05	—	0.05	0.05	—	0.05	0.00
H_2O	2.3	2.03	5.58	2	1.12	4.5	2.45	2.85	1.58
Total	99.11	99.13	99.66	100.75	99.96	99.84	99.58	100.13	
§FeO(t)	12.80	13.30	11.90	14.00	8.54	11.91	12.50	12.43	
¶Mg#	59.41	48.18	74.70	45.31	56.44	72.05	61.52	61.6	

* Fe_2O_3 calculated on basis of stoichiometry; † FeO calculated on basis of stoichiometry; § Total measured iron represented as FeO; ¶ Mg# is mol ratio 100Mg/(Mg+Fe) in which Fe is total Fe reported as FeO.

118 - A2-HD: Fine-grained chilled margin of mafic sill. Deer Lake West quadrangle, 61-25-1CC. From Ripley and others (1982).
119 - 3-CD-2: Fine-grained chilled margin of mafic sill. Deer Lake West quadrangle, 61-25-1CC. From Ripley and others (1982).
120 - 1-1-Z: Fine-grained chilled margin of mafic sill. Deer Lake West quadrangle, 61-25-1C. From Berkley (1972).
121 - 3-CD-1: Fine-grained chilled margin of mafic sill. Deer Lake West quadrangle, 61-25-1CC. From Ripley and others (1982).
122 - 1-1-Y: Fine-grained chilled margin of mafic sill. Deer Lake West quadrangle, 61-25-1C. From Berkley (1972).
123 - 2-8-D: Fine-grained chilled margin of mafic sill. Deer Lake West quadrangle, 61-25-1C. From Berkley (1972).
124 - 29-02: Fine-grained chilled margin of mafic sill. Deer Lake West quadrangle, 61-25-1CC. From Ripley and others (1982).

Table Ap(23). Dacite porphyry dikes and sills, and dacite flows, Soudan-Bigfork area

[Q porph, contains quartz phenocrysts; P porph, contains plagioclase phenocrysts; dacite fl., dacite flow; major elements in weight percent oxides; minor elements in parts per million; —, no data; totals below 96 wt. percent italicized]

Rock type	Q porph	Q porph	Q porph	Q porph	Q porph	Q porph	Q porph	Q porph	Q porph	P porph	P porph	P porph
Sample	125	126	127	128	129	130	131	132	133	134	135	136
SiO_2	64.5	65.8	65.8	65.42	63.77	66.54	64.20	68.00	64.75	61.15	61.6	61.60
TiO_2	0.27	0.21	0.19	0.43	0.44	0.35	0.23	0.21	0.25	0.36	0.31	0.48
Al_2O_3	14.98	16.23	17.7	14.89	15.44	15.80	17.21	16.32	16.68	16.48	16.7	16.40
*Fe_2O_3	0.51	0.92	0.9	1.32	—	—	1.36	1.92	2.92	1.33	1	3.19
†FeO	2.12	0.76	0.63	2.67	3.83	3.3	—	—	—	2.48	1.67	1.6
MnO	0.03	0.02	0.03	0.08	0.10	0.06	0.02	0.04	0.02	0.07	0.05	0.08
MgO	2.11	0.6	1.73	2.68	2.33	2.56	1.32	1.67	1.38	2.58	3.65	2.55
CaO	3.75	3.2	3.95	4.95	4.58	1.20	4.19	3.45	2.67	4.29	5.53	3.96
Na_2O	4.72	5.11	5.77	4.66	4.37	5.41	4.18	5.20	6.42	5.04	4.43	5.52
K_2O	1.61	2.8	1.24	0.41	1.26	2.27	2.59	1.61	1.46	1.43	2.12	1.09
P_2O_5	0.12	0.1	0.1	0.25	0.17	0.16	0.12	0.11	0.14	0.18	—	0.24
CO_2	2.94	2.54	0.44	0.29	—	—	—	—	—	2.29	—	0.87
H_2O	1.85	1.48	1.05	0.18	2.5	1.8	—	—	—	2.02	2.94	1.30
Total	99.51	99.77	99.53	98.23	94.79	99.45	*95.42*	98.53	96.69	99.70	100	98.88
§FeO(t)	2.58	1.59	1.44	3.86	3.83	3.30	1.22	1.73	2.63	3.68	2.57	4.47
Rb	—	—	32	10	—	—	68.01	43.64	38.81	—	—	24
Sr	—	—	657	490	32	19	500.65	534.63	489.45	—	—	1690
Ba	—	—	836	220	39	20	877.42	790.37	444.7	—	—	956
Sc	—	—	—	7	—	—	—	—	—	—	—	5.8
Nb	—	—	—	<20	—	—	—	—	—	—	—	13
Hf	—	—	—	2.8	—	—	1.97	1.68	2.14	—	—	3.6
Zr	—	—	—	92	—	—	61.56	60.74	69.81	—	—	137
Y	—	—	—	<20	—	—	—	—	0.97	—	—	7
Cr	—	—	—	110	79	69	16.37	51.93	16.8	—	—	89
Ni	—	—	—	52	22	20	17.28	35.99	17.69	—	—	11
Cu	—	—	—	18	27	26	71.11	66.3	79.28	—	—	13.2
Zn	—	—	—	51	58	108	26.75	43.85	35.38	—	—	65.1
V	—	—	—	56	51	49	20.95	23.43	26.5	—	—	83
La	—	—		16	23	18	8.9257	11.573	12.594	—	—	32.2
Ce	—	—	33.7	40	—	—	20.387	25.878	28.218	—	—	65.5
Nd	—	—	15.9	14	—	—	9.4491	11.183	13.236	—	—	33.7
Sm	—	—	3	2.6	—	—	2.2435	2.0284	2.4881	—	—	5.1
Eu	—	—	0.803	0.8	—	—	0.9512	0.6375	0.6386	—	—	1.38
Tb	—	—	—	<1	—	—	0.4514	0.1422	0.1631	—	—	0.3
Yb	—	—	0.28	0.3	—	—	0.2906	0.1455	0.2809	—	—	0.5
Lu	—	—	0.044	<1.0	—	—	0.2576	0.0387	0.0595	—	—	0.06
Au	—	—	—	0.002	—	—	—	—	—	—	—	0.005

* Fe2O3 calculated on basis of stoichiometry; † FeO calculated on basis of stoichiometry; §Total measured iron represented as FeO.

125 - PK-H-8: Dacite porphyry. Tower quadrangle, 61-15-5ABCD. Analyst (4).
126 - PK-169W: Dacite porphyry. Soudan quadrangle, 62-14-20BABB. Analyst (4).
127 - JAMN-51: Dacite porphyry. Soudan quadrangle, 62-14-16DDA. Analyst (6).
128 - I022X: Tonalite porphyry. Sherry Lake quadrangle, 60-22-8BBD. Analyst (7).
129 - SNT-1-3: Dacite porphyry, drill core sample. Togo quadrangle, 61-22-21DDC. Analyst (8).
130 - SNT-1-6: Dacite porphyry, drill core sample. Togo quadrangle, 61-22-21DDC. Analyst (8).
131 - S-46: Dacite porphyry, Soudan quadrangle, 62-14-18CCBCB. Analyst (9).
132 - S-474: Dacite porphyry, Soudan quadrangle, 61-15-3CBBCA. Analyst (9).
133 - S-711: Dacite porphyry, Soudan quadrangle, island NW of Birch I., 62-15-10DAADA. Analyst (9).
134 - PK-169: Dacite porphyry. Eagles Nest Lake quadrangle, 62-14-15CCBA. Analyst (4).
135 - JAMN-53: Dacite porphyry. Soudan quadrangle, 62-14-19ADA. Analyst (6).
136 - I558B: Dacite porphyry. Effie SE quadrangle, 61-25-17ADCA. Analyst (1).

Table Ap(23) continued.

[Q porph, contains quartz phenocrysts; P porph, contains plagioclase phenocrysts; dacite fl., dacite flow; major elements in weight percent oxides; minor elements in parts per million; —, no data; totals below 96 wt. percent italicized]

Rock type	P porph	P porph	P porph	dacite fl	dacite fl	dacite fl	dacite fl	grand average	std. dev.	mean Q porph	mean P porph	mean dac. fl.
Sample	137	138	139	140	141	142	143					
SiO_2	61.76	63.57	60.52	66.10	60.98	56.49	62.77	63.44	2.73	65.42	61.70	61.59
TiO_2	0.45	0.28	0.44	0.92	0.61	0.63	0.67	0.41	0.19	0.29	0.39	0.71
Al_2O_3	16.12	17.19	15.70	15.46	16.10	15.43	16.13	16.16	0.75	16.14	16.43	15.78
*Fe_2O_3	1.68	2.91	4.80	1.29	—	2.73	1.83	1.91	1.12	1.41	2.49	1.95
†FeO	2.9	—	—	2.85	5.75	4.6	5.1	2.88	1.54	2.22	2.16	4.58
MnO	0.10	0.06	0.08	0.07	0.13	0.12	0.09	0.07	0.03	0.04	0.07	0.10
MgO	2.19	2.96	5.15	1.56	3.06	5.63	3.10	2.57	1.24	1.82	3.18	3.34
CaO	3.68	4.74	4.70	2.25	4.00	8.16	2.46	3.98	1.46	3.55	4.48	4.22
Na_2O	4.11	4.27	4.62	5.14	3.31	2.82	4.23	4.70	0.84	5.09	4.67	3.87
K_2O	4.14	2.33	1.93	1.95	2.37	0.72	2.28	1.87	0.84	1.69	2.17	1.83
P_2O_5	0.26	0.13	0.20	0.19	0.17	0.13	0.19	0.16	0.05	0.14	0.20	0.17
CO_2	0.07	—	—	—	—	0.04	<0.01	1.19	1.20	1.55	1.08	0.04
H_2O	0.94			0.30	1.16	1.14	0.95	1.40	0.77	1.48	1.80	0.89
Total	98.4	98.44	98.14	98.08	97.64	98.64	99.80	100.74		100.84	100.82	99.07
§FeO(t)	4.41	2.62	4.32	4.01	5.75	7.06	6.75	4.60		3.49	4.40	6.63
Rb	42	82.02	51.69	55	80	2	65	46	25	38	50	51
Sr	774	411.52	317.84	505	500	200	379	500	389	389	798	396
Ba	1164	392.72	866.02	1030	—	167	472	591	386	461	845	556
Sc	2	—	—	13.3	—	<1	7	7	4	7	4	10
Nb	—	—	—	<20	29.0	—	—	21	11		13	29
Hf	5.3	2.21	2.34	5	—	2.3	3.0	3	1	2	3	3
Zr	168	73.06	83.97	211	130	85	126	108	47	71	116	138
Y	11	—	5.01	<20	—	<2	9	7	4	1	8	9
Cr	14	124.95	314.7	124	137	50	135	95	77	57	136	112
Ni	8	55.59	79.43	45	—	85	70	40	27	27	39	67
Cu	20	48.7	61.61	6	—	110	50	46	31	48	36	55
Zn	52	34.77	60.39	40	—	35	41	50	21	54	53	39
V	80	38.46	79.25	102	—	50	150	62	36	38	70	101
La	41.0	11.52	13.151	29	—	8.2	24.0	19.17	10.06	15.02	24.47	20.40
Ce	76	24.819	29.113	56	—	19	48	38.88	18.60	29.64	48.86	41.00
Nd	40	11.242	13.601	44	—	8	21	19.61	12.48	12.75	24.64	24.33
Sm	6.2	2.0289	2.7823	4.4	—	1.8	3.3	3.16	1.37	2.47	4.03	3.17
Eu	1.44	0.6448	0.9143	1.1	—	0.53	0.80	0.89	0.29	0.77	1.09	0.81
Tb	0.5	0.1349	0.2795	<1	—	0.3	0.4	0.30	0.13	0.25	0.30	0.35
Yb	1.53	0.1452	0.66	1.1	—	1.37	1.46	0.67	0.54	0.26	0.71	1.31
Lu	0.20	0.0457	0.1165	<1.0	—	0.21	0.33	0.14	0.11	0.10	0.11	0.27
Au	0.006	—	—	<.001	—	0.019	0.008	0.008	0.01	0.002	0.006	0.014

137 - I388BX: Dacite porphyry dike. Deer Lake West quadrangle, 62-24-17BDA. Analyst (1).
138 - S-515: Dacite porphyry, Soudan quadrangle, 62-14-20DCACB. Analyst (9).
139 - S-646: Dacite porphyry, Soudan quadrangle, 61-15-2DCCDA. Analyst (9).
140 - I156EX: Dacite flow. Sherry Lake quadrangle, 60-23-36CDD. Analyst (7).
141 - 3223: Dacite. Deer Lake West quadrangle, 61-25-1DD. Analyst (?).
142 - DL41X: Dacite flow. Effie SE quadrangle, 61-25-3AAB. Analyst (1).
143 - I357B: Felsic flow. Togo quadrangle, 62-22-17AA. Analyst (1).

Table Ap(24). Lamprophyres, Soudan-Bigfork area

[divided into high-Cr group (144-150) and low-Cr group (151-156); major elements given in weight percent oxides; minor elements in parts per million; —, no data; blank, not present as normative mineral]

Cr group	high	high	high	high	high	high	high	mean high Cr
Sample	144	145	146	147	148	149	150	
SiO_2	46.1	55.2	51.5	51.2	48.9	48.8	49.46	50.17
TiO_2	0.71	0.62	0.69	0.67	1.13	0.92	0.5	0.75
Al_2O_3	8.95	13.3	10.2	11	12.2	11.4	10.92	11.14
*Fe_2O_3	2.76	1.89	1.76	2.5	3.77	1.72	1.31	2.24
†FeO	9.4	4.8	6.1	6.5	6.3	7.8	6.3	6.74
MnO	0.22	0.12	0.17	0.17	0.17	0.17	0.14	0.17
MgO	15.4	8.12	12.1	9.87	10.8	12.2	13.67	11.74
CaO	10.8	7.26	8.56	11.7	6.05	8.12	7.56	8.58
Na_2O	0.82	3.6	2.75	2.08	3.26	1.65	0.73	2.13
K_2O	0.24	1.91	1	1.24	1.61	0.19	3.569	1.39
P_2O_5	0.03	0.22	0.28	0.17	0.17	0.31	0.42	0.23
CO_2	0.03	0.53	0.06	0.04	0.27	1.61	0.06	0.37
H_2O	2.2	1.1	1.6	0.9	2.1	4.1	1.99	2.00
Total	97.66	98.67	96.77	98.04	96.73	98.99	96.73	97.65
§FeO(t)	11.88	6.50	7.68	8.75	9.69	9.35	7.48	8.76
¶Mg#	69.81	69.03	73.75	66.81	66.53	69.96	76.53	70.34
Rb	4	78	23	37	40	<2	14	33
Sr	29	813	982	339	453	417	262	471
Ba	36	324	1320	557	455	107	760	508
Nb	<2	<2	6	2	<2	3	—	4
Hf	1	2.7	2.4	1.8	2	3.8	3.4	2
Zr	36	106	95	64	75	114	107	85
Y	12	12	13	11	14	17	7	12
Cr	1600	460	970	660	720	720	540	810
Ni	337	161	182	136	260	257	260	228
Cu	167	65	144	30	123	93	36	94
Zn	91	75	69	99	94	119	61	87
V	252	167	193	199	194	206	100	187
La	2.6	26.4	18.2	12.1	10.4	15.7	27	16.06
Ce	3.7	51.1	38.3	25.8	19.6	33.8	59	33.04
Nd	4.8	27.4	19.8	15.9	13.8	20.8	35	19.64
Sm	1.4	4.8	4.2	3.3	3.5	4.5	6.5	4.03
Eu	0.569	1.44	1.51	0.91	1.07	1.25	1.48	1.18
Tb	0.4	0.5	0.5	0.3	0.5	0.6	0.06	0.41
Yb	1.4	1.1	1.2	1.2	1.4	1.7	1.17	1.31
Lu	0.17	0.16	0.21	0.17	0.2	0.25	0.17	0.19
Au	<.001	0.002	<.001	<.001	<.001	<.001	0.004	0.003
norm. quartz		1.35				1.11		
norm. olivine	13.14		5.09	1.24	12.56		11.5	5.08

* Fe_2O_3 calculated on basis of stoichiometry; † FeO calculated on basis of stoichiometry; § Total measured iron represented as FeO; ¶ Mg# is mol ratio 100Mg/(Mg+Fe) in which Fe is total Fe reported as FeO.

144 - BNW-2A: Lamprophyre. Biwabik NW quadrangle, 61-16-21CDDD. Analyst (1).
145 - BNW-1C: Lamprophyre. Biwabik NW quadrangle, 61-16-21DBBB. Analyst (1).
146 - C192B: Lamprophyre, fine-grained, massive; sill within metabasalt sequence. Sassas Creek quadrangle, 61-17-16DBDA. Analyst (1).
147 - C645B: Lamprophyre, hornblende-rich; sill or flow(?) interstratified with breccia of similar composition. Britt quadrangle, 61-18-24CCBD. Analyst (1).
148 - T-864: Lamprophyre. Tower quadrangle, 61-15-20CBAB. Analyst (1).
149 - RO-T-688D: Lamprophyre; small dike in metagraywacke of Lake Vermilion Formation. Tower quadrangle, 62-15-21DBDB. Analyst (1).
150 - I407AX: Lamprophyre, Deer Lake East quadrangle, 61-23-7ACC. Analyst (1).

Table Ap(24) continued.

[divided into high-Cr group (144-150) and low-Cr group (151-156); major elements given in weight percent oxides; minor elements in parts per million; blank, not present as normative mineral]

Cr group	low	low	low	low	low	low	mean low Cr
Sample	151	152	153	154	155	156	
SiO_2	43.6	50.3	49.6	53.9	55	49.7	50.35
TiO_2	0.95	1.14	0.96	0.72	0.71	2.47	1.16
Al_2O_3	13.2	12.6	13.6	17.3	14.2	12.7	13.93
*Fe_2O_3	4.08	3.48	2.67	2.79	2.71	7.24	3.83
†FeO	7.2	11.2	8.3	4.3	5	9.6	7.60
MnO	0.18	0.25	0.2	0.12	0.14	0.3	0.20
MgO	6.64	6.1	7.25	5.16	6.13	3.38	5.78
CaO	13.2	8.85	10.2	7.94	6.84	8.03	9.18
Na_2O	1.86	2.1	2.28	2.79	3.89	3.04	2.66
K_2O	1.03	0.29	0.24	1.57	2.39	0.48	1.00
P_2O_5	0.23	0.12	0.13	0.12	0.23	0.1	0.16
CO_2	3.38	0.11	0.06	0.33	0.04	0.05	0.66
H_2O	2.7	1.9	3.2	2.2	1	1.1	2.02
Total	98.25	98.44	98.69	99.24	98.28	98.19	98.53
§FeO(t)	10.87	14.33	10.70	6.81	7.44	16.12	11.05
¶Mg#	52.15	43.16	54.72	57.48	59.52	27.23	49.04
Rb	18	<2	<2	33	63	7	30
Sr	782	98	88	202	790	97	343
Ba	207	38	86	244	745	169	248
Nb	3	2	7	6	6	5	5
Hf	2.5	2.2	2.2	2.4	3.3	3.2	3
Zr	79	60	66	92	117	73	81
Y	18	23	24	12	18	21	19
Cr	410	25	180	92	280	5	165
Ni	59	45	61	61	43	2	45
Cu	135	105	53	28	94	10	71
Zn	94	158	100	69	104	161	114
V	293	408	238	162	186	325	269
La	12.7	7.3	6.2	10.6	25.3	4.2	11.05
Ce	27.3	14.6	12.2	23.9	49.5	12.3	23.30
Nd	17.5	9.6	9.6	12.5	27.6	10.3	14.52
Sm	3.7	2.4	2.6	2.7	5.3	3	3.28
Eu	1.18	0.91	0.97	1.01	1.44	1.51	1.17
Tb	0.6	0.6	0.6	0.4	0.6	0.6	0.57
Yb	1.7	2.5	2.6	1.4	1.7	2.8	2.12
Lu	0.23	0.36	0.4	0.16	0.28	0.37	0.30
Au	0.002	0.003	<.001	0.002	<.001	<.001	0.002
norm. quartz		6.17	2.96	7.27	1.32	9.01	3.77
norm. olivine	7.62						

* Fe_2O_3 calculated on basis of stoichiometry; † FeO calculated on basis of stoichiometry; § Total measured iron represented as FeO; ¶ Mg# is mol ratio 100Mg/(Mg+Fe) in which Fe is total Fe reported as FeO.

151 - ENW-379C: Lamprophyre. Shagawa Lake quadrangle, 63-13-36DAAC. Analyst (1).
152 - S-431: Lamprophyre. Soudan quadrangle, 61-15-11BACD. Analyst (1).
153 - ENW-358: Lamprophyre, pyroxene-phyric. Shagawa Lake quadrangle, 62-13-1DBDC. Analyst (1).
154 - T-114: Lamprophyre or hornblende dolerite. Tower quadrangle, 62-15-33BACA. Analyst (1).
155 - BNW-11B: Lamprophyre or hornblende dolerite. Biwabik NW quadrangle, 61-17-26DDAB. Analyst (1).
156 - BNE-92A: Lamprophyre, hornblende-rich, strongly foliated and lineated. Biwabik NE quadrangle, 61-16-25ACAD. Analyst (1).